JOURNAL OF PETROLOGY | VOLUME 55 | NUMBER 12 | PAGES 2419–2456 | 2014 | doi:10.1093/petrology/egu062

Interaction of Biotite–Amphibole Gneiss with H_2O–CO_2–(K, Na)Cl Fluids at 550 MPa and 750 and 800°C: Experimental Study and Applications to Dehydration and Partial Melting in the Middle Crust

OLEG G. SAFONOV[1,2,3]*, SVETLANA A. KOSOVA[1] AND DIRK D. VAN REENEN[3]

[1]INSTITUTE OF EXPERIMENTAL MINERALOGY, RUSSIAN ACADEMY OF SCIENCES, ACADEMICIAN OSSIPIAN STR., 4, CHERNOGOLOVKA, MOSCOW DISTRICT, 142432 RUSSIA

[2]DEPARTMENT OF PETROLOGY, MOSCOW STATE UNIVERSITY, VOROB'EVY GORY, MOSCOW, 119899 RUSSIA

[3]DEPARTMENT OF GEOLOGY, UNIVERSITY OF JOHANNESBURG, JOHANNESBURG, SOUTH AFRICA

RECEIVED JUNE 5, 2013; ACCEPTED OCTOBER 23, 2014

To constrain effects of chloride-bearing H_2O–CO_2 fluids on complex natural assemblages during high-grade metamorphism and anatexis, we report the results of experiments on the interaction of biotite–hornblende tonalitic gneiss from the Sand River Formation (Limpopo Complex, South Africa) with H_2O–CO_2, H_2O–CO_2–KCl, H_2O–CO_2–NaCl, and H_2O–CO_2–(K, Na)Cl fluids at 550 MPa, 750 and 800°C, and varying chloride/($H_2O + CO_2$) ratios with molar $CO_2/(CO_2 + H_2O) = 0{\cdot}5$. Heating of solid cylinders of gneiss at both temperatures in the absence of a free fluid phase produced no changes in the gneiss phase assemblage. The equimolar H_2O–CO_2 fluid at 750°C also did not significantly influence the phase assemblage. Addition of KCl to the fluid at 750°C resulted in formation of the clinopyroxene + K-feldspar (+ ilmenite/titanite) assemblage after biotite, hornblende and plagioclase. Orthopyroxene accompanied by amphibole appeared only at 800°C as a result of biotite breakdown in the presence of H_2O–CO_2 and low-salinity H_2O–CO_2–KCl fluids. Increase in the KCl content in the fluid at 800°C resulted in the production of a clinopyroxene-bearing assemblage. Increase of the NaCl content stabilized amphibole in an assemblage with either orthopyroxene (at low NaCl concentrations) or clinopyroxene. Nevertheless, clinopyroxene (+ albite) is stable only at high salt concentrations. Comparison of the experimental results with the results of thermodynamic modeling using the Gibbs free energy minimization method (PERPLE_X software) showed that mineral reactions and assemblages in the run products were governed by the activities of alkali components imposed by KCl and NaCl in the H_2O–CO_2 fluids, and decrease of the water activity served as an additional factor stabilizing anhydrous assemblages. No melts formed at 750°C in the presence of the H_2O–CO_2–KCl fluids. These fluids provoked melting only at 800°C with formation of rhyolitic melts. With increasing KCl content of the fluid, the melt composition changed to potassic rhyolitic with $Al_2O_3 < 13{\cdot}5$ wt %, $CaO < 2$ wt %, $K_2O + Na_2O > 7$ wt %, $FeO/(FeO + MgO) > 0{\cdot}8$, $K_2O/Na_2O > 1$, and moderate enrichment in Cl (0·2–0·6 wt %). Increasing NaCl content caused melting at 750°C and shifted the melt composition towards trachytic and trachyandesitic compositions at both 750 and 800°C. The experiments support a model for the formation of ferroan A-type granite–syenite complexes via crustal melting in the presence of H_2O–CO_2–salt fluids in extensional tectonic settings. They demonstrate a possible link between A-type granitoids and mid-crustal dehydration zones in amphibolite- to granulite-facies terrains and allow a new interpretation of mineral assemblages within these zones in terms of variations in fluid salinity.

*Corresponding author. Present address: Institute of Experimental Mineralogy, Russian Academy of Sciences, Academician Ossipian str., 4, Chernogolovka, Moscow district, 142432 Russia. Telephone and fax: +7-496-525-44-25. E-mail: oleg@iem.ac.ru

KEY WORDS: *biotite–amphibole gneiss; aqueous–carbonic and aqueous–salt fluids; partial melting; alkali activity, water activity, dehydration; middle crust; charnockite; syenite; granite*

Mineral and end-member abbreviations: Ab – albite, Aeg – aegirine, Amph – amphibole, An – anorthite, Ap – apatite, Bar – barroisite, Bt – biotite, Cal – calcite, Cor – corundum, Cpx – clinopyroxene, Di – diopside, Ed – edenite, En – enstatite, Ep – epidote, Fl – fluorite, Fs – ferrosilite, Fsp – alkali feldspar, Hal – halite, Hbl – hornblende, Hed – hedenbergite, Hyp – hypersthene, Ilm – ilmenite, Kfs – K-feldspar, Ks – kalsilite, Lc – leucite, Ms – magnesite, Mt – magnetite, Ne – nepheline, Ol – olivine, Opx – orthopyroxene, Or – orthoclase, Phl – phlogopite, Pl – plagioclase, Prg – pargasite, Qtz – quartz, San – sanidine, Sp – spinel, Tr – tremolite, Ts – tschermakite, Ttn – titanite, Uvs – ulvöspinel, Win – winchite, Zrc – zircon

Compositional parameters: $X_{Mg} = Mg/(Mg + Fe + Mn)$, $X_{Al} = Al/(Si + Al + Ti + Mg + Fe + Mn)$ (for amphiboles, biotites and orthopyroxenes), $X_{Ca} = Ca/(Ca + Na + K)$ (for plagioclase and amphibole), $X_{Ca} = Ca/(Ca + Mg + Fe + Mn)$ (for garnet), $X_K = K/(K + Na)$ (for alkali feldspar and amphibole)

INTRODUCTION

The participation of chloride-bearing aqueous–salt fluids in high-grade metamorphism and deep-crustal anatexis in addition to, or as an alternative to, CO_2-rich fluids was first recognized in the 1980s on the basis of petrological data, fluid inclusion studies and thermodynamic considerations (Condie *et al.*, 1982; Touret, 1985; Aranovich *et al.*, 1987). Later, Perchuk and co-authors (Perchuk & Gerya, 1993; Perchuk *et al.*, 1994), following theoretical predictions by Korzhinskii (1959, 1962), showed that some metamorphic processes, for example charnockite formation, could be governed by an increase of K and Na activities in fluids bearing alkali salts. This conclusion was based on an interpretation of K-feldspar reaction textures and regular variations of mineral compositions associated with these textures as a result of the interaction of the minerals with alkali-bearing fluids. Subsequently, these conclusions were repeatedly supported for charnockite (Perchuk *et al.*, 2000; Ravindra Kumar, 2004; Safonov *et al.*, 2012; Rajesh *et al.*, 2013) and successfully extended to high-grade metamorphism (Hansen *et al.*, 1995; Newton, 1995; Franz & Harlov, 1998; Harlov *et al.*, 1998; Markl & Bucher, 1998; Markl *et al.*, 1998; Newton *et al.*, 1998, 2014; Safonov, 1998; Harlov & Förster, 2002; Yardley & Graham, 2002; Montanini & Harlov, 2006; Touret, 2009; Newton & Manning, 2010; Huizenga *et al.*, 2011; Touret & Huizenga, 2011, 2012; Harlov, 2012; Manning & Aranovich, 2014; Tsunogae & van Reenen, 2014). These studies proved that apart from major components of the ternary system C–O–H, fluids participating in high-grade metamorphism in the middle and lower crust also contain diverse dissolved salts, of which K, Na, and Ca chlorides are the principal components. The presence of alkali chlorides in granulite-related fluids is supported globally by the presence of chloride-bearing fluid inclusions in minerals (Srikantappa & Malathi, 2008; Srikantappa & Zargar, 2009; Touret, 2009; Touret & Huizenga, 2011, 2012), intergranular crystalline chlorides (Markl & Bucher, 1998), and Cl-rich (>1 wt %) amphiboles, biotites, and apatite (Markl *et al.*, 1998; Safonov, 1998) in granulites. Experiments have shown that, in contrast to CO_2-rich fluids, chloride-bearing aqueous solutions at high P and T are much better solvents for many silicate minerals, as well as for carbonates, sulphates, phosphates, and fluorides (see review by and references in Newton & Manning, 2010; Manning, 2013; Manning & Aranovich, 2014). Such fluids are able to dissolve various accessory minerals and actively exchange alkali components with feldspars and biotite, thus assisting with the transport of rare earth elements (REE), Rb and Cs (Hansen *et al.*, 1995, 2002; Harlov & Melzer, 2002; Harlov *et al.*, 2005; Harlov, 2011; Tropper *et al.*, 2011, 2013). Strong ionization of the concentrated (K, Na)Cl–H_2O fluids at $P > 400$ MPa and $T = 600$–$900°C$ results in a decrease of water activity in such solutions (Aranovich *et al.*, 1987, 2013, 2014; Aranovich & Newton, 1996, 1997, 1998; Shmulovich & Graham, 1996; Manning, 2013; Manning & Aranovich, 2014), stabilizing anhydrous mineral assemblages. At granulite P–T conditions, aqueous chloride fluids are immiscible with CO_2 (Bowers & Helgeson, 1983; Johnson, 1991; Duan *et al.*, 1995; Gilbert *et al.*, 1998; Shmulovich & Graham, 2004; Heinrich, 2007; Aranovich *et al.*, 2010), resulting in the coexistence of two fluids with low water activity and contrasting mobility (Watson & Brenan, 1987; Holness, 1997; Gilbert *et al.*, 1998). This effect is evidenced in granulites and charnockites by heterogeneous trapping of brine (aqueous solutions coexisting with a solid salt phase) and dense CO_2 inclusions in minerals (Perchuk *et al.*, 2000; Srikantappa & Malathi, 2008; Srikantappa & Zargar, 2009; Touret, 2009; Touret & Huizenga, 2011, 2012; Rajesh *et al.*, 2013). Low water activity, which characterizes major high-grade fluids, inhibits partial melting of quartz–feldspar assemblages (Aranovich & Newton, 1996; Shmulovich & Graham, 1996; Aranovich *et al.*, 2013, 2014). In addition, concentrated aqueous chloride solutions show limited solubility in silicic melts (Ryabchikov & Hamilton, 1971; Kilink & Burnham, 1972; Shmulovich & Graham, 1996; Webster, 1997) that usually form during anatexis of metamorphic rocks. In equilibrium with an aluminosilicate melt, chlorides strongly partition into any coexisting aqueous fluid. Therefore, the appearance of melts and partitioning of H_2O into them increases the salinity of the coexisting fluid (e.g. Shmulovich & Graham, 1996). Nevertheless, the solubility of chloride-bearing fluids in magmas critically depends on

the composition of the melt (Webster, 1997; Webster & De Vivo, 2002), which, in turn, is a function of the bulk chemical and mineral composition of the original protolith. In contrast to haplogranitic compositions, the presence of Ca and Fe and high peralkalinity assist the solubility of Cl in melts and, therefore, could promote the progress of melting.

Thermodynamic properties of aqueous chloride solutions and H_2O–CO_2–chloride fluids are well known from experiments in model systems (Bowers & Helgeson, 1983; Duan *et al.*, 1995; Aranovich & Newton, 1996, 1997, 1998; Shmulovich & Graham, 1996; Aranovich *et al.*, 2010, 2013, 2014; Newton & Manning, 2010; Manning, 2013; Manning & Aranovich, 2014). However, such data are not sufficient to evaluate the behavior of chloride-bearing fluids during crustal high-grade metamorphism and anatexis in complex mineral–fluid systems. Model systems do not account for all possible reactions between minerals and complex fluids. For this purpose, experiments on the interaction of aqueous–chloride and aqueous–carbonic–chloride fluids with natural metamorphic rocks are a valuable addition to the data obtained from model systems. Such experiments reveal possible fluid–mineral–melt reactions, which can subsequently be thermodynamically constrained in model systems. So far, the results for only a few such experimental studies are available. Tropper & Manning (2008) studied the transformation of a garnet–biotite–sillimanite gneiss to a jadeite–phengite–quartz assemblage via interaction with H_2O–NaCl fluids at 2000 MPa and 600°C, and reproduced some mineral assemblages in subduction-related metamorphic complexes. Khodorevskaya (2004) performed experiments on the 'granitization' of amphibolite via infiltration of chloride-bearing aqueous solutions at 500 MPa and 750°C. Larikova & Zaraisky (2009) experimentally investigated the influence of NaCl concentration in aqueous fluid on the formation of amphibole and garnet coronas in metagabbro at 500 MPa and 670 and 700°C. Harlov (2004) showed that chlorides stabilize orthopyroxene and clinopyroxene with K-feldspar after biotite and plagioclase in tonalite biotite gneiss interacted with KCl- and NaCl-bearing fluids at 1000 MPa and 900°C. However, no systematic experimental studies on the interaction of metamorphic rocks with chloride-bearing fluids of varying chloride content and KCl/NaCl ratio are available.

In this study we present the results of experiments on the interaction of a biotite–hornblende gneiss with H_2O–CO_2, H_2O–CO_2–KCl, H_2O–CO_2–NaCl and H_2O–CO_2–(K, Na)Cl fluids at a pressure of 550 MPa and temperatures of 750 and 800°C. The major purpose of the experiments was to investigate the dependence of mineral–fluid reactions, melting processes, compositions of crystalline phases and melts on temperature, the chloride content and KCl/NaCl ratio in the fluid. Our experiments did not aim to provide constraints on the thermodynamic properties of aqueous–carbonic–salt fluids. From the start, they were initiated to reproduce the processes accompanying formation of pyroxene-bearing dehydration domains at the Causeway locality, Limpopo Complex, South Africa at 750–800°C and 550–620 MPa under the influence of H_2O–CO_2–salt fluids (Safonov *et al.*, 2012; Rajesh *et al.*, 2013). Safonov *et al.* (2012) demonstrated the applicability of the experimental results with H_2O–CO_2 and H_2O–CO_2–KCl fluids to this specific example of a dehydration zone. Here we report additional textural and compositional data for experiments with H_2O–CO_2 and H_2O–CO_2–KCl fluids and expand the range of fluid compositions to H_2O–CO_2–NaCl and H_2O–CO_2–(K, Na)Cl. The results of our study can thus be readily applied to a much greater diversity of examples of fluid–rock interaction processes during high-grade metamorphism and anatexis.

EXPERIMENTAL AND ANALYTICAL PROCEDURES

Starting materials

A metaluminous biotite–hornblende orthogneiss 173/1 (Safonov *et al.*, 2012; Rajesh *et al.*, 2013) from the Sand River Gneiss formation, Limpopo Complex, Southern Africa, was used in the experiments (Table 1). The orthogneiss is a texturally homogeneous fine- to medium-grained rock with a gneissic texture expressed by alternating broad bands enriched either in quartz and plagioclase or in biotite and hornblende. The gneissic texture is not evident at the thin-section scale (Fig. 1). Hornblende and biotite form clusters in a quartz–plagioclase granoblastic matrix (Fig. 1). Magnetite appears as irregular grains with lamellae of ilmenite. Fluorapatite is present as rounded grains attached mostly to clusters of biotite and hornblende, whereas small grains of zircon are dispersed in the plagioclase–quartz matrix (Fig. 1). Rare pyrite is also present in the rock. K-feldspar appears only as minute antiperthite inclusions in plagioclase (Fig. 1). No pyroxenes are present in the orthogneiss 173/1.

Cylindrical samples of the gneiss, 4–6 mm in length and 3 mm in diameter, were prepared for experiments using a diamond drill. These were placed tightly into 3 mm diameter gold capsules of 40 mm length and with walls 0·2 mm thick. Free volume in the capsules was filled with homogeneous mixtures of oxalic acid and chlorides of analytical purity. Concentrations of chloride in the fluid mixtures varied from 0·2 to 8·3 mol % (Table 2). The weight of the mixture in single capsules was estimated from molar volumes of H_2O and CO_2 at run conditions, neglecting the volume of crystalline chloride. The rock/fluid weight ratio varied from 0·15 to 0·70 for single runs (Table 2). Capsules

Table 1: Bulk chemical composition and average composition of major rock-forming minerals of the orthogneiss 173/1 (Rajesh et al., 2013) used in the experiments

Component:	Rock	Hbl	Bt	Pl	Ap	Mt	Ilm
n:	1	8	12	17	4	1	1
SiO_2	61·22	42·07 (1·03)	34·78 (0·16)	59·14 (0·74)	0·43 (0·06)	0·17	0·37
TiO_2	0·70	1·11 (0·09)	3·68 (0·14)	0·00 (0·00)	0·00 (0·00)	0·07	52·72
Al_2O_3	17·19	11·61 (0·55)	14·82 (0·18)	25·77 (0·47)	0·00 (0·00)	0·67	0·28
FeO	5·86	20·82 (0·86)	21·60 (0·46)	0·00 (0·00)	0·00 (0·00)	98·20	40·60
MnO	0·08	0·47 (0·06)	0·16 (0·16)	0·00 (0·00)	0·00 (0·00)	0·24	10·98
MgO	2·22	8·35 (0·60)	10·07 (0·20)	0·00 (0·00)	0·00 (0·00)	0·00	0·18
CaO	5·26	11·89 (0·12)	0·00 (0·00)	7·93 (0·50)	55·13 (0·21)	0·04	0·00
Na_2O	3·37	1·06 (0·07)	0·10 (0·10)	6·93 (0·31)	0·00 (0·00)	0·00	0·00
K_2O	1·80	1·29 (0·12)	9·69 (0·10)	0·20 (0·04)	0·00 (0·00)	0·00	0·00
P_2O_5	0·19	0·00 (0·00)	0·00 (0·00)	0·00 (0·00)	41·97 (0·25)	0·00	0·00
Cl	n.d.	0·19 (0·11)	0·17 (0·02)	0·00 (0·00)	0·34 (0·08)	0·00	0·00
F	n.d.	0·18 (0·08)	0·27 (0·03)	0·00 (0·00)	2·42 (0·14)	0·00	0·00
Total	98·61*	98·86	95·07	99·97	100·29†	99·95‡	105·63§
Si		6·401	2·718	2·641	0·011	0·008	0·009
Ti		0·127	0·216	0·000	0·000	0·003	0·959
Al		2·082	1·365	1·136	0·000	0·038	0·008
Fe		2·648	1·411	0·000	0·000	3·911	0·821
Mn		0·061	0·011	0·000	0·000	0·010	0·225
Mg		1·893	1·172	0·000	0·000	0·000	0·006
Ca		1·938	0·000	0·379	1·588	0·002	0·000
Na		0·313	0·015	0·600	0·000	0·000	0·000
K		0·250	0·966	0·011	0·000	0·000	0·000
P		0·000	0·000	0·000	0·955	0·000	0·000
Cl		0·049	0·022	0·000	0·015	0·000	0·000
F		0·082	0·060	0·000	0·206	0·000	0·000
X_{Mg}		0·41	0·45				
X_{Al}		0·16	0·20				
X_{Ca}		0·77		0·38			

n, number of analyses; numbers in parentheses represent one standard deviation; n.d., not determined.
*Includes 0·72 wt % loss on ignition.
†Includes 0·88 (0·55) wt % SrO.
‡Includes 0·44 wt % V_2O_5 and 0·12 wt % Cr_2O_3.
§Includes 0·5 wt % V_2O_5.

were sealed by arc welding, with their bases cooled by water to prevent H_2O and CO_2 loss.

Starting fluid composition

The major purpose of the experiments was to investigate the dependence of mineral–fluid reactions and melting processes in the gneiss on the chloride content and KCl/NaCl ratio in the fluid at constant $H_2O/(H_2O + CO_2)$ ratio. Therefore, oxalic acid producing an equimolar H_2O–CO_2 ($X_{CO2} = 0·5$) fluid was used for the entire series of experiments. However, addition of given amounts of salt into such a fluid results in immiscibility with the formation of aqueous–carbonic and aqueous–salt fluids (Bowers & Helgeson, 1983; Duan *et al.*, 1995; Shmulovich & Graham, 2004; Aranovich *et al.*, 2010). To estimate the possibility of the presence of an immiscible fluid and the water activity of the starting fluid in each run, we used a model by Aranovich *et al.* (2010) for an H_2O–CO_2–NaCl fluid implemented in the PERPLEX software (Connolly, 2005) (version 6.6.8 for Windows with the database

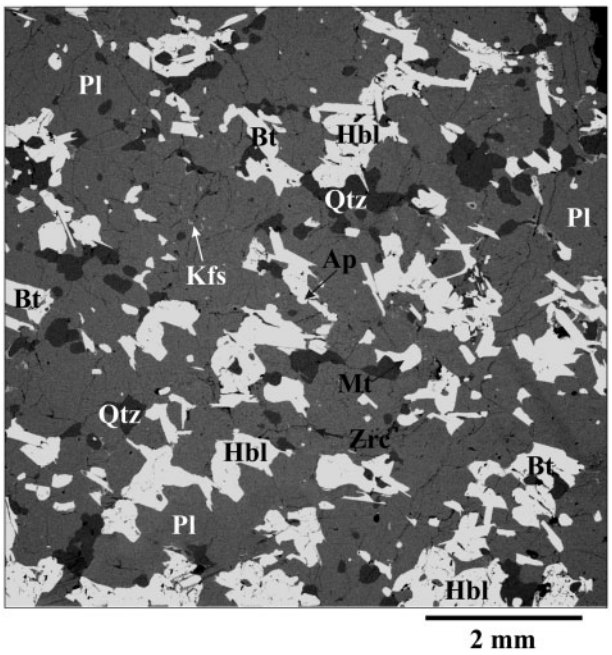

Fig. 1. Representative back-scattered electron image of the biotite–hornblende Sand River orthogneiss.

hp02ver.with.salt.dat; http://www.perplex.ethz.ch). The same model was used for H_2O–CO_2–KCl and H_2O–CO_2–(K, Na)Cl fluids, taking into account that a_{H2O} is very similar for H_2O–CO_2–NaCl, H_2O–CO_2–KCl and H_2O–CO_2–(K, Na)Cl fluids within the range of $X_{salt} = (KCl + NaCl)/(KCl + NaCl + H_2O + CO_2) < 0{\cdot}1$ (Aranovich & Newton, 1997). Calculations show that maximum solubility of chloride in the H_2O–CO_2 fluid at 750 and 800°C and 550 MPa is about 1·57 mol % ($X_{salt} = 0{\cdot}0157$). Two immiscible fluids coexist at salt concentrations above this value (Table 2). Table 2 shows that the experiments included both runs in which two fluids could coexist (italicized X_{salt} and a_{H2O} values) and runs in which only a homogeneous fluid was present. For example, the starting fluid in run N12 (Table 2) is the closest in composition to the miscibility gap. This fluid splits into 0·51 vol. % of an aqueous–salt portion with $X_{CO2} = 0{\cdot}123$, $X_{H2O} = 0{\cdot}645$, $X_{salt} = 0{\cdot}232$, and 99·49 vol. % of an aqueous–carbonic portion with $X_{CO2} = 0{\cdot}494$, $X_{H2O} = 0{\cdot}490$, $X_{salt} = 0{\cdot}016$. In the experiments with the H_2O–CO_2 fluid, the water activity was above 0·6 and decreased with increasing salt concentration (Table 2). The lowest water activity (0·37) corresponds to the fluid in run K7 containing 8·3 mol % of KCl (Table 2). Calculations show that such a fluid splits into 22·7 vol. % of an aqueous–salt portion with $X_{CO2} = 0{\cdot}104$, $X_{H2O} = 0{\cdot}630$, $X_{salt} = 0{\cdot}266$ and 77·3 vol. % of an aqueous–carbonic portion with $X_{CO2} = 0{\cdot}608$, $X_{H2O} = 0{\cdot}384$, $X_{salt} = 0{\cdot}008$.

Oxygen fugacity was not specifically buffered in the experiments. Compositions of coexisting ilmenite and Ti-bearing magnetite (glass contamination was corrected for by assuming no silica in the oxides) in the products of runs 24, K31, K32, and N11 used in the oxygen barometer of Andersen & Lindsley (1985) define log f_{O2} value between −12·7 and −12·0 for a run temperature of 800°C. Values between −12·7 and −12·2 for a temperature of 800°C were calculated from the equilibrium $6Fs + O_2 = 2Mt + 6Qtz$ for runs 24, K31, K32, K33, and N11 (Table 2) using the thermodynamic database of Berman & Aranovich (1996) implemented into the win TWQ software, version 2.32 (Berman, 2007). The calculated log f_{O2} values are about 1 log unit above the Ni–NiO buffer. We assume similar oxygen fugacity for other experiments. The log f_{O2} values are within the stability range of the H_2O–CO_2 fluid. Because the starting fluid was kept in excess with respect to the biotite–hornblende gneiss, no significant modifications in H_2O/CO_2 ratio during the experiments are expected. No significant absorption of Fe from both solids and melts by the Au capsules is expected at these redox conditions (e.g. Ratajeski & Sisson, 1999).

Experimental procedure

Experiments were carried out at a pressure of 550 MPa and temperatures of 750 and 800°C using an internally heated gas pressure vessel, which allowed seven capsules to be run at the same time. None of the experiments was reversed. The duration of all experiments was 10 days. Each capsule was weighed before and after each run. A specific hissing noise after pinching and the presence of bubbles in glasses indicate that the fluid has been preserved during isobaric quenching of the runs. After the runs, the samples were sealed in polyester mounts, cut along the vertical axis and polished with sandpaper and oil-based diamond pastes. Brittle samples were impregnated with epoxy using a vacuum impregnator before polishing.

Analytical procedures

Run products were studied by optical microscopy and scanning electron microscopy using a CamScan MV2300 (VEGA TS 5130MM) electron microscope equipped with an EDS INCA-Energy-350 and Tescan VEGA-II XMU microscope equipped with EDS INCA-Energy-450 and WDS Oxford INCA Wave 700 at the Institute of Experimental Mineralogy, Chernogolovka, Russia. Each sample was mapped to recognize areas extensively affected by fluid–mineral reactions and/or partial melting. Images of some run samples are provided in Fig. S1a–d in the Supplementary Material (supplementary material is available for downloading at http://www.petrology.oxfordjournals.org). Analyses of minerals were performed at 20 kV accelerating voltage with a beam current of 10 nA, a beam diameter of 3 μm and counting times of 100 s for all elements. A ZAF matrix correction was applied.

Table 2: Conditions and products of the runs on interaction of the Sand River biotite–amphibole gneiss with H_2O–CO_2, H_2O–CO_2–KCl, H_2O–CO_2–NaCl and H_2O–CO_2–(K, Na)Cl fluids at a pressure of 550 MPa

Run no.	T (°C)	m_g (g)	m_{oa} (g)	m_{ch} (g)	$m_g/(m_{oa}+m_{ch})$	X_{salt}	a_{H2O}	Products of experiments	Remarks
Fluid H_2O–CO_2									
1	750	0·0527	0·1743	0	0·30	0	0·625	Mt	1
24	800	0·0162	0·0806	0	0·20	0	0·613	Opx, Amph, Ti-Mt, Ilm, Pl, glass, (Mt)	2, 11
Fluid H_2O–CO_2–KCl									
K2	750	0·0471	0·1766	0·0036	0·26	0·007	0·595	Cpx, Kfs, Ti-Mt	3
K3	750	0·0456	0·1892	0·0049	0·23	0·009	0·587	Cpx, Kfs, (Bt, $CaCO_3$)	3, 4, 5
K4	750	0·0611	0·2076	0·0072	0·28	0·012	0·576	Cpx, Kfs, Ti-Mt, (Bt, glass)	3, 4
K5	750	0·0637	0·1881	0·0099	0·32	*0·019*	*0·549*	Cpx, Kfs, Ttn, (Grt)	3, 6
K6	750	0·0400	0·1878	0·0209	0·19	*0·039*	*0·483*	Cpx, Kfs, Ttn, (Bt)	3, 4
K7	750	0·047	0·1708	0·0427	0·22	*0·083*	*0·370*	Cpx, Kfs, Ilm, (Bt, KCl)	3, 4
K31	800	0·0412	0·1001	0·0007	0·40	0·002	0·605	Amph, Opx, Ilm, Ti-Mt, glass	2, 8
K32	800	0·0582	0·1000	0·0010	0·58	0·004	0·598	Amph, Opx, Ilm, Ti-Mt, glass	2, 8
K33	800	0·0483	0·0701	0·0010	0·68	0·005	0·594	Cpx, Opx, Pl, Ilm, glass	2
K8	800	0·0686	0·1487	0·0038	0·45	0·009	0·579	Cpx, Kfs, Ilm, glass, (Grt)	2, 6
K9	800	0·0437	0·1400	0·0100	0·29	*0·025*	*0·525*	Cpx, Kfs, Ilm, Ttn, glass	2
K10	800	0·0440	0·1360	0·0151	0·29	*0·039*	*0·484*	Cpx, Kfs, glass, (Ks, $CaCO_3$, Grt)	2, 5, 7
Fluid H_2O–CO_2–NaCl									
N20	750	0·0264	0·1413	0·0029	0·18	0·009	0·587	Amph, Cpx, Ti-Mt, glass	9
N19	750	0·0473	0·1194	0·0041	0·38	*0·016*	*0·560*	Amph, Cpx, Ti-Mt, glass	9
N18	750	0·0347	0·0674	0·0075	0·46	*0·049*	*0·453*	Amph, Cpx, Ti-Mt, glass	9
N11	800	0·0655	0·1510	0·0039	0·42	0·012	0·569	Amph, Opx, Ilm, Ti-Mt, glass	8
N12	800	0·0349	0·1427	0·0075	0·23	*0·023*	*0·532*	Cpx, glass	2
N13	800	0·0432	0·1428	0·0102	0·28	*0·032*	*0·504*	Cpx, Ab, Ttn, glass	10
Fluid H_2O–CO_2–(K, Na)Cl									
NK23	750	0·0243	0·1516	0·0031	0·16	0·008*	0·591	Amph, Cpx, Ilm, Pl, glass	9
NK22	750	0·0295	0·0831	0·0029	0·34	0·014*	0·568	Cpx, Pl, Kfs, Ilm, glass	2
NK27	800	0·0337	0·0798	0·0016	0·41	0·008*	0·583	Amph, Cpx, Ilm, glass	9
NK26	800	0·0571	0·0809	0·0028	0·68	0·014*	0·562	Cpx, Ilm, Pl, glass, (Mt)	2, 11
NK25	800	0·0252	0·0986	0·0110	0·23	*0·044**	*0·470*	Cpx, Kfs, Ilm, glass	2
NK28	800	0·0403	0·0910	0·0101	0·40	*0·041*†	*0·478*	Cpx, Ilm, Ttn, glass	2
NK29	800	0·0555	0·0807	0·0090	0·62	*0·046*‡	*0·464*	Cpx, Ilm, Kfs, glass	2

m_g, mass of a gneiss sample; m_{oa}, mass of oxalic acid; m_{ch}, mass of chloride; $m_g/(m_{oa}+m_{ch})$, starting rock/fluid ratio; X_{salt}, molar ratio $(KCl+NaCl)/(KCl+NaCl+H_2O+CO_2)$ in the starting fluid; water activity a_{H2O} in the starting fluid is calculated using equations for the H_2O–CO_2–NaCl fluid (Aranovich *et al.*, 2010); italicized values of X_{salt} and a_{H2O} mark heterogeneous fluids, where, according to the model by Aranovich *et al.* (2010), aqueous–carbonic and aqueous–salt portions coexist. Free fluid was present in all runs. Remarks: 1, no significant changes in phase assemblage; Mg-rich rims on original biotite crowded with magnetite; 2, glass zones with euhedral pyroxenes, Ti-magnetite and/or ilmenite around biotite; 3, Cpx + Kfs coronas between plagioclase and biotite; 4, newly formed biotite (Bt) is developed along cleavage in the original biotite or intergrown with Cpx and Kfs in the coronas; 5, small grains of $CaCO_3$ are present within the Cpx + Kfs intergrowths; 6, lace-like intergrowths of iron-rich garnet and K-feldspar are present within the Cpx + Kfs coronas; 7, garnet, kalsilite and calcite are locally present in zones in which plagioclase is extensively replaced by K-feldspar; 8, euhedral amphibole crystals armor biotite flakes or are present along with orthopyroxene in glass; 9, glass zones around biotite with euhedral clinopyroxene, amphibole, Ti-magnetite and/or ilmenite; 10, euhedral albite crystals along with clinopyroxene in the glass; 11, magnetite (Mt) forms rims on original pyrite grains, whereas ilmenite is present in the coronas around biotite.
*Weight ratio $KCl/(KCl+NaCl)=0{\cdot}5$.
†Weight ratio $KCl/(KCl+NaCl)=0{\cdot}25$.
‡Weight ratio $KCl/(KCl+NaCl)=0{\cdot}75$.

The following standards were used: SiO_2 for Si, albite for Na, microcline for K, wollastonite for Ca, pure titanium for Ti, corundum for Al, pure manganese for Mn, pure iron for Fe, periclase for Mg, BaF_2 for Ba, NaCl for Cl, CaF_2 for F and $LaPO_4$ for P.

To avoid loss of Na, glasses were analyzed by rastering the beam over areas of 180–20 μm^2. Some 20–30 analyses per sample were performed in different areas to confirm homogeneity of the glasses in the run samples (Table 3). Small traverses across glass films were analyzed to check for diffusional effects on the glass composition (e.g. Acosta-Vigil *et al.*, 2006). To support the results obtained by the rastering method, glasses were additionally analyzed using a Jeol JXA-8230 Superprobe equipped with WDS at the Laboratory of the Local Methods of Substance Analysis of the Petrology Department at the Moscow State University, Moscow, Russia, using analytical conditions recommended by Morgan & London (1996) for analysis of hydrous granitic glasses; that is, 20 kV acceleration voltage, 2 nA beam current, a beam diameter of 20 μm, and counting times of 40 s for Na and Al (analyzed first) and 20 s for other elements. Comparison of the analyses produced using the procedure recommended by Morgan & London (1996) with the analyses obtained by rastering the electron beam showed very good consistency for all major components. The Na_2O concentrations in glasses measured using the method of Morgan & London (1996) are always higher than the values obtained by the rastering method. However, the mean difference is below 0·4 wt % for most samples. It increases to 1–1·5 wt % for glasses containing above 6 wt % Na_2O. A similar difference is found for K_2O measured in the K_2O-rich glasses. Nevertheless, this difference does not influence the geochemical characteristics of the corresponding melts.

To qualitatively identify the presence of H_2O and CO_3^{2-} groups in the quenched melts, glasses from several run samples were analyzed by Raman spectroscopy using the JY Horiba XPloRa Jobin spectrometer (at the Department of Petrology, Moscow State University, Moscow, Russia) equipped with a polarized Olympus BX41 microscope. Spectra were obtained using a 532 nm laser within the range 200–4000 cm^{-1} for 40 s (two times 20 s each). The spectra were refined using LabSpec (version 5.78.24) software. Fitting of Raman spectra was performed with FITYK software (http://www.unipress.waw.pl/fityk/) assuming a Gaussian shape for the bands. Assignment of the Raman bands was carried out using web-based databanks (http://rruff.geo.arizona.edu/rruff/), as well as references cited below.

Approach to equilibrium

Reaction textures and melting zones are irregularly distributed in the samples (Supplementary Material, Fig. S1a–d). They reflect the distribution of biotite and hornblende grains in the original gneiss. Usually, both contacts of minerals are extensively affected by fluid–mineral reactions and/or partial melting and unaffected contacts are present in the samples. In some samples, reaction textures and melting zones are well developed only in the portions, which were closely in contact with a source of fluid, whereas they are weak or absent in the central portions of run samples (Supplementary Material, Fig. S1a and d). Other samples show a more or less regular distribution of reaction products (Supplementary Material, Fig. S1b and c). Relics of precursor minerals with newly formed phases and zoning of original crystalline phases in contact with the reaction textures are evidence for the absence of total equilibrium in the run products. However, a number of observations imply that long run durations (10 days), the presence of mobile aqueous–carbonic–salt fluids and volatile-rich melts facilitated an acceptable approach to local (on the scale of the reaction textures) equilibrium in the experiments, as follows.

(1) Despite the irregular distribution of reaction textures around biotite or amphibole (Supplementary Material, Fig, S1b–e), the appearance of newly formed phases does not notably depend on the precursor minerals. In the experiment K33 only (Table 2), orthopyroxene and clinopyroxene are unequally distributed in the reaction textures. In this case, orthopyroxene is a predominant phase in the reaction textures around biotite (although clinopyroxene is also present), whereas clinopyroxene is more abundant in the reaction textures around hornblende (although orthopyroxene is also present).
(2) Despite compositional variations and local zoning of crystalline phases, their compositions are nearly uniform throughout any given sample with the exception of relic phases inherited from the starting materials. The average composition of any specific phase does not obviously depend on its position in the run sample.
(3) Newly formed phases usually show equilibrium subhedral to euhedral shapes. Their chemical zoning is usually weak. The most zoned crystals of the newly formed phases are produced in the experiments at 750°C with fluids with high salt concentrations.
(4) Average compositions of crystalline phases vary regularly with both temperature and fluid composition (see below).
(5) Glasses in all run samples are homogeneous in texture. Visible quenched crystals of silicate and chloride phases are rare in the glasses. Compositions of quenched melts are uniform, at least with respect to major components (Table 3), throughout the volume of the experimental charges and vary regularly with the composition of the starting fluid (see below). Melt forms interconnected veins and pools even at

Table 3: Mean oxide (wt %), normalized, normative compositions and compositional indices of quenched melts

Fluid:	H_2O–CO_2	H_2O–CO_2–KCl				
Run no.:	24	K10	K8	K33	K32	K31
T (°C):	800	800	800	800	800	800
X_{salt}:*	0	0·039	0·009	0·005	0·004	0·002
a_{H2O}:*	0·613	0·484	0·579	0·594	0·598	0·605
n:	22	20	7	25	26	31
SiO_2	69·15 (1·09)	70·38 (0·91)	71·66 (1·17)	67·88 (1·30)	70·06 (2·10)	69·02 (1·36)
TiO_2	0·17 (0·10)	0·47 (0·21)	0·21 (0·10)	0·20 (0·08)	0·14 (0·13)	0·30 (0·10)
Al_2O_3	13·15 (0·24)	6·18 (0·27)	10·00 (0·12)	12·50 (0·43)	13·92 (0·33)	13·07 (0·57)
Cr_2O_3	0·05 (0·06)	0·02 (0·02)	0·05 (0·03)	0·03 (0·03)	0·04 (0·05)	0·04 (0·05)
FeO	1·84 (0·10)	3·94 (0·69)	1·62 (0·24)	1·96 (0·17)	2·13 (0·22)	2·06 (0·18)
MnO	0·06 (0·04)	0·08 (0·07)	0·05 (0·06)	0·05 (0·06)	0·05 (0·06)	0·08 (0·07)
MgO	0·30 (0·07)	0·44 (0·10)	0·06 (0·07)	0·32 (0·07)	0·37 (0·09)	0·34 (0·07)
CaO	1·98 (0·11)	0·65 (0·12)	0·41 (0·24)	1·93 (0·21)	2·28 (0·17)	2·11 (0·19)
Na_2O	2·40 (0·33)	1·29 (0·10)	1·21 (0·13)	2·48 (0·16)	2·64 (0·23)	2·50 (0·32)
K_2O	3·97 (0·20)	11·50 (0·44)	7·48 (0·65)	4·47 (0·13)	4·61 (0·15)	4·26 (0·21)
P_2O_5	0·01 (0·01)	0·07 (0·06)	0·05 (0·06)	0·07 (0·06)	n.d.	0·03 (0·04)
SO_3	0·03 (0·05)	0·04 (0·03)	0·19 (0·07)	0·09 (0·08)	n.d.	0·06 (0·06)
Cl	0·02 (0·02)	0·47 (0·09)	0·25 (0·07)	0·27 (0·05)	0·29 (0·04)	0·24 (0·05)
F	0·45 (0·36)	0·88 (0·34)	1·15 (0·39)	0·34 (0·20)	0·34 (0·34)	0·32 (0·29)
Total	93·59	96·43	94·39	92·61	96·86	94·43
Normalized to 100 %						
SiO_2	73·80	72·94	75·82	73·21	72·25	73·00
TiO_2	0·18	0·49	0·22	0·22	0·14	0·31
Al_2O_3	14·03	6·41	10·59	13·48	14·35	13·83
Cr_2O_3	0·05	0·02	0·05	0·03	0·04	0·04
FeO	1·97	4·08	1·71	2·12	2·19	2·18
MnO	0·06	0·08	0·05	0·06	0·05	0·08
MgO	0·32	0·46	0·06	0·34	0·38	0·36
CaO	2·11	0·67	0·44	2·08	2·35	2·23
Na_2O	2·56	1·34	1·28	2·68	2·72	2·64
K_2O	4·24	11·92	7·91	4·82	4·75	4·50
P_2O_5	0·01	0·08	0·05	0·08	n.d.	0·03
SO_3	0·03	0·05	0·20	0·09	n.d.	0·07
Cl	0·02	0·49	0·26	0·29	0·30	0·26
F	0·48	0·91	1·22	0·37	0·35	0·34
CIPW norms						
Qtz	35·52	40·75	38·06	34·61	33·93	35·38
Cor	2·59	0·00	0·87	2·03	2·19	2·20
Or	23·46	33·74	44·20	26·42	27·24	25·18
Pl	26·48	0·00	5·30	23·08	26·87	25·16
Ne	0·00	0·00	0·00	0·00	0·00	0·00
Di	0·00	0·00	0·00	0·00	0·00	0·00
Hyp	3·90	7·70	2·87	4·16	4·69	4·28
Ol	0·00	0·00	0·00	0·00	0·00	0·00
Ilm	0·32	0·89	0·40	0·38	0·27	0·57
Ap	0·02	0·17	0·12	0·17	0·00	0·07
Hal	0·04	0·88	0·47	0·51	0·54	0·45
Fl	1·11	2·16	2·84	0·83	0·84	0·79
Na_2SO_4	0·00	0·07	0·34	0·16	0·00	0·11
K_2SiO_3	0·00	9·48	0·00	0·00	0·00	0·00
Na_2SiO_3	0·00	0·86	0·00	0·00	0·00	0·00
Indices						
ASI	1·110	0·393	0·923	1·005	1·033	1·042
A/NK	1·594	0·424	0·993	1·400	1·492	1·501
MALI	4·690	12·590	8·750	5·420	5·120	4·910
Fe#	0·860	0·899	0·966	0·862	0·852	0·858

(continued)

Table 3: Continued

Fluid:	H_2O–CO_2–NaCl					
Run no.:	N20	N19	N18	N11	N12	N13
T (°C):	750	750	750	800	800	800
X_{salt}:*	0·009	0·016	0·049	0·012	0·023	0·032
a_{H2O}:*	0·587	0·560	0·453	0·569	0·532	0·504
n:	23	20	22	21	20	22
SiO_2	60·85 (0·84)	57·84 (0·56)	56·16 (0·47)	71·68 (0·52)	54·63 (0·40)	54·49 (0·86)
TiO_2	0·48 (0·12)	0·55 (0·10)	0·73 (0·11)	0·18 (0·09)	0·26 (0·10)	0·26 (0·12)
Al_2O_3	16·00 (0·24)	16·73 (0·26)	16·25 (0·31)	12·11 (0·28)	20·24 (0·58)	18·86 (1·01)
Cr_2O_3	0·05 (0·04)	0·02 (0·03)	0·03 (0·04)	0·04 (0·04)	0·05 (0·06)	0·06 (0·06)
FeO	3·27 (0·24)	3·94 (0·13)	4·62 (0·17)	1·49 (0·15)	1·95 (0·21)	2·04 (0·23)
MnO	0·07 (0·05)	0·11 (0·06)	0·11 (0·06)	0·03 (0·04)	0·05 (0·05)	0·08 (0·06)
MgO	0·68 (0·13)	1·08 (0·07)	1·03 (0·09)	0·19 (0·08)	0·19 (0·06)	0·19 (0·06)
CaO	3·11 (0·20)	4·24 (0·11)	2·74 (0·08)	0·56 (0·07)	0·77 (0·10)	0·94 (0·09)
Na_2O	5·80 (0·52)	7·03 (0·19)	8·60 (0·31)	4·12 (0·51)	12·56 (0·31)	12·93 (0·54)
K_2O	1·97 (0·09)	1·65 (0·07)	1·57 (0·09)	3·21 (0·43)	1·95 (0·24)	1·00 (0·09)
P_2O_5	0·10 (0·08)	0·13 (0·07)	0·26 (0·11)	0·06 (0·06)	0·11 (0·09)	0·11 (0·10)
SO_3	0·03 (0·04)	0·07 (0·08)	0·23 (0·32)	0·05 (0·05)	0·06 (0·06)	0·05 (0·07)
Cl	1·19 (0·07)	1·19 (0·08)	1·63 (0·06)	0·47 (0·07)	0·75 (0·06)	0·83 (0·21)
F	0·33 (0·27)	1·30 (0·27)	0·30 (0·33)	0·37 (0·19)	0·43 (0·27)	0·17 (0·20)
Total	93·88	95·87	94·07	94·59	94·00	92·00
Normalized to 100 %						
SiO_2	64·75	60·24	59·59	75·67	58·04	59·23
TiO_2	0·52	0·57	0·78	0·19	0·28	0·28
Al_2O_3	17·02	17·43	17·25	12·79	21·50	20·50
Cr_2O_3	0·05	0·02	0·04	0·05	0·05	0·06
FeO	3·41	4·11	4·90	1·57	2·07	2·21
MnO	0·08	0·11	0·12	0·03	0·05	0·09
MgO	0·72	1·13	1·09	0·20	0·20	0·20
CaO	3·31	4·41	2·91	0·59	0·81	1·03
Na_2O	6·17	7·32	9·13	4·35	13·35	14·05
K_2O	2·10	1·72	1·66	3·39	2·07	1·08
P_2O_5	0·11	0·13	0·28	0·07	0·12	0·11
SO_3	0·03	0·07	0·02	0·06	0·06	0·06
Cl	1·27	1·24	1·73	0·50	0·80	0·90
F	0·35	1·35	0·32	0·39	0·46	0·19
CIPW norms						
Qtz	23·00	13·83	8·53	39·02	0·00	0·00
Cor	3·23	2·95	1·77	3·27	0·00	0·00
Or	11·64	9·75	9·28	18·97	11·52	6·38
Pl	43·70	52·18	57·02	27·58	53·98	64·76
Ne	0·00	0·00	0·00	0·00	21·28	18·81
Di	0·00	0·00	0·00	0·00	0·02	2·69
Hyp	7·04	9·20	10·05	2·97	0·00	0·00
Ol	0·00	0·00	0·00	0·00	2·83	2·18
Ilm	0·91	1·04	1·39	0·34	0·49	0·53
Ap	0·24	0·31	0·63	0·14	0·26	0·26
Hal	2·23	2·23	3·05	0·88	1·41	1·69
Fl	0·79	3·19	0·69	0·90	1·04	0·45
Na_2SO_4	0·05	0·12	0·41	0·09	0·11	0·11
K_2SiO_3	0·00	0·00	0·00	0·00	0·00	0·00
Na_2SiO_3	0·00	0·00	0·00	0·00	0·36	1·35
Indices						
ASI	0·923	0·795	0·780	1·075	0·837	0·784
A/NK	1·370	1·254	1·026	1·181	0·888	0·844
MALI	4·960	4·630	7·880	7·150	14·610	14·100
Fe#	0·826	0·784	0·818	0·887	0·912	0·917

(continued)

Table 3: Continued

Fluid:	H_2O–CO_2–(K, Na)Cl					
Run no.:	NK23	NK22	NK27	NK26	NK28	NK29
T (°C):	750	750	800	800	800	800
X_{salt}:*	0·008	0·014	0·008	0·014	0·041	0·046
a_{H2O}:*	0·591	0·568	0·583	0·562	0·478	0·464
n:	23	23	22	27	21	21
SiO_2	55·79 (0·69)	67·80 (0·92)	70·89 (0·75)	67·73 (2·31)	67·80 (1·21)	72·91 (1·41)
TiO_2	0·38 (0·11)	0·21 (0·11)	0·16 (0·10)	0·22 (0·12)	0·35 (0·15)	0·25 (0·09)
Al_2O_3	18·09 (0·19)	14·24 (0·41)	12·90 (0·30)	12·98 (0·58)	14·41 (0·52)	11·24 (0·53)
Cr_2O_3	0·04 (0·04)	0·04 (0·05)	0·06 (0·04)	0·04 (0·04)	0·04 (0·04)	0·02 (0·03)
FeO	3·15 (0·17)	1·38 (0·14)	1·55 (0·18)	1·67 (0·19)	1·49 (0·26)	2·28 (0·45)
MnO	0·07 (0·06)	0·06 (0·06)	0·08 (0·08)	0·05 (0·06)	0·05 (0·04)	0·04 (0·04)
MgO	1·21 (0·13)	0·20 (0·07)	0·25 (0·09)	0·20 (0·06)	0·21 (0·07)	0·13 (0·06)
CaO	5·13 (0·12)	0·99 (0·10)	1·62 (0·10)	1·32 (0·17)	0·62 (0·08)	0·35 (0·10)
Na_2O	4·92 (0·24)	4·26 (0·16)	3·40 (0·19)	3·53 (0·26)	6·32 (0·29)	2·26 (0·21)
K_2O	3·78 (0·08)	5·81 (0·12)	4·06 (0·13)	4·54 (0·10)	3·89 (0·09)	7·99 (0·37)
P_2O_5	0·19 (0·08)	0·07 (0·07)	0·04 (0·04)	0·06 (0·06)	0·05 (0·05)	0·04 (0·03)
SO_3	0·02 (0·03)	n.d.	n.d.	n.d.	n.d.	n.d.
Cl	1·09 (0·06)	0·55 (0·05)	0·34 (0·06)	0·33 (0·11)	0·64 (0·07)	0·39 (0·09)
F	0·23 (0·21)	0·50 (0·26)	0·18 (0·18)	0·34 (0·20)	0·37 (0·30)	0·33 (0·23)
Total	94·09	96·12	95·52	93·11	96·25	98·28
Normalized to 100 %						
SiO_2	59·19	70·48	74·12	72·75	70·38	74·08
TiO_2	0·40	0·22	0·16	0·23	0·36	0·26
Al_2O_3	19·19	14·80	13·49	13·94	14·96	11·42
Cr_2O_3	0·04	0·04	0·06	0·04	0·05	0·30
FeO	3·35	1·44	1·62	1·79	1·55	2·32
MnO	0·07	0·06	0·09	0·06	0·06	0·04
MgO	1·28	0·21	0·26	0·22	0·22	0·14
CaO	5·44	1·02	1·70	1·42	0·64	0·36
Na_2O	5·22	4·43	3·55	3·79	6·56	2·30
K_2O	4·02	6·04	4·24	4·87	4·03	8·12
P_2O_5	0·21	0·07	0·04	0·06	0·06	0·04
SO_3	0·02	n.d.	n.d.	n.d.	n.d.	n.d.
Cl	1·15	0·57	0·35	0·36	0·66	0·40
F	0·24	0·52	0·19	0·37	0·38	0·34
CIPW norms						
Qtz	9·88	24·67	36·32	30·01	22·18	31·81
Cor	0·76	2·22	1·59	1·85	1·69	0·00
Or	22·34	34·33	25·12	26·83	23·87	48·10
Pl	48·03	28·75	31·61	28·69	45·78	13·52
Ne	0·00	0·00	0·00	0·00	0·00	0·00
Di	0·00	0·00	0·00	0·00	0·00	0·00
Hyp	8·30	2·80	3·49	3·29	2·89	4·25
Ol	0·00	0·00	0·00	0·00	0·00	0·00
Ilm	0·72	0·40	0·32	0·42	0·68	0·47
Ap	0·46	0·17	0·10	0·14	0·12	0·10
Hal	2·04	1·03	0·67	0·62	1·26	0·75
Fl	0·53	1·22	0·46	0·83	0·93	0·83
Na_2SO_4	0·04	0·00	0·00	0·00	0·00	0·00
K_2SiO_3	0·00	0·00	0·00	0·00	0·00	0·00
Na_2SiO_3	0·00	0·00	0·00	0·00	0·00	0·01
Indices						
ASI	0·841	0·944	0·998	0·989	0·917	0·863
A/NK	1·483	1·070	1·293	1·212	0·987	0·908
MALI	3·800	9·450	6·090	7·240	9·950	10·060
Fe#	0·724	0·873	0·862	0·891	0·876	0·943

n, number of analyses. Numbers in parentheses represent one standard deviation.
*See Table 2.

low melt fractions. This result is consistent with the observations of Acosta-Vigil *et al.* (2006) on the melting of a solid core of leucogranite in the presence of an aqueous fluid at 690, 740 and 800°C and 200 MPa. However, those researchers found very wide variations in melt composition (for example, SiO_2 variations within a range of 8–10 wt %) in the runs well above the solidus and concluded that partial melting at these conditions produced heterogeneous liquids with compositions determined by diffusion in the melt at contacts with neighboring crystalline phases. Microprobe traverses across melt films in the products of our experiments also showed slight gradients in concentration, mostly of SiO_2 and Al_2O_3. However, these are minor. In general, in contrast to the observations of Acosta-Vigil *et al.* (2006), melt compositions in our experiments show much smaller variations (Table 3). The SiO_2 content in the melts produced at 800°C varies within 4–5 wt %, whereas variations of Al_2O_3 do not exceed 1·5–2 wt % at almost uniform concentrations of K_2O, Na_2O, CaO and FeO (Table 3). Variations in the melt composition at 750°C are even smaller (Table 3).

(6) All charges are saturated with an H–O–C fluid phase, the presence of which in the run products is marked by the occurrence of bubble voids in glasses.

PHASE ASSEMBLAGES AND RELATIONS IN THE RUN PRODUCTS

Experiments without fluid and with equimolar H_2O–CO_2 fluid

Heating of the biotite–hornblende gneiss at both 750 and 800°C without fluid produced no visible changes in the phase assemblage. Interaction with an equimolar H_2O–CO_2 fluid at 750°C only caused formation of narrow Mg-rich outer zones on biotite flakes (see below) crowded with minute inclusions of magnetite. The sample that interacted with equimolar H_2O–CO_2 fluid at 800°C shows distinct glass areas at the contacts of plagioclase and quartz with biotite and hornblende (Fig. 2). The glass includes euhedral orthopyroxene, Ti-magnetite, ilmenite, and, locally, plagioclase crystallites (Fig. 2). No clinopyroxene was identified in the reaction textures, even in the vicinity of hornblende. Original hornblende (Hbl-1 in Fig. 2) shows re-equilibration zones containing rounded inclusions of Ti-magnetite and lamellae of ilmenite (Hbl-2 in Fig. 2). Relics of biotite were found in these zones, suggesting that formation of Hbl-2 involved decomposition of biotite. Voids formed by fluid bubbles (see inset in Fig. 2) contain quartz, $CaCO_3$ and rare $MgCO_3$ produced during quenching of the fluid.

Experiments with H_2O–CO_2–KCl fluid

Addition of KCl to the equimolar H_2O–CO_2 fluid at 750°C resulted in the formation of reaction textures consisting of clinopyroxene and K-feldspar around biotite and hornblende at the contacts with plagioclase. No partial melting was detected. K-feldspar microveins are extensively developed in plagioclase along cracks and in contact with quartz. The abundance of these clinopyroxene–K-feldspar textures increases with increase in the KCl content in the fluid. Locally, the reaction textures in the peripheral portions of the samples are developed very extensively and consist of large euhedral crystals of clinopyroxene in a K-feldspar matrix (Fig. 3a). In addition to clinopyroxene and K-feldspar, reaction textures in samples K3, K4, K6 and K7 (Table 2) locally contain new biotite (Fig. 3b). Usually it is developed after hornblende, but it also appears along cleavages in the original biotite. Ca-rich garnet is found in the clinopyroxene–K-feldspar reaction textures in run sample K5. In sample K4, clinopyroxene–K-feldspar reaction textures contain minute $CaCO_3$ crystals, whereas in sample K7, they involve tiny crystallites of KCl. The reaction textures are accompanied by Ti-bearing phases. Ti-magnetite is characteristic of reaction textures formed at $X_{KCl} < 0{\cdot}015$ in the fluid, whereas ilmenite and titanite appear in reaction textures produced by fluids richer in KCl (Table 2).

Melting is a characteristic process during interaction of the gneiss with the H_2O–CO_2–KCl fluid at 800°C At $X_{KCl} = 0{\cdot}002$ and 0·004 (runs K31 and K32; Table 2), pargasite–edenite amphibole forms along with orthopyroxene as a product of biotite decomposition (Fig. 4a). Amphibole grains armor biotite flakes and appear along with orthopyroxene as euhedral crystals in glass. Both Ti-magnetite and ilmenite are present in the orthopyroxene–amphibole–melt reaction textures in these run samples (Fig. 4a). At $X_{KCl} = 0{\cdot}005$ (run K33; Table 1), amphibole and Ti-magnetite disappear from the reaction assemblage, and orthopyroxene coexists with clinopyroxene and ilmenite (Fig. 4b). Clinopyroxene prevails over orthopyroxene in these reaction textures. Further increase of the KCl content in the fluid results in the disappearance of orthopyroxene. Glass zones around biotite contain numerous euhedral crystallites of clinopyroxene, tablets of K-feldspar, and small pores (Fig. 4c). Aggregates of euhedral K-feldspar crystallites outline biotite and plagioclase grains. Original plagioclase is usually intensively replaced by K-feldspar in contact with the clinopyroxene–K-feldspar–glass textures (Fig. 4c). In sample K10 (Table 2), Ca-rich garnet, kalsilite, and calcite are locally attached to zones in which plagioclase is extensively replaced by K-feldspar.

Experiments with H_2O–CO_2–NaCl fluid

At both 750 and 800°C run samples produced by interaction of the gneiss with H_2O–CO_2–NaCl fluids contain

glass (Fig. 5a and b). The characteristic newly formed crystalline phases produced at 750°C are amphibole, clinopyroxene, and Ti-magnetite (Fig. 5a). At 800°C, sodic amphibole was identified only in run N11, produced at $X_{NaCl} = 0{\cdot}012$ (Table 2). In this run, it coexists with orthopyroxene, ilmenite and melt in reaction textures around biotite, plagioclase and quartz (Fig. 5b). Increase of the NaCl content in the fluid resulted in disappearance of both amphibole and orthopyroxene. Clinopyroxene is stable with silicate melt only at $X_{NaCl} = 0{\cdot}023$ (run N12, Table 2). At higher NaCl content in the starting fluid large crystals of albite join clinopyroxene (run N13, Table 2). Their euhedral shapes suggest that this phase crystallized along with clinopyroxene from the melt, rather than being formed by replacement of plagioclase (Fig. 5c). In a fluid bubble in run N13, $CaCO_3$ is associated with Al_2O_3.

Experiments with H_2O–CO_2–(K, Na)Cl fluid

Phase assemblages formed after gneiss in equilibrium with the mixed H_2O–CO_2–(K, Na)Cl fluid, to some extent, combine the textural and compositional features of the phase assemblages formed respectively in equilibrium with H_2O–CO_2–KCl and H_2O–CO_2–NaCl fluids. The Cpx–Amph–Ilm–melt assemblage appears at both 750 and 800°C at $X_{salt} = 0{\cdot}008$ in the starting fluid (Table 2). At 750°C, newly formed plagioclase joins this assemblage. No amphibole was found in the run products at higher salt content of the fluid (Table 2).

Compositions of crystalline phases in the run products

Micas in the run samples are mostly represented by relict biotites from the starting gneiss (Table 1). Their core compositions are similar to the average composition of original biotite (Supplementary Material, Table S1). However, the compositions of biotite rims contacting the reaction textures differ from the core compositions (Supplementary Material, Table S1). Usually, the Mg-number of biotites increases by 4–8 mol % in contact with the reaction textures. The largest increase of Mg-number (14–20 mol %) is observed in biotite from run 1, the rims of which are crowded with magnetite micro-inclusions (Supplementary Material, Table S1). Despite variations in Mg-number, concentrations of TiO_2 and Al_2O_3 in biotite rims in contact with the reaction textures are similar to the concentrations of these components in the original biotite (Supplementary Material, Table S1).

Newly formed biotite flakes are locally present in the clinopyroxene–K-feldspar intergrowths after biotite and amphibole produced in runs with H_2O–CO_2–KCl fluids at 750°C (runs K3, K4, K6, K7; Table 2). This biotite has a variable Al_2O_3 content that is much lower in comparison with the original biotite. For example, newly formed biotites from run K3 contain just 4·5–6·5 wt % Al_2O_3 (Supplementary Material, Table S1). Deficiency of Al in this biotite is partially compensated by Ti (up to 5 wt % TiO_2) as well as by Fe^{3+}. However, this deficiency at a K content close to 1 a.p.f.u. implies the presence of the montdorite component, $K(Mg, Fe)_{2\cdot5}Si_4O_{10}(OH)_2$ in the biotite solid solution. Mg-numbers of the biotites included in the clinopyroxene–K-feldspar intergrowth are higher (above 50 mol %) than the Mg-number of the original biotite (except micas in the sample K3). Newly formed biotites in the reaction textures of sample K7 produced at the highest X_{KCl} content of the fluid contain 0·65–0·75 wt % Cl (Supplementary Material, Table S1).

Amphiboles in the run products can clearly be subdivided into relic hornblende and newly formed hornblende. Relic hornblendes are distinguishable by their composition, which is close to the mean composition of hornblendes from the precursor gneiss (Table 1). The average composition of relic amphibole is located within the Prg–Ed–Ts–Tr quadrangle of the Al/(Al + Si + Mg + Fe + Ti)–Ca/(Ca + Na + K) diagram (Fig. 6a). They have $X_{Mg} = 0{\cdot}37$–$0{\cdot}44$, K/(K + Na) ratios close to 0·45 and a total K + Na content of about 0·6 a.p.f.u. (Supplementary Material, Table S2; Fig. 6b). Chemical variations of original hornblendes in contact with reaction textures are insignificant (Supplementary Material, Table S2).

Amphiboles formed in the experiments always occur as euhedral crystals in glass or as overgrowths with clear crystallographic facets on original hornblende or biotite. The Mg-number of the newly formed amphibole is always higher than the X_{Mg} of the original hornblende (Supplementary Material, Table S2). Therefore, it always appears darker in BSE images compared with the original hornblende (e.g. Fig. 2). These amphiboles usually contain inclusions of Ti-bearing phases (Figs 2 and 5a, b). Mg-numbers of amphiboles produced in the experiments at 800°C (0·51–0·54) are lower than Mg-numbers of amphiboles at 750°C (0·65–0·75) (Supplementary Material, Table S1). The Ca/(Ca + Na + K) ratios of newly formed amphiboles are lower than this ratio in the original hornblende (Fig. 6a). For amphibole from run 24 that equilibrated with the H_2O–CO_2 fluid (Fig. 2), this ratio varies from 0·72 to 0·75 (in contrast to 0·76–0·78 in the initial hornblende). At similar K + Na content this amphibole also has distinctly lower K/(K + Na) ratios (Fig. 6b). A higher total K + Na content (Fig. 6b) characterizes amphiboles formed in equilibrium with chloride-bearing fluids. Data points for amphiboles in runs with the H_2O–CO_2–KCl fluid (runs K31 and K32; Table 2) are slightly displaced toward the Prg–Ed tie-line (Fig. 6a). Their K/(K + Na) ratio is lower (0·25–0·35) in comparison with the original hornblende. A tendency for a decrease of the Ca/(Ca + Na + K) ratio continues for the amphiboles produced in the (K, Na)Cl-bearing runs. Their compositions lie closer to the Prg–Ed tie-line (Fig. 6a), and the

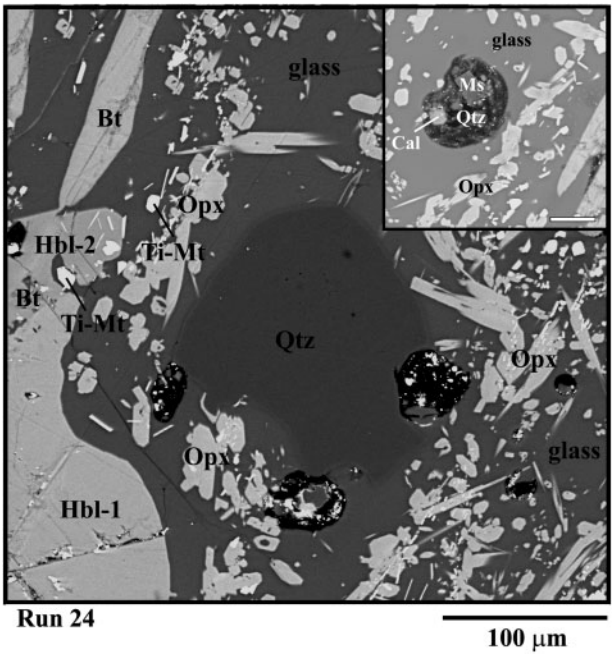

Fig. 2. Orthopyroxene, Ti-magnetite, ilmenite, and melt (glass) formed after biotite and hornblende in run 24 that interacted with a salt-free equimolar H_2O–CO_2 fluid at 800°C. Hbl-1, original hornblende; Hbl-2, re-equilibrated zone of hornblende with higher Mg-number and containing inclusions of Ti-magnetite (isometric grains) and ilmenite (acicular crystallites). Dark rounded patches are voids formed by fluid bubbles. The inset image shows a detailed view of a large void containing quartz, calcite (Cal), and magnesite (Ms) formed by fluid quenching. The scale bar in the inset image represents 20 μm.

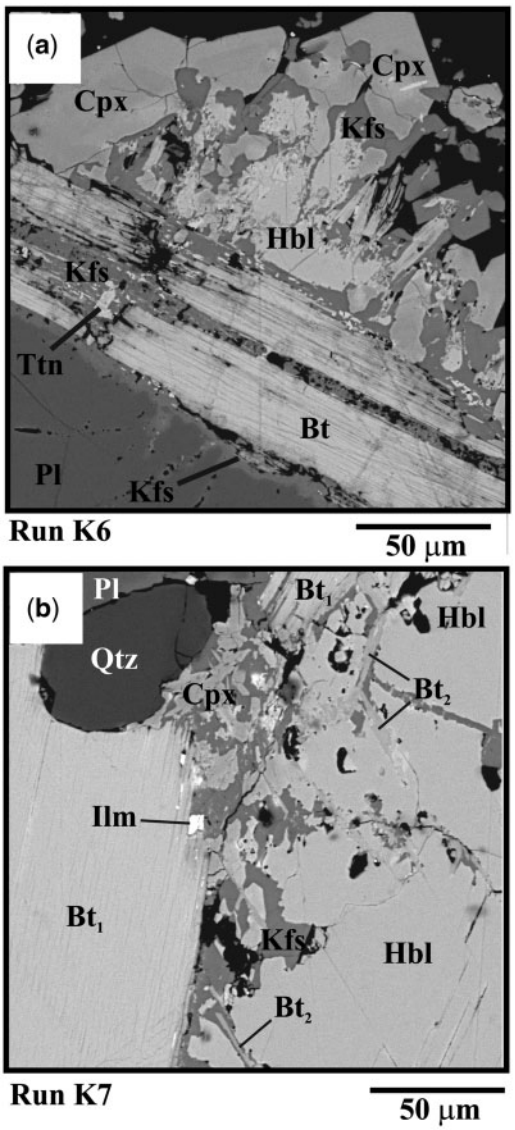

Fig. 3. Phase assemblages produced by interaction of the biotite–amphibole gneiss with an H_2O–CO_2–KCl fluid at 750°C. (a) Large euhedral crystals of clinopyroxene and K-feldspar formed after biotite and hornblende as a result of the gneiss interacting with the fluid at $X_{KCl} = 0{\cdot}039$ (run K6, Table 2); titanite appears as minute crystals in the products of biotite decomposition. (b) Newly formed biotite (Bt_2) associated with clinopyroxene–K-feldspar intergrowths developed along the contacts of hornblende and original biotite (Bt_1) in run K7 at $X_{KCl} = 0{\cdot}083$ (Table 2).

K/(K + Na) ratio decreases to 0·25–0·30 (Fig. 6b). Low K/(K + Na) ratios reflect preferential partitioning of Na into amphibole with respect to K, which remains in the fluid or in the silicate melt. Compositions of amphiboles in runs with the H_2O–CO_2–NaCl fluid are displaced further beyond the Prg–Ed tie-line toward barroisite and winchite compositions (Fig. 6a). All amphiboles crystallizing in the presence of the H_2O–CO_2–NaCl fluid are characterized by K/(K + Na) ratios below 0·15 and total K + Na content above 0·7 a.p.f.u. (up to 1·2) (Fig. 6b).

Despite variations in alkali content, all amphiboles show similar Al/(Al + Si + Mg + Fe + Mn + Ti) ratios near 0·15, comparable with the original hornblende (Fig. 6a). Only amphibole coexisting with orthopyroxene in run N11 (Fig. 5b) shows lower alumina content; that is, enriched in the richterite component. The K/(K + Na) ratio of the newly formed amphiboles reflects the KCl/NaCl ratio in the fluids, whereas their total K + Na content depends on the X_{salt} of the starting fluid; that is, reflects the bulk chloride content of the fluid. For example, hornblende in run N18 that reacted with fluid $X_{NaCl} = 0{\cdot}049$ at 750°C contains more than 1·0 a.p.f.u of K + Na per 23 O, whereas amphibole in run N20 at the same temperature, but at $X_{NaCl} = 0{\cdot}009$, contains less than 1·0 a.p.f.u of K + Na per 23 O.

In contrast to the initial hornblende (Table 1), the TiO_2 content in the experimentally produced hornblendes varies from 1·4 to above 3·0 wt %. The most Ti-rich hornblendes (up to 3·5 wt % TiO_2) are formed in equilibrium with NaCl-rich fluids. Elevated concentrations of TiO_2 in

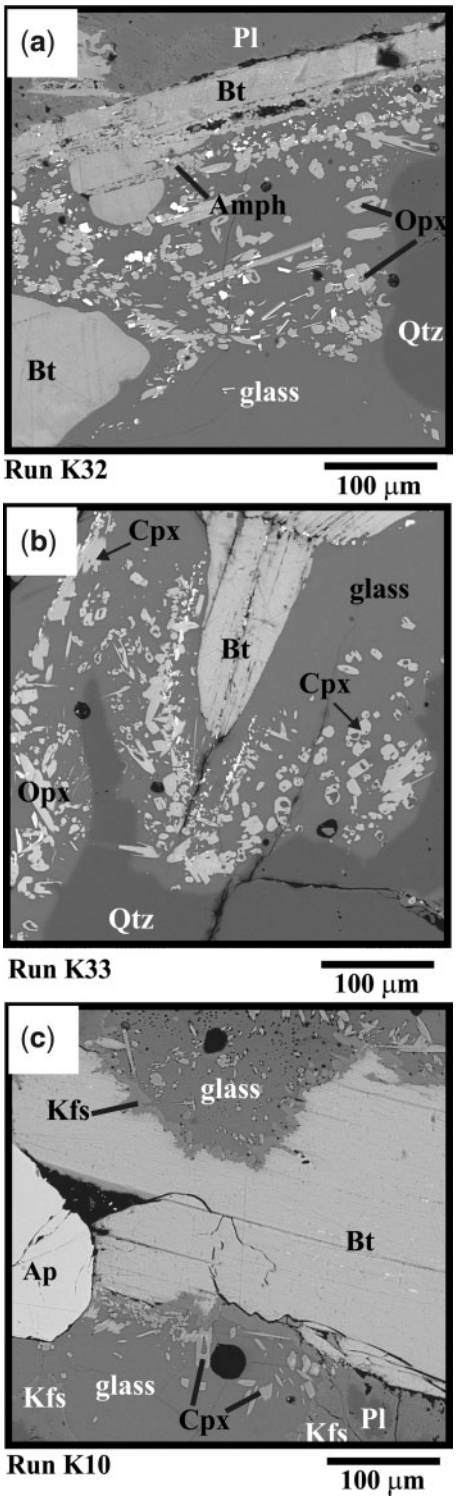

Fig. 4. Phase assemblages produced by interaction of the biotite–amphibole gneiss with an H_2O–CO_2–KCl fluid at 800°C. (a) Orthopyroxene, pargasite–edenite amphibole, Ti-magnetite, and ilmenite coexisting with a melt (glass) in the run sample that interacted with fluid at $X_{KCl} = 0{\cdot}004$ (run K32, Table 2); bright isometric grains are Ti-magnetite, whereas elongated platelets are ilmenite. (b) Two pyroxenes and ilmenite coexisting with a melt in the run sample that interacted with fluid at $X_{KCl} = 0{\cdot}005$ (run K33, Table 2); bright elongated platelets are ilmenite. (c) Clinopyroxene and K-feldspar coexisting with a melt in the run sample that interacted with fluid at $X_{KCl} = 0{\cdot}039$ (run K10, Table 2); extensive metasomatic replacement of plagioclase by K-feldspar is clearly seen in the lower right corner of the image.

the newly formed amphiboles and their coexistence with Ti-magnetite or/and ilmenite are an indication that they were formed via decomposition of the original Ti-rich biotite.

The Cl content of the newly formed amphiboles ranges from 0·15 to 0·35 wt % (Supplementary Material, Table S2) without clear dependence on temperature and starting fluid composition. These values are generally higher than the Cl content of initial amphiboles (Table 1). The average $K_{Cl}^{Amph/melt}$ values at 800°C vary from about 1 for amphiboles coexisting with K-rich melts down to 0·12–0·18 for amphiboles coexisting with Na-rich melts.

Appearance of pyroxenes in the run samples is exclusively related to reactions of the gneiss with the H_2O–CO_2–salt fluids. Clinopyroxenes show wide, but regular, variations of X_{Mg} with temperature and X_{salt} of the fluids (Supplementary Material, Table S3). Clinopyroxenes produced at 750°C have lower X_{Mg} compared with clinopyroxenes produced at 800°C (Supplementary Material, Table S3). Their Na/Al ratios are close to unity (Fig. 7), corresponding to the jadeite component in the solid solution (Supplementary Material, Table S3). Nevertheless, clinopyroxenes produced at 800°C in the runs with high X_{salt} in the fluids show an excess of Na over Al (data points above the Na = Al line in Fig. 7). The most Na-rich clinopyroxenes (>0·3 a.p.f.u.) are produced in NaCl-rich fluids (runs N12 and N13). Recalculation of clinopyroxene formulae to 6 O atoms shows that excess Na over the jadeite and Na–Ti-end-member might be bound to Fe^{3+} as the aegirine component. The sodic clinopyroxenes from runs N12 and N13 contain 0·2–0·3 a.p.f.u. of Fe^{3+} (Supplementary Material, Table S3).

Orthopyroxenes are identified in reaction textures only at 800°C (Table 2). At similar X_{Mg} (0·52–0·54) (Supplementary Material, Table S4), orthopyroxene in run 24 produced by interaction of the gneiss with the chloride-free H_2O–CO_2 fluid has higher Al_2O_3 content (1·7–3·0 wt %) in comparison with orthopyroxene that crystallized in equilibrium with both KCl- and NaCl-bearing fluids (Fig. 8). Orthopyroxenes coexisting with pargasite–edenite amphiboles and clinopyroxene in runs with the KCl-bearing fluid (K31 and K32) contain 0·7–1·5 wt % Al_2O_3 (Supplementary Material, Table S4). At similar Al_2O_3 content, orthopyroxene associated with sodic amphibole in run N11 has a lower Mg-number of about 0·48 (Supplementary Material, Table S4). Orthopyroxenes formed in equilibrium with KCl-bearing fluids have

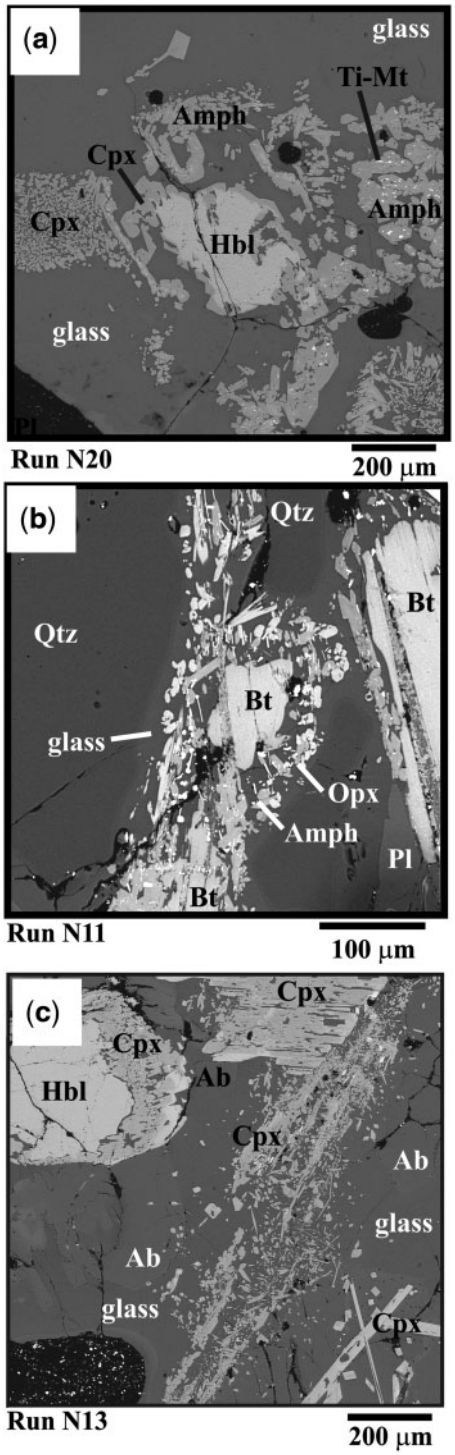

Fig. 5. Phase assemblages produced by interaction of the biotite–amphibole gneiss with an H_2O–CO_2–NaCl fluid at 750 and 800°C. (a) Sodic amphibole, containing inclusions of Ti-magnetite, and clinopyroxene in the glass in the sample that interacted with fluid at $X_{NaCl} = 0{\cdot}009$ (run N20, Table 2) at 750°C. (b) Orthopyroxene, sodic amphibole, and ilmenite coexisting with melt (glass) in the run sample that interacted with fluid at $X_{NaCl} = 0{\cdot}012$ (run N11, Table 2); elongated platelets in the glass are ilmenite crystallites. (c) Large euhedral albite crystals and clinopyroxene coexisting with melt (glass) in the sample that interacted with fluid at $X_{NaCl} = 0{\cdot}032$ (run N13, Table 2); a large fluid bubble is visible in the lower left corner of the image; clinopyroxene crystallites developed on the original hornblende are zoned with an increase in Na content toward the rims.

higher CaO contents (>1·5 wt %) compared with orthopyroxenes that equilibrated with H_2O–CO_2 and H_2O–CO_2–NaCl fluids.

No grains of original magnetite or ilmenite were found in the run samples, although these are constituents of the assemblage of the gneiss (Fig. 1; Table 1). Both phases are present as euhedral crystallites in reaction textures formed during the experiments. In contrast to the original magnetite, which does not contain TiO_2 (Table 1), the experimental magnetite contains 6–11 wt % TiO_2 (Supplementary Material, Table S5). In contrast to the original Mn-rich and Mg-poor ilmenite (Table 1), the experimental ilmenite contains less than 1 wt % MnO, but more than 1·5 wt % MgO (Supplementary Material, Table S5). These differences are reflections of the formation of ilmenite and/or Ti-bearing magnetite in the run products via the decomposition of the original Ti-bearing, but Mn-poor, biotite (Table 1). Formation of these phases seems to be controlled by X_{salt} in the starting fluids. Both ilmenite and Ti-bearing magnetite (6–7 wt % TiO_2) form along with orthopyroxene, amphibole, and silicate melt via the decomposition of biotite in the presence of the salt-free H_2O–CO_2 fluid and KCl-poor fluids at 800°C (runs 24, K31, K32; Table 2; Figs 2 and 3a). However, increasing X_{KCl} results in the disappearance of Ti-magnetite from the reaction assemblages, whereas ilmenite coexists with orthopyroxene and clinopyroxene only in run K33 (Fig. 4b), and with clinopyroxene in runs K8 and K9. Both Ti-bearing magnetite and ilmenite are associated with orthopyroxene and amphibole in run N11 produced at 800°C by the H_2O–CO_2–NaCl fluid with $X_{NaCl} = 0{\cdot}012$, but these phases are absent in runs N12 and N13 produced by more saline H_2O–CO_2–NaCl fluids (Table 2). Magnetite, with 10–11 wt % TiO_2, appears as lamellae-like inclusions in amphibole from runs N18 and N20 with the H_2O–CO_2–NaCl fluid at 750°C (Fig. 5a). In run NK26 (Table 2) Ti-bearing magnetite (about 8 wt % TiO_2) forms shells around primary pyrite grains in Cpx + melt reaction zones around biotite flakes, whereas ilmenite crystallites are characteristic for reaction textures further away from pyrite grains.

In runs with H_2O–CO_2–KCl fluid, titanite is associated with the clinopyroxene–K-feldspar textures around biotite (Supplementary Material, Table S6). Titanite occurs as a result of biotite decomposition in run N13 at 800°C (Table 2), where it is associated with clinopyroxene, albite, and Na-rich melt. Titanites produced at 750°C are richer in Al_2O_3 and F in comparison with titanites from the runs at 800°C (Supplementary Material, Table S6).

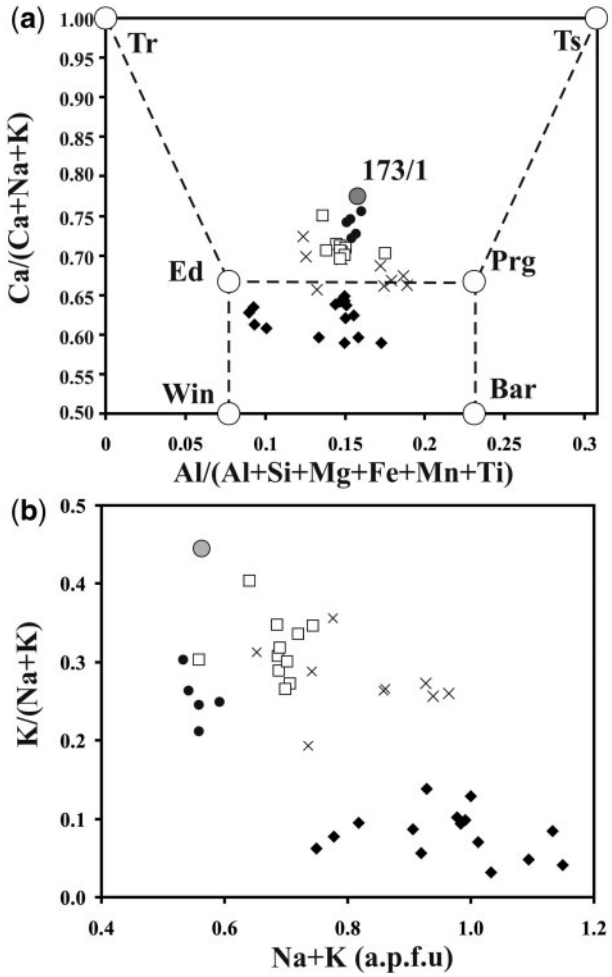

Fig. 6. Compositional characteristics of amphibole produced in equilibrium with H_2O–CO_2 (black dots; run 24), H_2O–CO_2–KCl (open squares; runs K31, K32), H_2O–CO_2–NaCl fluid (black rhombs; runs N11, N18, N20), and H_2O–CO_2–(K, Na)Cl fluid (crosses, runs NK23, NK27). (a) Variations of the amphibole composition in terms of Al/(Al + Si + Mg + Fe + Mn + Ti) and Ca/(Ca + Na + K) in comparison with major Ca and Ca–Na amphibole end-members (Tr, tremolite; Ts, tschermakite; Ed, edenite; Prg, pargasite; Win, winchite; Bar, barroisite). (b) Variations of the amphibole composition in terms of total alkali content and K/(Na + K) ratio. Large gray circle marks the average composition of amphibole in the initial gneiss sample 173/1 (Table 1).

Apatite in the run products is clearly a relic from the original assemblage of the gneiss 173/1. However, the Cl content varies from 0·4 to 0·75 wt %, which is notably higher than the Cl content in apatite from the starting gneiss (Table 1). This means that apatite compositions are greatly influenced by Cl–OH exchange with fluids. No evidence for the decomposition or dissolution of apatite was observed in the run samples.

Plagioclase in most of the run products is a remnant of the original plagioclase. Usually, plagioclase does not show any zoning in contact with reaction textures (Supplementary Material, Table S7). However, high-Ca plagioclase finely intergrown with K-feldspar is observed in the K-feldspar rims in the run samples produced by the H_2O–CO_2–KCl fluids at 750°C (see run K4 in Table S7 in Supplementary Material). Some run products (Table 2) contain newly formed tabular or subhedral crystals of plagioclase attached to the reaction textures around biotite and amphibole. The anorthite content of plagioclase produced in the runs with the H_2O–CO_2–KCl fluids is higher than the anorthite content of the original plagioclase (see analyses of plagioclases in samples 24, K32 and K33 in Table S7, Supplementary Material). In contrast, the anorthite content of plagioclase produced in the runs with the H_2O–CO_2–(K, Na)Cl fluids is similar to or lower than the anorthite content of the original plagioclase (see analyses of plagioclases in samples NK26, NK23, NK22 in Table S7, Supplementary Material).

The mole fraction X_K in newly formed alkali feldspars directly depends on the KCl/(KCl + NaCl) ratio of the starting fluid. It varies from 0·96 to 0·99 in alkali feldspar formed in equilibrium with KCl-rich fluids, but decreases to 0·70–0·78 in feldspars produced by mixed KCl–NaCl fluids (runs NK22 and NK25 in Table S8, Supplementary Material). Albite coexists with clinopyroxene, titanite, and sodic melt in reaction textures from run sample N13 (Supplementary Material, Table S10).

Kalsilite is associated with K-feldspar in zones of strong K-feldspathization of plagioclase in the products of run K10 at 800°C and KCl/(H_2O + CO_2) = 0·1. This phase contains 1·1–1·3 wt % Na_2O (Supplementary Material, Table S8).

Ca-rich garnet is a minor phase in reaction textures produced by KCl-rich fluids. The ratio Ca/(Ca + Fe + Mg + Mn) in garnets varies from 0·69–0·70 in sample K5 to 0·88 in sample K10. Garnet in run sample K10 is deficient in Al and shows an excess of Fe indicating the andradite component.

Compositions of quenched melts

Melting of the gneiss in the presence of an H_2O–CO_2 fluid at 800°C (run 24) produces a rhyolitic melt containing 6–7 wt % K_2O + Na_2O (Fig. 9a; Table 3). Its normative composition is richer in quartz and orthoclase (Fig. 10) in comparison with the minimum melt in the system Ab–Or–Qtz–H_2O–CO_2 at 500 MPa and a_{H2O} between 1·0 and 0·3 (Ebadi & Johannes, 1991; Johannes & Holtz, 1996). The K_2O content (Fig. 11) and the modified alkali–lime index (MALI; Frost *et al.*, 2001) of the rhyolitic melts formed in the presence of the KCl-bearing fluids positively depend on X_{KCl} in the fluid. In contrast, the molar ratio Al_2O_3/(K_2O + Na_2O + CaO) (aluminium saturation index; ASI; Acosta-Vigil *et al.*, 2003) decreases (Table 3). The CaO content in these melts decreases from about 2–2·5 wt % in melts produced in the presence of low-KCl fluids (runs K31, K32 and K33 in Table 3) to 0·4–0·6 wt % in melts produced by high-KCl fluids (runs K8 and

K10 in Table 3). The melts are characterized by Al_2O_3 contents less than 14·5 wt % (Table 3), and this parameter systematically decreases with increasing X_{KCl} of the starting fluid (Fig. 11). As a result, melts shift toward more peralkaline compositions. The K_2O/Na_2O ratio of melts in equilibrium with KCl-poor fluids is close to that of melts produced in equilibrium with the chloride-free H_2O–CO_2 fluid, but increases with an increase of the KCl content of the fluid. Normative compositions of melts produced at low KCl fluid contents (runs K31, K32 and K33) are similar to the melt in run 24 (Fig. 10) and close to the normative composition of the minimum melts in the system Ab–Or–Qtz–H_2O–KCl–NaCl (Aranovich *et al.*, 2013). An increasing KCl content results in displacement of the normative composition towards orthoclase and quartz (Fig. 11). Peralkaline K_2SiO_3- and Na_2SiO_3-normative melt forms at $X_{KCl} = 0·039$ (run K10, Table 3).

Melts produced with the H_2O–CO_2–NaCl–KCl fluids at 800°C also show CaO contents below 2 wt % (Table 3). These drop below 1 wt % for melts produced in equilibrium with fluids with X_{salt} above 0·04 (runs NK28 and NK29 in Table 3). At KCl/(KCl + NaCl) weight ratios of 0·5 and 0·25 and X_{salt} above 0·04 (runs NK25 and NK28 in Tables 2 and 11), the compositions of melts are shifted toward the trachytic field at 800°C in terms of SiO_2 and $K_2O + Na_2O$ contents (Fig. 9a). Even more silica-deficient (trachyandesitic) melts formed at 750°C (Fig. 9b). In general, fluids with low concentrations of KCl + NaCl produce melts of regular granitic composition at 800°C (runs NK26 and NK27). Their normative composition is close to that of the melts produced with low-salinity H_2O–CO_2 fluids (Fig. 10). Increase of both KCl and NaCl results in an increase of the peralkalinity of the melts. At constant X_{salt}, the K_2O/Na_2O ratio of the melts at 800 and 750°C positively depends on the K/Na ratio of the fluid (Fig. 12). The K_2O/Na_2O values of the melts from our experiments are in a good agreement with the K_2O/Na_2O values for the model melts in the system Ab–Or–Qtz–H_2O–KCl–NaCl at 600 MPa, 700–850°C and variable X_{salt} in the aqueous–salt fluids from the experiments by Aranovich *et al.* (2013).

The composition of melts formed in the presence of the H_2O–CO_2–NaCl fluids depends on the X_{NaCl} of these fluids. So, at $X_{NaCl} = 0·012$, the melt formed at 800°C (run N11; Tables 2 and 11) has a quartz- and hypersthene-normative rhyolitic composition (Figs 9a and 10) with a K_2O/Na_2O ratio of about 0·8. However, at $X_{NaCl} > 0·02$ the melt composition corresponds to a phonolite with respect to SiO_2 and $K_2O + Na_2O$ content (Figs 9a and 10). The K_2O/Na_2O ratio of the melts is less than 0·15. The Na_2O content of melts formed in the presence of the H_2O–CO_2–NaCl fluids increases with X_{NaCl} of the fluid. However, in contrast to potassic melts formed via H_2O–CO_2–KCl fluids at 800°C, sodic melts show a significant

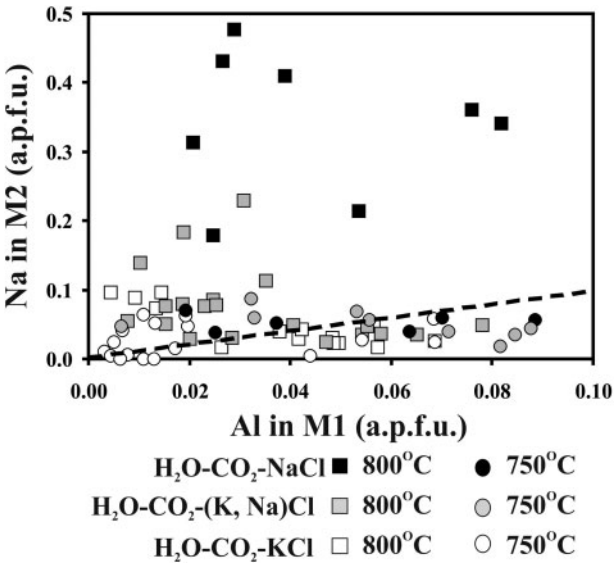

Fig. 7. M2 Na and M1 Al contents per formula unit of clinopyroxene produced at 750°C (circles) and 800°C (squares) in equilibrium with H_2O–CO_2–KCl (open symbols), H_2O–CO_2–(K, Na)Cl (gray filled symbols), and H_2O–CO_2–NaCl (black filled symbols) fluids. Dashed line shows Na/Al = 1 corresponding to the jadeite component. Data points above this line indicate the presence of the aegirine end-member in clinopyroxene.

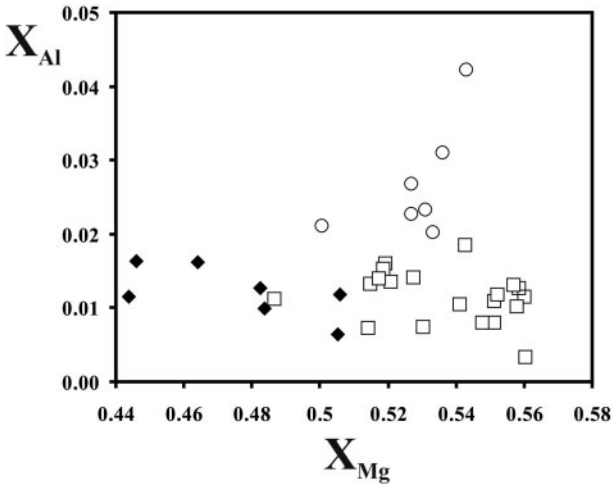

Fig. 8. X_{Mg} vs X_{Al} plot for orthopyroxene produced at 800°C in equilibrium with equimolar H_2O–CO_2 fluid (open circles; run 24), H_2O–CO_2–KCl fluid (open squares; runs K31, K32, K33), and H_2O–CO_2–NaCl fluid (black rhombs; run N11).

increase in the Al_2O_3 content (up to 21 wt %) with increasing X_{NaCl} of the fluid. For example, the melt produced in run N13, with the highest X_{NaCl}, contains up to 14 wt % of Na_2O and up to 20·5 wt % of Al_2O_3, thus making it Ne- and Ol-normative (Fig. 10; Table 3). The SiO_2 and $K_2O + Na_2O$ content of the Na-rich melts produced at

750°C corresponds to a trachyandesite composition (Fig. 9b). The Al_2O_3 content of these melts (up to 17·5 wt %) is comparable with that of sodic melts formed at 800°C, but is significantly higher than the Al_2O_3 content of potassic melts. The normative composition of these melts directly depends on the X_{NaCl} of the fluid (runs N18, N19 and N20 in Table 3; Fig. 10). At $X_{NaCl} = 0·09$, the melt contains about 23 wt % normative quartz (run N20), whereas at lower X_{NaCl} it drops to about 8 wt % (run N18).

Thus, NaCl-rich and KCl-rich fluids have different effects on melt compositions. The NaCl-rich fluids produce silica-undersaturated melts, especially at 750°C, whereas melts produced by KCl-rich fluids are predominantly of rhyolitic composition (Fig. 9a and b). The H_2O–CO_2–NaCl fluids produce melts enriched in Al_2O_3 (up to 20 wt % at 800°C; Table 3), whereas the Al_2O_3 content of melts produced by H_2O–CO_2–KCl fluids does not exceed 15 wt % (Table 3). Albite and nepheline become normative in sodic melts with increasing X_{NaCl} of the fluid, whereas the normative composition of potassic melts moves towards quartz or K-silicate with increasing X_{KCl} of the fluid (Fig. 10).

All melts contain Cl. The Cl content of the melt, 0·02 ± 0·02 wt % (Table 3), produced by the chloride-free H_2O–CO_2 fluid resulted from the decomposition of Cl-bearing biotite, amphibole, and, partially, apatite from the gneiss. The Cl content in the melt that equilibrated with the chloride-bearing fluids shows a tendency to decrease with increasing SiO_2 content (Fig. 13a) and increase with total alkalinity $K_2O + Na_2O$ (Fig. 13b). Melts produced at 750°C are richer in Cl than melts produced at 800°C (Fig. 13a and b). This conclusion is supported by Fig. 13c, in which the dependence of Cl content in the melt on its K_2O/Na_2O ratio is compared. This diagram also indicates that sodic melts are richer in Cl in comparison with potassic melts at similar temperatures. All the above compositional regularities regarding Cl solubility in the melts are in good agreement with available experimental data (see Webster, 1997) and with the model of Webster & De Vivo (2002), which predicts that Cl solubility in felsic melts increases with increasing $(Na + K + Al + Ca + Mg + Fe + Mn + F)/Si$, $Al_2O_3/(K_2O + Na_2O)$, and Na_2O/K_2O ratios. The Cl concentrations in the melts are also within the range reported by Aranovich *et al.* (2013) for minimum granite melts in the system Or–Ab–Qtz that equilibrated with H_2O–KCl–NaCl fluids.

In addition to Cl, all glasses contain F (Table 3), which resulted from the decomposition of biotite, amphibole, and, to a lesser extent, apatite from the gneiss. In most cases, the concentration of F varies from 0·2 to 0·4 wt %. However, glasses in runs K10, K8 and N19 are enriched in F (0·8–1·3 wt %) (Table 3).

Analyses of glasses give oxide totals below 100 % (Table 3). Taking into account the low solubility of CO_2 in rhyolitic melts that have equilibrated with mixed H_2O–CO_2 fluids [see review by Ni & Keppler (2013)], the 100 minus anhydrous total (wt %) difference can be mostly attributed to H_2O dissolved in the melt (Morgan & London, 1996; Acosta-Vigil *et al.*, 2003). The difference from 2 to 8 wt % (Table 3) is well within the range of H_2O solubility in rhyolitic melts that have equilibrated with mixed H_2O–CO_2 fluids (Holtz *et al.*, 2001; Tamic *et al.*, 2001; Ni & Keppler, 2013). It is also consistent with the water content in the melts reported for the system Ab–Or–Qtz–H_2O–KCl–NaCl (Aranovich *et al.*, 2013). To qualitatively identify the presence of H_2O and CO_3^{2-} groups in the melts, glasses from several run samples were analyzed by Raman spectroscopy (Supplementary Material, Fig. S2). All spectra show a wide asymmetric band at 3500–3600 cm^{-1} assigned to H–O–H stretching and a band at 1630 cm^{-1}, which might correspond to bending of molecular H_2O (e.g. Mysen *et al.*, 1980; McMillan *et al.*, 1983). Thus, both OH groups and molecular H_2O are present in the glasses. The low-frequency region of the Raman spectra of glasses produced in runs with H_2O–CO_2 and H_2O–CO_2–KCl fluids shows complex bands corresponding to variably polymerized SiO_4^{4-} groups. In addition, the glasses produced in runs with H_2O–CO_2–(K, Na)Cl and H_2O–CO_2–NaCl fluids also show sharp bands at 1095–1098 cm^{-1}, which can be assigned to symmetric stretching C–O vibrations in the CO_3^{2-} groups. Bands at 1095 cm^{-1} could correspond to $MgCO_3$ and $CaMgCO_3$-like complexes in the quenched melts (see web databanks at http://rruff.geo.arizona.edu/rruff/), whereas higher frequency bands (1098 cm^{-1}) could correspond to lasfordite $MgCO_3.5H_2O$ (e.g. Coleyshaw *et al.*, 2003). Thus, the Raman data clearly show that solubility of CO_2 as CO_3^{2-} in the melts that equilibrated with the NaCl-bearing fluids is higher than in the melts produced in the presence of H_2O–CO_2 and H_2O–CO_2–KCl fluids. Taking into account the data on Cl content in the melts (Fig. 13a–c) we can conclude that the sodic melts are much richer in volatiles in comparison with the potassic melts.

DISCUSSION AND APPLICATIONS TO NATURAL ASSEMBLAGES

Fluid–mineral–melt reactions between gneiss and H_2O–CO_2–chloride fluids

Reactions with participation of the equimolar H_2O–CO_2 fluid

The Sand River gneiss did not show any notable mineral reactions and did not produce melt at 800°C in the absence of a free fluid. This result is consistent with experimental data on diverse tonalitic assemblages at pressures up to 1000 MPa (Rutter & Wyllie, 1988; Skjerlie & Johnston, 1993; Patiño Douce & Beard, 1995; Patiño Douce, 1997; Gardien *et al.*, 2000; Watkins *et al.*, 2007) indicating that

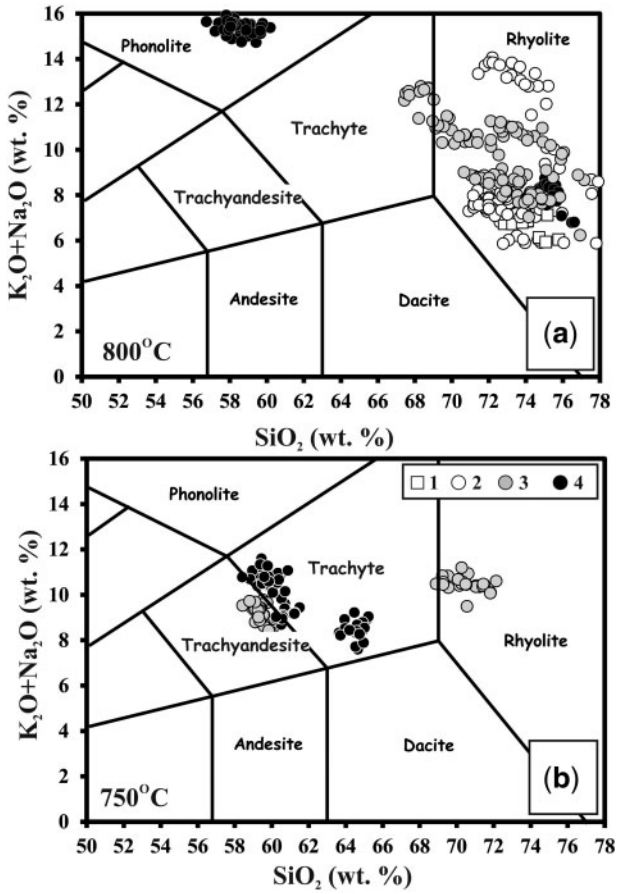

Fig. 9. Total alkalis–silica diagrams showing the compositions normalized to 100% of the quenched melts produced at 800°C (a) and 750°C (b) in equilibrium with (1) H_2O–CO_2, (2) H_2O–CO_2–KCl, (3) H_2O–CO_2–(K, Na)Cl and (4) H_2O–CO_2–NaCl fluids (see Table 3 for mean compositions) compared with common volcanic rocks types designated by the IUGS Subcommission on the Systematics of Igneous Rocks (Le Maitre *et al.*, 2002).

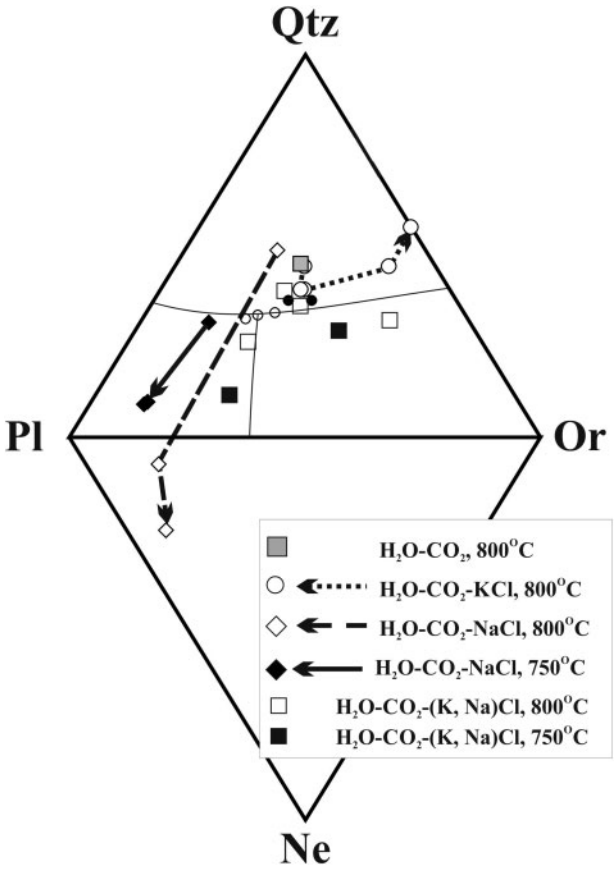

Fig. 10. Normative compositions of melts produced from interaction of the gneiss with the H_2O–CO_2 and H_2O–CO_2–KCl at 800°C, and H_2O–CO_2–NaCl and H_2O–CO_2–(K, Na)Cl fluids at 750 and 800°C. Small open circles and fine lines mark the normative composition of the minimum melts and cotectic lines in the system Ab–Or–Qtz–H_2O–CO_2 at 500 MPa (Ebadi & Johannes, 1991; Johannes & Holtz, 1996). Small filled circles mark the normative composition of the minimum melts in the system Ab–Or–Qtz–H_2O–KCl–NaCl at 600 MPa (Aranovich *et al.*, 2013).

dehydration melting with decomposition of biotite and amphibole begins at temperatures above 800–850°C depending on bulk composition (Patiño Douce & Beard, 1995; Patiño Douce, 1997; Watkins *et al.*, 2007). Nevertheless, Singh & Johannes (1996) experimentally demonstrated that dehydration melting of tonalite vitally depends on the Mg-number of biotite; at pressure 500 MPa biotite with $X_{Mg} = 0{\cdot}5$ melts out with plagioclase and quartz at 710–730°C to produce Opx + Cpx ± Amph + Kfs + melt. In addition, melting temperatures drop significantly in the presence of an H_2O fluid (Gardien *et al.*, 2000; Watkins *et al.*, 2007). Watkins *et al.* (2007) found that melting of biotite and biotite–hornblende rocks at 600 MPa in the presence of H_2O begins at temperatures of about 680 and 690°C, respectively. Taking into account these data and the rate of increase in melting temperature with decrease of X_{H2O} in an H_2O–CO_2 fluid

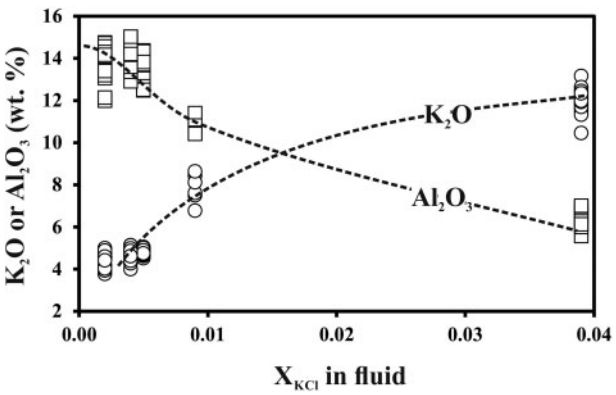

Fig. 11. Variation of the K_2O and Al_2O_3 content in the melts produced from interaction of the gneiss with H_2O–CO_2–KCl fluids at 800°C vs X_{KCl} in the fluid.

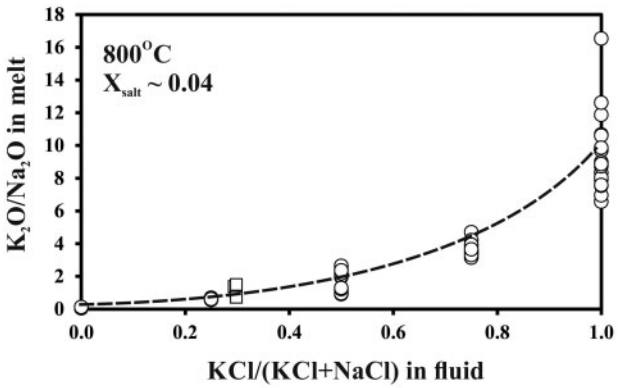

Fig. 12. Dependence of the K_2O/Na_2O ratio in the melt on the KCl/(KCl + NaCl) ratio of the starting fluid at 800°C at X_{salt} in the fluid of about 0·04 (open circles). Open squares show the compositions of the model melts in the system Ab–Or–Qtz–H_2O–KCl–NaCl at 600 MPa and 700–850°C (Aranovich *et al.*, 2013).

for the granitic minimum (Ebadi & Johannes, 1991), it can be roughly estimated that melting of tonalite at $X_{H2O} = 0·5$ would begin at temperatures 760–780°C. This estimation is consistent with our data indicating that the Sand River gneiss did not melt in the presence of an equimolar H_2O–CO_2 fluid at 750°C, but produced about 20% melt at 800°C.

Dehydration melting of biotite-rich tonalite produces assemblages with predominant orthopyroxene (Patiño Douce & Beard, 1995; Patiño Douce, 1997; Watkins *et al.*, 2007). Formation of the orthopyroxene-dominant assemblage during partial melting in the presence of the equimolar H_2O–CO_2 fluid in run 24 (Table 2) is similar to the dehydration melting process (Rutter & Wyllie, 1988; Skjerlie & Johnston, 1993; Patiño Douce & Beard, 1995; Patiño Douce, 1997; Gardien *et al.*, 2000; Watkins *et al.*, 2007). However, dehydration melting results in decomposition of amphibole, rather than its formation after biotite as it is observed in run 24. Relics of biotite in new amphibole (Fig. 2) and its elevated TiO_2 content (Supplementary Material, Table S2) imply that formation of the assemblage Opx + Amph + Ilm + Ti-Mt + melt proceeded at the expense of Ti-bearing biotite. Balanced reaction (r24-1) (Table 4) written for the specific mineral and melt compositions from run 24 shows that Bt_2 forming zones of higher Mg-number on the original biotite (Bt_1) at the contacts with the reaction textures (Fig. 2, Table 3) serves as a reactant component. This is comparable with the results of Gardien *et al.* (2000), who demonstrated that H_2O stabilized amphibole with respect to biotite. At H_2O contents above 4 wt %, the biotite-rich tonalite melts at about 800°C (at 1000 MPa) with formation of amphibole, calcic plagioclase and a Ti-bearing phase (Gardien *et al.*, 2000). Thus, the melting of tonalite in the presence of equimolar H_2O–CO_2 fluid seems to combine the characteristics of dehydration and hydrous melting.

Previous experiments were conducted on bulk compositions, which differ from the bulk composition of the Sand River gneiss and, thus, do not allow a substantiated comparison with the results of our present experiments. To further compare modifications of the Sand River biotite–hornblende gneiss caused by H_2O–CO_2 fluids with theoretical predictions, we have calculated a T–a_{H2O} pseudosection for the gneiss (Table 1) at 550 MPa using the Gibbs energy minimization method implemented into the PERPLEX software (Connolly, 2005) (version 6.7.0 for Windows with the standard properties database hp02ver.dat and solution model database solution_model.dat; http://www.perplex.ethz.ch) (Fig. 14). In our calculations, we assumed that the system was saturated with a fluid with the water activity indicated along the y-axis (Fig. 14). This assumption corresponds to the experimental setup with rock/fluid weight ratio below unity and is supported by the presence of large fluid bubbles in the experimental glasses. The pseudosection closely reproduces the results of the experiments with H_2O–CO_2 fluids. The data point for run 24 at 800°C and $a_{H2O} = 0·613$ (Table 2) is situated between the calculated phase fields melt + Opx + Amph + Pl + Ilm and melt + Opx + Amph + Pl + Qtz + Ilm, which is perfectly consistent with the experimentally produced assemblages (Fig. 2). The data point for run 1 at 750°C and $a_{H2O} = 0·625$ (Table 2) is situated in the subsolidus region close to the field Bt + Amph + Pl + Qtz + Ilm.

Assemblages involving Opx + Amph + Ilm + Ti-Mt + melt produced by low-salinity H_2O–CO_2–KCl and H_2O–CO_2–NaCl fluids in the experiments at 800°C (runs K31, K32 and N11 in Table 2) also agree with the corresponding phase fields in the T–a_{H2O} pseudosection (Fig. 14). The data point for the run K33 (Table 2) with the assemblage Cpx + Opx + Ilm + melt is also close to the phase fields melt + Opx + Cpx + Pl + Ilm and melt + Opx + Cpx + Pl + Qtz + Ilm in Fig. 14. However, the T–a_{H2O} pseudosection does not contain the Cpx-dominated assemblages that are characteristic for runs involving high-salinity fluids. It shows that a_{H2O} is not the only thermodynamic parameter controlling mineral assemblages and partial melting in presence of chloride-bearing fluids, and that the activities of alkali chlorides have a definitive role.

Reactions with participation of chloride components

Mineral assemblages produced during interaction of the gneiss with H_2O–CO_2–chloride fluids vary with temperature, X_{salt} and the KCl/(KCl + NaCl) ratio of the starting fluid (Fig. 15a and b). The schematic grid of mineral assemblages at 750°C (Fig. 15a) shows that clinopyroxene is the major newly formed phase over the entire range of fluid composition. Formation of the Cpx + Kfs assemblage in runs with H_2O–CO_2–KCl fluids by decomposition of biotite or/and amphibole in contact with plagioclase and quartz (Fig. 3a and b) can be expressed in terms of the

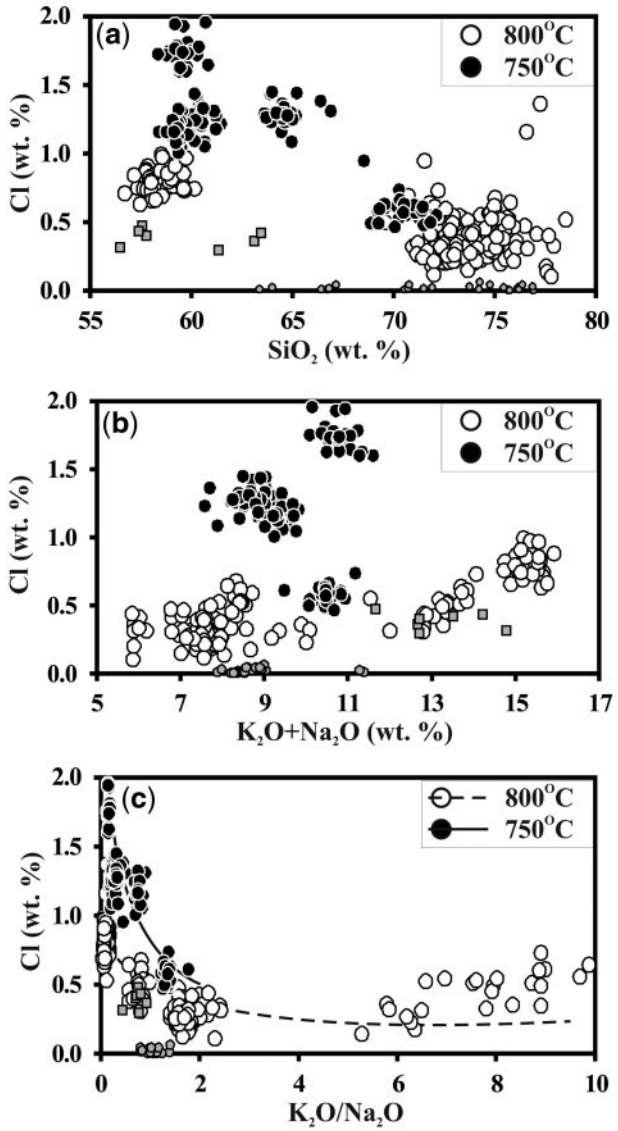

Fig. 13. Variations in Cl content of the melts produced at 750 and 800°C with (a) SiO_2 content, (b) total alkalinity ($K_2O + Na_2O$), and (c) K_2O/Na_2O ratio of the melts. The Cl contents of A-type granitoids (Whalen *et al.*, 1987; Landenberger & Collins, 1996) (small gray-filled circles) and syenites from the Soustov intrusive complex in the Kola Peninsula (Bea *et al.*, 2001) (small gray-filled squares) are plotted as examples of melts presumably produced via melting of Archean tonalitic gneisses for comparison.

following end-member reactions:

$$\mathrm{Phl} + 3\mathrm{An} + 18\mathrm{Qtz} + 6\mathrm{KCl} + 2\mathrm{H_2O} = 3\mathrm{Di} + 7\mathrm{Kfs} + 6\mathrm{HCl} \quad (1a)$$

$$\mathrm{Prg} + 2\mathrm{An} + \mathrm{Ab} + 19\mathrm{Qtz} + 7\mathrm{KCl} + 2\mathrm{H_2O} = 4\mathrm{Di} + 7\mathrm{Kfs} + \mathrm{NaCl} + 6\mathrm{HCl} \quad (1b)$$

Because of the net-transfer nature of the reactions, the compositions of the original biotite and hornblende change (Supplementary Material, Tables S1 and S2). In several runs, this process is expressed by the appearance of biotite flakes within the Cpx + Kfs intergrowths (Fig. 3b). The Mg-number of this biotite is higher than or similar to that of the original biotite (Supplementary Material, Tables S1). The reaction balanced for the specific mineral compositions in sample K7 (Table 4) indicates that biotite inside the Cpx + Kfs reaction textures [Bt_2 in the reaction (rK7-1) in Table 4] serves as a reactant phase along with the original biotite (Bt_1). Thus, the original assemblage Bt + Hbl + Pl + Qtz, which is stable in the presence of an H_2O–CO_2 fluid, is outside its stability field in the presence of H_2O–CO_2–KCl fluids at 750°C.

Decrease of the KCl/(KCl + NaCl) ratio at low X_{salt} stabilizes amphibole in association with clinopyroxene at 750°C (Fig. 15a). Reactions (rNK23-1)–(rNK23-5) (Table 4) balanced using the phase compositions from run NK23 (Table 2) show that crystallization of amphibole ($Amph_2$) in the assemblage with clinopyroxene, sodic plagioclase (Pl_2), ilmenite and melt can proceed either with or without the participation of the original hornblende ($Amph_1$). Formation of amphibole after biotite as a result of interaction with the KCl- and NaCl-bearing fluid and an increase of the winchite–barroisite component in amphibole with increasing NaCl content (Fig. 6a and b) can be expressed by the following end-member reactions:

$$4/3\mathrm{Phl} + 2\mathrm{An} + 5\mathrm{Qtz} + \mathrm{KCl} + \mathrm{NaCl} + 2/3\mathrm{H_2O} = \mathrm{Prg} + 7/3\mathrm{Kfs} + 2\mathrm{HCl} \quad (2a)$$

$$\mathrm{Phl} + 3/4\mathrm{An} + 18/4\mathrm{Qtz} + 3/2\mathrm{NaCl} + 1/2\mathrm{H_2O} = 3/4\mathrm{Win} + 3/4\mathrm{Ab} + \mathrm{Kfs} + 3/2\mathrm{HCl}. \quad (2b)$$

Because amphibole formation in the runs with NaCl-bearing fluids at 750°C is accompanied by partial melting (see below), Ab and Kfs in reactions (2a) and (2b) represent components of the melt.

Increase of X_{salt} in the fluid at constant KCl/(KCl + NaCl) ratio stabilizes clinopyroxene (Fig. 15a). The reactions (rNK22-1), (rNK22-2) and (rNK22-3) balanced using the phase compositions from run NK22 (Table 4) show that both Bt_1 and Bt_2 serve as reactant components, suggesting that biotite reacts out during formation of the assemblage Cpx + Ilm + Pl + Kfs + melt.

Opx-bearing assemblages form at 800°C in presence of low-salinity H_2O–CO_2 fluids only (Fig. 15b). At low X_{salt}, orthopyroxene coexists with new amphibole, which forms at the expense of Ti-bearing biotite. In contrast to the balanced reaction (r24-1) (Table 4) for the formation of the assemblage Opx + Amph + Ilm + melt via the salt-free H_2O–CO_2 fluid in run 24, reactions (rK32-1)–(rK32-5)

(Table 4) for the phase compositions in run K32 produced from interaction with the H_2O–CO_2–KCl fluid show Bt_2 as a product. A similar conclusion follows for the reaction (rN11-1) (Table 4), which describes the formation of the assemblage of orthopyroxene with sodium-enriched amphibole in the presence of the low-salinity H_2O–CO_2–NaCl fluid (Figs 5b and 6a, b). Further increase of X_{salt} in the fluid results in orthopyroxene and amphibole breakdown to form the assemblage Cpx + Ilm ± Pl ± Kfs + melt (Fig. 15b). The reactions producing this assemblage are exemplified in Table 4 by the runs NK26, NK27, and NK29. The negative slope of the 'Amph-out' boundary (Fig. 15b) indicates that NaCl in the fluid expands the stability field of amphibole-bearing assemblages to higher salt concentrations.

Thus, our results indicate that an increase of alkali chloride content in the H_2O–CO_2 fluid causes systematic changes in the mineral assemblages coexisting with alkali feldspar, albite or/and alkali-rich silicate melt, from Amph + Bt through Opx + Amph and Opx + Cpx to Cpx. This succession of mineral assemblages as a function of total salt concentration and the KCl/NaCl ratio of the fluid closely reproduces predictions by Korzhinskii (1959), who, on the basis of a Schreinemakers analysis, deduced variability of the mineral paragenesis of granitic and syenitic rocks as a function of K_2O and Na_2O chemical potentials in the fluids or melts. According to Korzhinskii (1959), quartz-free assemblages involving Cpx + Kfs or Cpx + Ab would correspond to the highest K_2O and Na_2O activities, respectively. Korzhinskii (1959) introduced a criterion for variable K_2O activity: the higher the anorthite content of plagioclase coexisting with K-feldspar, the higher the K_2O activity corresponding to this assemblage because of the exchange reaction

$$Ab + 1/2K_2O = Kfs + 1/2Na_2O \quad (3a)$$

which can be rewritten with participation of KCl and NaCl as

$$Ab + KCl = Kfs + NaCl. \quad (3b)$$

Relict plagioclase does not show any distinct zoning at contacts with reaction textures in the run products, because the anorthite component of the plagioclase contributes to the formation of clinopyroxene, amphibole, and melt. However, Ca-rich plagioclase intergrown with K-feldspar has been locally found in the K-feldspar rims on plagioclase grains (see, for example, run K4 in Table S7 in Supplementary Material) providing evidence for reaction (3b). Following Korzhinskii (1959, 1962), Perchuk and co-authors (Perchuk & Gerya, 1993; Perchuk *et al.*, 1994) added another criterion for variable K_2O activity in the fluid: the lower the Al_2O_3 content of the Fe–Mg mineral (biotite, amphibole, pyroxenes) that coexists with K-feldspar, the higher the K_2O activity of the fluid. This criterion is also reflected in compositions of minerals in the reaction textures. The Al content of biotite flakes included in clinopyroxene–K-feldspar textures is much lower than the Al content of the original biotite (Supplementary Material, Table S1). The Al content of orthopyroxene produced in equilibrium with chloride-bearing fluids is lower than the Al content of orthopyroxene produced in equilibrium with the H_2O–CO_2 fluid (Fig. 8). Increase of the salt concentration in the fluid assists in the formation of the aegirine component of clinopyroxene (Fig. 7) because of the extraction of Al from clinopyroxene to form K-feldspar, albite or melt and its replacement by Fe^{3+} (Fig. 7).

Activities of alkali chlorides are also responsible for the appearance of specific minor phases in the run products. Grossular-rich garnet associated with clinopyroxene–K-feldspar reaction textures in samples that interacted with H_2O–CO_2–KCl fluid (Table 2) forms via decomposition of the anorthite component in plagioclase that has interacted with a potassic fluid according to the end-member reaction (Safonov, 1998)

$$An + 3Qtz + 4/3KCl + 2/3H_2O = 1/3Grs + 4/3Kfs + 4/3HCl. \quad (4)$$

In run sample K10, garnet is associated with strongly K-feldspathized and desilicitized zones in plagioclase, which are characterized by the presence of kalsilite and calcite inclusions. End-member reactions

$$Uvs + An + 6Qtz + 2KCl + H_2O = Hed + Ilm + 2Kfs + 2HCl \quad (5a)$$

and

$$Ilm + 2An + 11Qtz + 4KCl + 2H_2O = Hed + Ttn + 4Kfs + 4HCl \quad (5b)$$

indicate that Ti-magnetite should be unstable with respect to ilmenite and titanite in the presence of KCl-rich fluid. This is observed in our experiments (Table 2).

Thus, the activity of chloride components is an important parameter in the formation of specific mineral assemblages. Unfortunately, it is difficult to compute pseudosections illustrating the activities of chloride, specifically. However, taking into account that elevated activities of alkali chloride in the fluids generally impose elevated activities of K_2O and Na_2O in the rock system (Safonov & Aranovich, 2014), pseudosections a_{H2O}–a_{K2O} and a_{H2O}–a_{Na2O} for 800°C have been computed using the PERPLEX software (Fig. 16a and b). Again, we assumed that the system was saturated with a fluid. Both pseudosections support the observation that orthopyroxene-bearing assemblages are characteristic for low activities of K_2O

Table 4: Selected mineral–fluid and mineral–fluid-melt reactions proceeding in the biotite–hornblende tonalite gneiss interacting with H_2O–CO_2, H_2O–CO_2–KCl, H_2O–CO_2–NaCl, and H_2O–CO_2–(K, Na)Cl fluids at 550 MPa and 750 and 800°C

Phase compositions used in calculations	Reactions
Dehydration reaction forming Cpx + Kfs + Ilm with participation of the H_2O–CO_2–KCl fluid at 750°C	
Run K7	
Bt_1: $KFe_{1.41}Mg_{1.175}Al_{1.29}Ti_{0.19}Si_{2.8}O_{10}(OH)_2$	$Bt_1 + 2.640Bt_2 + 9.155Pl_1 + 5.227Pl_2 + 38.944Qtz + 19.704KCl + 2.659H_2O = 7.501Cpx + 0.560Ilm$
Bt_2: $KFe_{1.07}Mg_{1.43}Al_{1.0}Ti_{0.14}Si_{3.11}O_{10}(OH)_2$	$+ 24.074Kfs + 7.105NaCl + 12.599HCl$ (rK7-1)
$Amph_1$: $K_{0.26}Na_{0.32}Ca_{1.96}Fe_{2.67}Mg_{1.90}Al_{2.08}Ti_{0.2}Si_{6.40}O_{22}(OH)_2$	
Pl_1: $K_{0.01}Na_{0.55}Ca_{0.41}Al_{1.42}Si_{2.59}O_8$	
Pl_2: $K_{0.03}Na_{0.56}Ca_{0.43}Al_{1.41}Si_{2.58}O_8$	
Cpx: $Na_{0.05}Ca_{0.80}Fe_{0.49}Mg_{0.66}Al_{0.03}Si_{1.99}O_6$ Kfs: $K_{0.98}Na_{0.02}AlSi_3O_8$	
Ilm: $FeTiO_3$	
Qtz: SiO_2	
Fluid components: H_2O, KCl, NaCl, HCl	
Dehydration–melting reactions forming Cpx + Amph + Ilm + Pl + melt with participation of the H_2O–CO_2–(K, Na)Cl fluid at 750°C	
Run NK23	
Bt_1: $KFe_{1.435}Mg_{1.09}Al_{1.33}Ti_{0.21}Si_{2.78}O_{10}(OH)_2$	$Bt_1 + 0.056Amph_1 + 7.507Pl_1 + 9.111Qtz + 1.214NaCl + 1.623KCl = 0.059Amph_2 + 3.748melt + 0.056Ilm$
$Amph_1$: $K_{0.27}Na_{0.38}Ca_{1.92}Fe_{2.67}Mg_{1.86}Al_{1.95}Ti_{0.13}Si_{6.52}O_{22}(OH)_2$	$+ 0.084H_2O + 1.825HCl$ (rNK23-1)
$Amph_2$: $K_{0.25}Na_{0.71}Ca_{1.9}Fe_{1.13}Mg_{3.1}Al_{2.42}Ti_{0.2}Si_{6.18}O_{22}(OH)_2$	$Bt_1 + 0.094Amph_1 + 8.690Pl_1 + 10.471Qtz + 1.468NaCl + 1.820KCl = 0.690Pl_2 + 0.215Cpx + 4.072melt + 0.059Ilm + 2.188HCl$ (rNK23-2)
Pl_1: $K_{0.01}Na_{0.55}Ca_{0.41}Al_{1.42}Si_{2.59}O_8$	$Bt_1 + 0.112Amph_1 + 8.378Pl_1 + 10.365Qtz + 1.333NaCl + 1.914KCl = 0.212Cpx + 4.206melt + 0.056Ilm + 0.056H_2O + 2.112HCl$ (rNK23-3)
Pl_2: $Na_{0.71}Ca_{0.29}Al_{1.21}Si_{2.77}O_8$	$Bt_1 + 8.386Pl_1 + 0.080H_2O + 9.374Qtz + 1.604NaCl + 1.335KCl = 0.061Amph_2 + 2.017Pl_2 + 3.338melt + 0.064Ilm + 2.037HCl$ (rNK23-4)
Cpx: $Na_{0.05}Ca_{0.95}Fe_{0.18}Mg_{0.77}Al_{0.13}Si_{1.94}O_6$	$Bt_1 + 10.297Pl_1 + 11.021Qtz + 0.291H_2O + 2.163NaCl + 1.332KCl = 4.242Pl_2 + 0.230Cpx + 3.382melt + 0.075Ilm + 2.582HCl$ (rNK23-5)
melt: $K_{0.72}Na_{1.42}Ca_{0.82}Fe_{0.39}Mg_{0.27}Al_{3.19}Ti_{0.04}Si_{8.36}Cl_{0.27}O_{24}$	
Ilm: $FeTiO_3$	
Qtz: SiO_2	
Fluid components: H_2O, NaCl, KCl, HCl	
Dehydration–melting reactions forming Cpx + Ilm + Pl + Kfs + melt with participation of the H_2O–CO_2–(K, Na)Cl fluid at 750°C	
Run NK22	
Bt_1: $KFe_{1.435}Mg_{1.09}Al_{1.33}Ti_{0.21}Si_{2.78}O_{10}(OH)_2$	
Bt_2: $KFe_{1.26}Mg_{1.22}Al_{1.36}Ti_{0.20}Si_{2.79}O_{10}(OH)_2$	(1) $Bt_1 + 1.583Bt_2 + 95.061Pl_1 + 3.563H_2O + 52.814Qtz + 13.345Na_{0.5}K_{0.5}Cl = 85.009Pl_2 + 4.220Cpx$
$Amph_1$: $K_{0.27}Na_{0.38}Ca_{1.92}Fe_{2.67}Mg_{1.86}Al_{1.95}Ti_{0.13}Si_{6.52}O_{22}(OH)_2$	$+ 8.101melt + 0.284Ilm + 12.292HCl$ (rNK22-1)
Pl_1: $K_{0.01}Na_{0.55}Ca_{0.41}Al_{1.42}Si_{2.59}O_8$	(2) $Bt_2 + 0.097Amph_1 + 42.461Pl_1 + 1.588H_2O + 22.541Qtz + 5.815Na_{0.5}K_{0.5}Cl = 38.293Pl_2 + 1.983Cpx$
Pl_2: $K_{0.02}Na_{0.58}Ca_{0.40}Al_{1.40}Si_{2.6}O_8$	+thinsp;3.421melt + 0.111Ilm + 5.370HCl (rNK22-2)
Cpx: $Na_{0.06}Ca_{0.89}Fe_{0.40}Mg_{0.62}Al_{0.08}Si_{1.97}O_6$	

(continued)

Table 4: Continued

Phase compositions used in calculations	Reactions
melt: $K_{1.05}Na_{1.16}Ca_{0.15}Fe_{0.18}Mg_{0.05}Al_{2.36}Ti_{0.03}Si_{9.49}Cl_{0.13}O_{24}$	(3) $Bt_2 + 54.476Pl_1 + 1.860H_2O + 19.321Qtz + 6.021Na_{0.5}K_{0.5}Cl = 51.006Pl_2 + 1.781Cpx + 2.318melt + 0.130Ilm + 1.694Kfs + 5.720HCl$ (rNK22-3)
Kfs: $K_{0.65}Na_{0.35}Si_3O_8$	
Ilm: $FeTiO_3$	
Qtz: SiO_2	
Fluid components: H_2O, $Na_{0.5}K_{0.5}Cl$, HCl	
Dehydration–melting reaction forming Opx + Amph + Ilm melt with participation of the low-salinity H_2O–CO_2 fluids at 800°C	
Run 24	
Bt_1: $KFe_{1.4}Mg_{1.1}Al_{1.3}Ti_{0.2}Si_{2.8}O_{10}(OH)_2$	$Bt_1 + 4.458Bt_2 + 1.895Amph_1 + 7.595Pl_1 + 4.055Pl_2 + 47.014Qtz = 3.867Amph_2 + 0.882Opx + 8.126melt + 0.535Ilm + 3.487H_2O$ (r24-1)
Bt_2: $KFe_{1.2}Mg_{1.3}Al_{1.3}Ti_{0.2}Si_{2.8}O_{10}(OH)_2$	
$Amph_1$: $K_{0.26}Na_{0.32}Ca_{1.96}Fe_{2.67}Mg_{1.90}Al_{2.08}Ti_{0.2}Si_{6.40}O_{22}(OH)_2$	
$Amph_2$: $K_{0.14}Na_{0.44}Ca_{1.58}Fe_{2.23}Mg_{2.39}Al_{2.06}Ti_{0.2}Si_{6.51}O_{22}(OH)_2$	
Pl_1: $K_{0.01}Na_{0.61}Ca_{0.38}Al_{1.16}Si_{2.785}O_8$	
Pl_2: $K_{0.05}Na_{0.41}Ca_{0.48}Al_{1.46}Si_{2.55}O_8$	
Opx: $Fe_{0.98}Mg_{0.87}Al_{0.1}Si_2O_6$	
melt: $K_{0.70}Na_{0.64}Ca_{0.3}Fe_{0.22}Mg_{0.06}Al_{2.18}Ti_{0.02}Si_{9.72}O_{24}$	
Ilm: $FeTiO_3$	
Qtz: SiO_2	
Fluid components: H_2O	
Run K32	
Bt_1: $KFe_{1.37}Mg_{1.18}Al_{1.34}Ti_{0.19}Si_{2.78}O_{10}(OH)_2$	$Bt_1 + 0.051Amph_1 + 2.722Pl_1 + 9.800Qtz + 0.265KCl = 1.206Pl_2 + 0.972H_2O + 1.149Opx + 1.524melt + 0.165Ilm + 0.158HCl$ (rK32-1)
Bt_2: $KFe_{1.20}Mg_{1.32}Al_{1.32}Ti_{0.20}Si_{2.80}O_{10}(OH)_2$	
$Amph_1$: $K_{0.30}Na_{0.32}Ca_{1.92}Fe_{2.78}Mg_{1.79}Al_{2.08}Ti_{0.11}Si_{6.43}O_{22}(OH)_2$	$Bt_1 + 0.104Amph_1 + 3.494Pl_1 + 14.268Qtz + 1.035KCl = 0.479Amph_2 + 0.194H_2O + 0.001Opx + 2.465melt + 0.047Ilm + 0.863HCl$ (rK32-2)
$Amph_2$: $K_{0.22}Na_{0.48}Ca_{1.66}Fe_{2.08}Mg_{2.44}Al_{1.98}Ti_{0.22}Si_{6.53}O_{22}(OH)_2$	$Bt_1 + 0.104Amph_1 + 3.495Pl_1 + 0.001Pl_2 + 14.272Qtz + 1.037KCl = 0.479Amph_2 + 0.193H_2O + 2.466melt + 0.047Ilm + 0.864HCl$ (rK32-3)
Pl_1: $K_{0.01}Na_{0.55}Ca_{0.41}Al_{1.42}Si_{2.59}O_8$	$Bt_1 + 2.183Pl_1 + 8.222Qtz + 0.299KCl = 0.217Bt_2 + 0.777Pl_2 + 0.679H_2O + 0.789Opx + 1.305melt + 0.120Ilm + 0.207HCl$ (rK32-4)
Pl_2: $K_{0.06}Na_{0.37}Ca_{0.51}Al_{1.49}Si_{2.52}O_8$	$Bt_1 + 2.281Pl_1 + 9.541Qtz + 0.677KCl = 0.323Bt_2 + 0.225Amph_2 + 0.170H_2O + 0.073Opx + 1.638melt + 0.043Ilm + 0.563HCl$ (rK32-5)
Opx: $Ca_{0.07}Fe_{0.84}Mg_{1.00}Al_{0.06}Si_2O_6$	
melt: $K_{0.81}Na_{0.70}Ca_{0.34}Fe_{0.25}Mg_{0.08}Al_{2.26}Ti_{0.02}Si_{9.59}Cl_{0.07}O_{24}$	
Ilm: $FeTiO_3$	
Qtz: SiO_2	
Fluid components: H_2O, KCl, HCl	
Run N11	
Bt_1: $KFe_{1.445}Mg_{1.12}Al_{1.33}Ti_{0.19}Si_{2.78}O_{10}(OH)_2$	$1.379Bt_1 + 0.870Pl1 + 3.874Qtz + 0.234NaCl = Bt_2 + 0.107Amph_1 + 0.052Amph_2 + 0.038Opx + 0.623melt + 0.026Ilm + 0.165HCl + 0.136H_2O$ (rN11-1)
Bt_2: $KFe_{1.41}Mg_{1.145}Al_{1.31}Ti_{0.19}Si_{2.8}O_{10}(OH)_2$	
$Amph_1$: $K_{0.26}Na_{0.32}Ca_{1.96}Fe_{2.67}Mg_{1.90}Al_{2.08}Ti_{0.2}Si_{6.40}O_{22}(OH)_2$	

(continued)

Table 4: Continued

Phase compositions used in calculations	Reactions
$Amph_2$: $K_{0.08}Na_{0.73}Ca_{1.3}Fe_{2.28}Mg_{2.475}Al_{1.26}Ti_{0.22}Si_{6.97}O_{22}(OH)_2$	
Pl_1: $K_{0.01}Na_{0.61}Ca_{0.38}Al_{1.16}Si_{2.785}O_8$	
Opx: $Ca_{0.05}Fe_{0.97}Mg_{0.89}Al_{0.06}Si_2O_6$	
melt: $K_{0.57}Na_{1.11}Ca_{0.08}Fe_{0.18}Mg_{0.05}Al_{1.99}Ti_{0.02}Si_{9.94}Cl_{0.11}O_{24}$	
Ilm: $FeTiO_3$	
Qtz: SiO_2	
Fluid components: H_2O, NaCl, HCl	
Dehydration–melting reaction forming Opx + Cpx + Ilm + melt with participation of H_2O–CO_2–KCl fluid at 800°C	
Run K33	
Bt_1: $KFe_{1.41}Mg_{1.09}Al_{1.32}Ti_{0.23}Si_{2.78}O_{10}(OH)_2$	$Bt_1 + 1{\cdot}523Pl_1 + 8{\cdot}175Qtz + 0{\cdot}236KCl = 0{\cdot}155Bt_2 + 0{\cdot}011Amph_1 + 0{\cdot}130Cpx + 0{\cdot}732Opx + 1{\cdot}334melt$
Bt_2: $KFe_{1.195}Mg_{1.22}Al_{1.27}Ti_{0.24}Si_{2.85}O_{10}(OH)_2$	$+ 0{\cdot}157Ilm + 0{\cdot}756H_2O + 0{\cdot}156HCl$ (rK33-1)
$Amph_1$: $K_{0.26}Na_{0.32}Ca_{1.96}Fe_{2.67}Mg_{1.90}Al_{2.08}Ti_{0.2}Si_{6.40}O_{22}(OH)_2$	
Pl_1: $K_{0.01}Na_{0.61}Ca_{0.38}Al_{1.16}Si_{2.785}O_8$	
Pl_2: $K_{0.06}Na_{0.37}Ca_{0.55}Al_{1.49}Si_{2.5}O_8$	
Opx: $Ca_{0.07}Fe_{0.92}Mg_{0.96}Al_{0.06}Si_{1.98}O_6$	
Cpx: $Na_{0.04}Ca_{0.815}Fe_{0.45}Mg_{0.65}Al_{0.07}Si_{1.98}O_6$	
melt: $K_{0.82}Na_{0.69}Ca_{0.3}Fe_{0.23}Mg_{0.07}Al_{2.11}Ti_{0.025}Si_{9.73}Cl_{0.06}O_{24}$	
Ilm: $FeTiO_3$	
Qtz: SiO_2	
Fluid components: H_2O, KCl, HCl	
Dehydration–melting reaction forming Cpx + Ilm ± Pl ± Kfs melt with participation of H_2O–CO_2–(K, Na)Cl fluids at 800°C	
Run NK26	
Bt_1: $KFe_{1.39}Mg_{1.11}Al_{1.36}Ti_{0.21}Si_{2.77}O_{10}(OH)_2$	$Bt_1 + 0{\cdot}086Bt_2 + 0{\cdot}853Amph_1 + 8{\cdot}054Pl_1 + 29{\cdot}668Qtz + 4{\cdot}191Na_{0.5}K_{0.5}Cl = 4{\cdot}296Cpx + 3{\cdot}933melt$
Bt_2: $KFe_{1.065}Mg_{1.41}Al_{1.27}Ti_{0.23}Si_{2.83}O_{10}(OH)_2$	$+ 0{\cdot}222Ilm + 4{\cdot}554Pl_2 + 3{\cdot}877HCl$ (rNK26-1)
$Amph_1$: $K_{0.27}Na_{0.38}Ca_{1.92}Fe_{2.67}Mg_{1.86}Al_{1.95}Ti_{0.13}Si_{6.52}O_{22}(OH)_2$	$Bt_1 + 0{\cdot}666Amph_1 + 7{\cdot}069Pl_1 + 0{\cdot}017H_2O + 25{\cdot}935Qtz + 3{\cdot}643Na_{0.5}K_{0.5}Cl = 3{\cdot}566Cpx + 3{\cdot}466melt + 0{\cdot}193Ilm + 3{\cdot}909Pl_2 + 3{\cdot}366HCl$ (rNK26-2)
Pl_1: $K_{0.01}Na_{0.55}Ca_{0.41}Al_{1.42}Si_{2.59}O_8$	$Bt_1 + 3{\cdot}561Pl_1 + 0{\cdot}077H_2O + 12{\cdot}636Qtz + 1{\cdot}689Na_{0.5}K_{0.5}Cl = 0{\cdot}305Bt_2 + 0{\cdot}968Cpx + 1{\cdot}801melt + 0{\cdot}086Ilm + 1{\cdot}612Pl_2 + 1{\cdot}545HCl$ (rNK26-3)
Pl_2: $K_{0.05}Na_{0.62}Ca_{0.28}Al_{1.27}Si_{2.74}O_8$	
Cpx: $Na_{0.04}Ca_{0.67}Fe_{0.64}Mg_{0.61}Al_{0.04}Si_2O_6$	
melt: $K_{0.83}Na_{0.98}Ca0{\cdot}2Fe_{0.2}Mg_{0.05}Al_{2.19}Ti_{0.03}Si_{9.67}Cl_{0.08}O_{24}$	
Ilm: $FeTiO_3$	
Qtz: SiO_2	
Fluid components: H_2O, $K_{0.5}Na_{0.5}Cl$, HCl	

(continued)

Table 4: Continued

Phase compositions used in calculations	Reactions
Run NK27	
Bt_1: $KFe_{1.37}Mg_{1.02}Al_{1.38}Ti_{0.21}Si_{2.81}O_{10}(OH)_2$	$Bt_1 + 0.164Bt_2 + 5.934Pl_1 + 0.313H_2O + 30.651Qtz + 1.149NaCl + 2.183KCl = 0.512Amph_2 + 1.456Cpx$
Bt_2: $KFe_{1.34}Mg_{1.11}Al_{1.34}Ti_{0.21}Si_{2.81}O_{10}(OH)_2$	$+ 7.532melt + 0.216Ilm + 4.471HCl$ (rNK27-3)
$Amph_1$: $K_{0.27}Na_{0.38}Ca_{1.92}Fe_{2.67}Mg_{1.86}Al_{1.95}Ti_{0.13}Si_{6.52}O_{22}(OH)_2$	$Bt_2 + 0.002Amph_1 + 3.146Pl_1 + 0.071H_2O + 15.249Qtz + 0.714NaCl + 0.788KCl = 0.418Amph_2 + 2.400melt + 0.058Ilm + 1.310HCl$ (rNK27-2)
$Amph_2$: $K_{0.22}Na_{0.57}Ca_{1.72}Fe_{2.05}Mg_{2.38}Al_{1.85}Ti_{0.25}Si_{6.59}O_{22}(OH)_2$	$Bt_1 + 1.359Bt_2 + 9.614Pl_1 + 0.389H_2O + 48.427Qtz + 1.992NaCl + 3.081KCl = 1.509Cpx + 4.732melt + 0.150Ilm + 2.954HCl$ (rNK27-1)
Pl_1: $K_{0.01}Na_{0.55}Ca_{0.41}Al_{1.42}Si_{2.59}O_8$	
Cpx: $Na_{0.04}Ca_{0.86}Fe_{0.39}Mg_{0.64}Al_{0.06}Si_2O_6$	
melt: $K_{0.72}Na_{0.92}Ca_{0.24}Fe_{0.18}Mg_{0.05}Al_{2.10}Ti_{0.02}Si_{9.78}Cl_{0.08}O_{24}$Ilm: $FeTiO_3$	
Qtz: SiO_2	
Fluid components: H_2O, KCl, NaCl, HCl	
Run NK29	
Bt_1: $KFe_{1.38}Mg_{1.11}Al_{1.30}Ti_{0.22}Si_{2.81}O_{10}(OH)_2$	$Bt_2 + 0.914Amph_1 + 5.590Pl_1 + 1.509H_2O + 44.211Qtz + 0.475NaCl + 6.901KCl = 4.449Cpx$
Bt_2: $KFe_{1.415}Mg_{1.28}Al_{1.11}Ti_{0.14}Si_{2.93}O_{10}(OH)_2$	$+ 5.902melt + 0.081Ilm + 6.845HCl$ (rNK29-1)
$Amph_1$: $K_{0.30}Na_{0.32}Ca_{1.92}Fe_{2.78}Mg_{1.79}Al_{2.08}Ti_{0.11}Si_{6.43}O_{22}(OH)_2$	$Bt_2 + 0.618Amph_1 + 5.133Pl_1 + 1.331H_2O + 35.399Qtz + 6.297KCl = 3.647Cpx + 4.410melt + 0.088Ilm + 1.506Kfs + 5.900HCl$ (rNK29-2)
Pl_1: $K_{0.01}Na_{0.55}Ca_{0.41}Al_{1.42}Si_{2.59}O_8$	
Cpx: $Na_{0.08}Ca_{0.83}Fe_{0.49}Mg_{0.63}Al_{0.02}Si_{1.99}O_6$	
melt: $K_{1.39}Na_{0.60}Ca_{0.06}Fe_{0.27}Mg_{0.03}Al_{1.82}Ti_{0.03}Si_{9.95}Cl_{0.09}O_{24}$	
Kfs: $K_{0.92}Na_{0.08}AlSi_3O_8$	
Ilm: $FeTiO_3$	
Qtz: SiO_2	

Fluid components: H_2O, KCl, NaCl, HCl. Subscripts 1 denote phases that are considered to be of the primary assemblage; subscripts 2 denote phases or zones of relic phases contacting reaction textures, which are considered to be formed during the experiments.

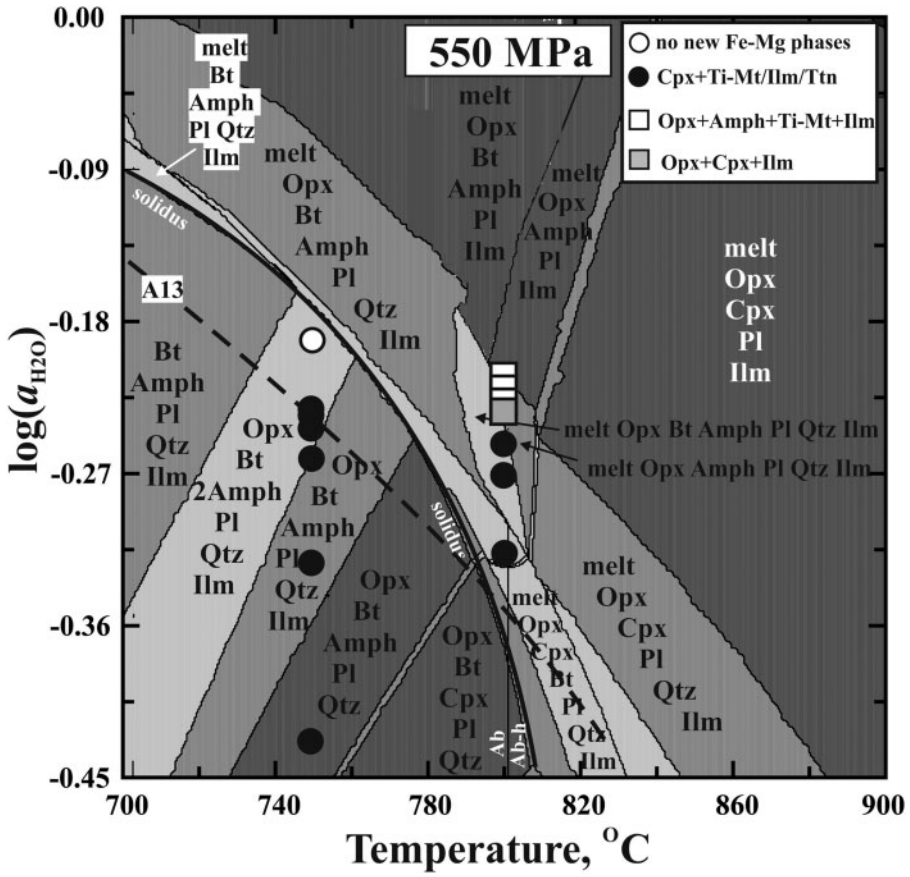

Fig. 14. Conditions and products of experiments with H_2O–CO_2 fluids containing variable concentrations of KCl in comparison with phase assemblages predicted by a T–a_{H2O} pseudosection constructed using the PERPLEX software for the Sand River biotite–hornblende gneiss at 550 MPa. Data points at 750°C are (from top to bottom) runs l, K2, K3, K4, K5, K6, and K7 in Table 2; data points at 800°C are (from top to bottom) runs 24, K3l, K32, K33, K8, K9, and K10 in Table 2. The log(a_{H2O}) values are calculated from the a_{H2O} values reported in Table 2. Only principal phase fields are labeled. All phase fields contain a free fluid phase. Dashed line marked Al3 is the minimum melting curve for the system Ab–San–Qtz–KCl–NaCl–H_2O approximated from fig. 6 of Aranovich *et al.* (2013).

and Na_2O only. Clinopyroxene-bearing assemblages are predominant at elevated a_{K2O} and a_{Na2O} over a wide range of a_{H2O}. The pseudosection a_{H2O}–a_{K2O} shows that titanite is stable instead of ilmenite at high a_{K2O} in correspondence to reaction (5b) and the results of our experiments. The appearance of kalsilite at high a_{K2O} (Fig. 16a) is also consistent with the observation of this phase in the products of run K10 (Table 2). The a_{H2O}–a_{Na2O} pseudosection (Fig. 16b) indicates that an increase of a_{Na2O} significantly expands the stability of amphibole in assemblages with clinopyroxene.

Figure 14 shows that runs involving H_2O–CO_2–KCl fluids at 800°C are above the melting curve of the haplogranite Or–Ab–Qtz minimum in the presence of H_2O–KCl–NaCl fluids (Aranovich *et al.*, 2013) and the calculated solidus. However, our experiments show that the degree of melting decreases with increasing KCl concentration in the fluid. This observation is consistent with the pseudosection a_{H2O}–a_{K2O} (Fig. 16a), which shows a generally negative slope for the solidus curve. The position of the solidus indicates that an increase of a_{K2O} at constant or decreasing a_{H2O} suppresses melting. In contrast, no melts form at 750°C in the presence of H_2O–CO_2–KCl fluids (Table 2; Fig. 3a and b). However, addition of NaCl causes extensive melting at this temperature, despite the fact that T–a_{H2O} conditions of the runs at both 800 and 750°C with H_2O–CO_2–(Na, K)Cl and H_2O–CO_2–NaCl fluids are significantly below the melting curve of albite–H_2O–NaCl (Shmulovich & Graham, 1996). The negative slope of the 'melt-in' boundary in Fig. 15a, which arbitrarily defines the appearance of a melt at 750°C, suggests that melting should be promoted by a decrease of X_{salt} and KCl/(KCl + NaCl) ratio in the fluid. The pseudosection a_{H2O}–a_{Na2O} (Fig. 16b) demonstrates significant expansion of the melt-bearing phase fields toward the lower a_{H2O} in comparison with the pseudosection a_{H2O}–a_{K2O} (Fig. 16b). This theoretical result supports an observation of much active melting in the presence of NaCl. In our opinion,

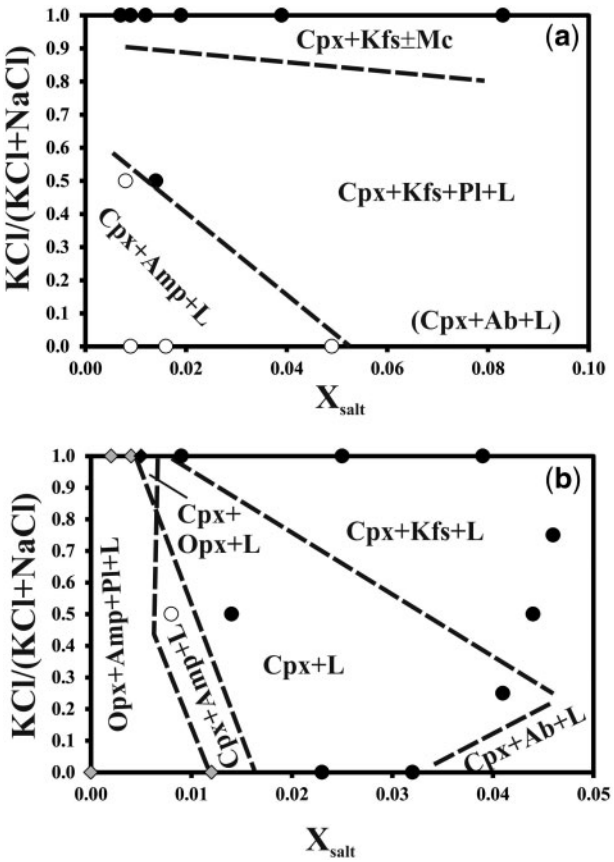

Fig. 15. Schematic grids of mineral assemblages formed by interaction of the biotite–amphibole gneiss with H_2O–CO_2, H_2O–CO_2–KCl, H_2O–CO_2–KCl–NaCl and H_2O–CO_2–NaCl fluids at (a) 750°C and (b) 800°C in dependence on the (X_{salt}) chloride/($H_2O + CO_2$) and KCl/(KCl + NaCl) ratios of the fluid. Dashed lines marking boundaries between assemblages are arbitrary. Black circles, Cpx + L, Cpx + Kfs, Cpx + Kfs + L, and Cpx + Pl + Kfs + L assemblages; open circles, Cpx + Amp + L assemblage; gray rhombs, Opx + Amp + L assemblage; black rhomb, Opx + Cpx + L assemblage.

the additional reason for the intensification of melting in presence of NaCl is the higher solubility of both Cl (Fig. 13c) and CO_2 as CO_3^{2-} species in sodic melts that form in equilibrium with NaCl-bearing fluids in comparison with the potassic melts that form in equilibrium with KCl-rich fluids. Higher solubility of volatiles in sodic melts thus assists with the initiation of melting.

Thus, the above pseudosections are in a perfect agreement with our experimental results and support the idea that specific mineral assemblages and reactions occurring in gneiss that has interacted with H_2O–CO_2–(K, Na)Cl fluids vitally depend on the activities of alkali components imposed by KCl and NaCl, whereas water activity serves only as an additional factor. The data points on the pseudosection in Fig. 14 are plotted assuming that the water activity in the equilibrium fluid was similar to the water activity in the starting fluid (Table 2). However, the equilibrium water activity in the fluids could be different from that in the starting fluid because of compositional modifications of the fluids during the course of re-equilibration with the gneiss. The presence of quartz, carbonate (runs 24 and K32), and an Al_2O_3 phase (run N13) daughter crystals in the bubble voids in glasses points to active dissolution of silicates and carbonates in the chloride-bearing fluids (e.g. Manning, 2013). The K–Na exchange with the gneiss is another way to modify the KCl- or NaCl-bearing fluid. For example, the K/(K + Na) ratio of amphiboles produced by the H_2O–CO_2–KCl and H_2O–CO_2–(K, Na)Cl fluids is always lower in comparison with the original hornblende (Fig. 6b; Supplementary Material, Table S2). This reflects K/(K + Na) equilibrium ratios in the fluid that were lower than in the starting H_2O–CO_2–KCl fluid owing to active K–Na–Ca exchange reactions between the chloride-bearing fluid and plagioclase. Along with modification of the KCl/(KCl + NaCl) molar ratio, X_{salt} in the fluid can also change because of the active partitioning of alkalis between the crystalline phases (feldspar, amphibole) and melt during reactions of chlorides with silicates (Table 4) and, thus, an increase of the fluid pH via the hydrolysis effect (Manning, 2013; Manning & Aranovich, 2014). Preferential dissolution of water in the melt would shift the fluid composition towards higher contents of CO_2 and chlorides and cause displacement of the bulk fluid composition toward the miscibility gap (Shmulovich & Graham, 2004; Aranovich *et al.*, 2010), assisting in the development of two low water activity fluids. However, the complex influence of the above effects on water activity in a fluid-dominated system cannot be fully predicted on the basis of our experiments and demands further investigation.

Melting of tonalite in the presence of H_2O–CO_2–chloride fluids and petrogenesis of A-type granitoid magmas

The compositions of melts produced in equilibrium with H_2O–CO_2–KCl fluids with X_{salt} up to about 0·009 and H_2O–CO_2–(K, Na)Cl fluids with X_{salt} up to about 0·014 at 800°C are comparable with the compositions of melts that result from dehydration and hydrous melting of tonalite (Rutter & Wyllie, 1988; Skjerlie & Johnston, 1993; Patiño Douce & Beard, 1995; Patiño Douce, 1997; Gardien *et al.*, 2000; Watkins *et al.*, 2007). Nevertheless, melts in the presence of KCl-bearing fluids clearly have lower Al_2O_3 concentrations and higher MALI indices in comparison with melts produced by dehydration and hydrous melting of tonalite (Fig. 17a and b). The higher the KCl content of the starting fluid the lower is the Al_2O_3 content of the melt (Fig. 10). This effect is probably related to the crystallization of K-feldspar that binds Al in the presence of KCl-rich fluids. The FeO/(FeO + MgO) ratios of melts produced in experiments with H_2O–CO_2 and

chloride-poor fluids are similar to those of melts formed by dehydration and hydrous melting. However, this ratio is much higher (>0·9) for melts that equilibrated with chloride-rich fluids (Fig. 17c) reflecting the effect of Fe–Cl affinity in the melt (Webster & De Vivo, 2002). Melts produced in experiments with fluids with $X_{KCl} > 0{\cdot}009$ (runs K8 and K10 in Table 3) or $X_{KCl+NaCl} > 0{\cdot}04$ (runs NK28 and NK29 in Table 3) are characterized by very low CaO contents (0·7–0·2 wt %), which is related to stabilization of clinopyroxene in equilibrium with these melts.

Increasing X_{salt} in the H_2O–CO_2–KCl and H_2O–CO_2–(K, Na)Cl fluids up to about 0·02 results in the formation at 800°C of peralkaline rhyolitic (granitic) melts characterized by low Al_2O_3 (<13·5 wt %), low CaO (<2 wt %), high $K_2O + Na_2O$ (>7 wt %), $FeO/(FeO + MgO) > 0{\cdot}8$ and $K_2O/Na_2O > 1$, which are moderately enriched in Cl (0·2–0·6 wt %). These melts coexist with predominantly non-hydrous assemblages (Cpx + Kfs + Pl ± Opx ± Amph) that reflect the low a_{H2O} of such melts. These characteristics are exactly those of the so-called non-orogenic ferroan (A-type) granitoids (Loiselle & Wones, 1979; Collins *et al.*, 1982; Whalen *et al.*, 1987; Eby, 1990; Creaser *et al.*, 1991; Martin, 2006; Bonin, 2007; Frost & Frost, 2011), which vary in composition from quartz syenite to peralkaline granite (Fig. 18a–c). Some models suggest that the magmas producing these granitoids might represent the products of high-temperature, vapour-absent partial melting of lower- and middle-crustal rocks, either a geochemically depleted F- and/or Cl-enriched dry granulitic source (Collins *et al.*, 1982; Whalen *et al.*, 1987; Clemens *et al.*, 1986; Landenberger & Collins, 1996; Rajesh, 2008) or a tonalitic or granodioritic I-type source (Anderson, 1983; Creaser *et al.*, 1991). Experimental studies show that dehydration melting of tonalite produces granitic melts with notably higher Al_2O_3 contents than A-type melts (Skjerlie & Johnston, 1993; Patiño Douce, 1997; Watkins *et al.*, 2007). Even low-pressure (about 400 MPa) dehydration melting of tonalite and granodiorite (e.g. Patiño Douce, 1997) cannot reproduce all the characteristics of A-type granitoids. According to some studies (e.g. Litvinovsky & Podladchikov, 1993), the mechanism of dehydration melting is shown to be questionable for the formation of intraplate A-type granitoid massifs, and the input of H_2O, alkalis and halogens must accompany formation of these complexes.

Many studies advocate an important role for halogens in the formation of ferroan (A-type) granitoid complexes (Collins *et al.*, 1982; Whalen *et al.*, 1987; Abdel-Rahman & Martin, 1990; Litvinovsky & Podladchikov, 1993; Skjerlie & Johnston, 1993; Martin, 2006). Most attention is paid to F, the concentration of which in A-type granites could be as high as 1·5–1·7 wt % (Eby, 1990). Skjerlie & Johnston (1993) experimentally showed that such concentrations of F in granitic melts could be reached via partial melting of tonalite gneiss, which contains F-bearing biotite and amphibole. Enrichment in F in the glasses produced in our experiments (Table 3) supports this conclusion.

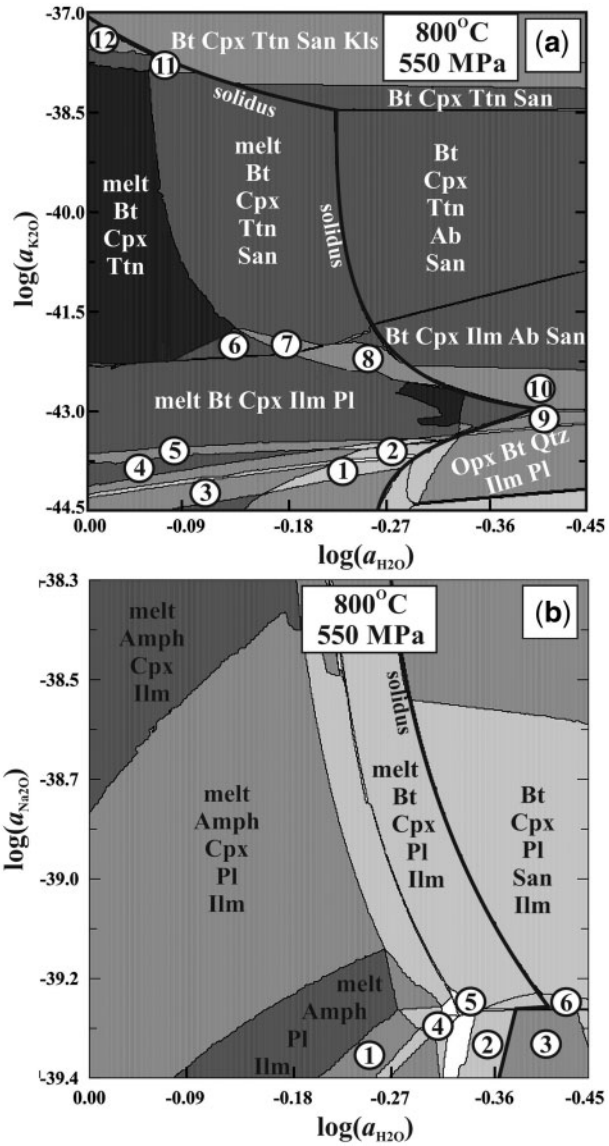

Fig. 16. a_{H2O}–a_{K2O} (a) and a_{H2O}–a_{Na2O} (b) pseudosections constructed using the PERPLEX software for the Sand River biotite–hornblende gneiss at 800°C and 550 MPa. Only the principal phase fields are labeled. All phase fields contain a free fluid phase. Numbered phase fields in (a): 1, melt, Opx, Amph, Qtz, Ilm, Pl; 2, melt, Opx, Amph, Bt, Ilm, Pl, Qtz; 3, melt, Opx, Amph, Ilm, Pl; 4, melt, Bt, Amph, Ilm, Pl; 5, melt, Bt, Amph, Cpx, Ilm, Pl; 6, melt, Bt, Cpx, Ttn, Pl; 7, melt, Bt, Cpx, Ttn, San, Pl; 8, melt, Bt, Cpx, Ilm, San, Pl; 9, Opx, Cpx, Bt, Ilm, Pl, Qtz; 10, Bt, Cpx, Ilm, San, Pl; 11, melt, Bt, Cpx, Ttn, San, Kls; 12, melt, Bt, Cpx, Ttn, Kls. Numbered phase fields in (b): 1, melt, Opx, Amph, Pl, Ilm; 2, melt, Opx, Bt, Pl, Qtz; 3, Opx, Bt, Pl, Qtz; 4, melt, Opx, Amph, Pl, Qtz, Ilm; 5, melt, Opx, Cpx, Bt, Pl, Ilm; 6, Cpx, Bt, Pl, San, Qtz.

Chlorine does not exceed 0·2 wt % in A-type granitoids (Eby, 1990; Fig. 13a–c). Collins *et al.* (1982) noted that Cl is more abundant in peralkaline members of the A-type series. In the above partial melting models, halogens in the A-type granites are considered to result from enrichment of these components in the source, either dehydrated granulite or tonalite. However, Martin (2006) (see also Abdel-Rahman & Martin, 1990) proposed that the formation of ferroan (A-type) granitic magmas is closely related to extensive alkali metasomatism of the crust by mantle-derived alkali–halogen H_2O–CO_2 fluids in rift-related tectonic settings. The metasomatism fenitized and fertilized the refractory lower crust and prepared the precursor source for melting to form both granitic and more alkalic (syenitic, nepheline syenitic) melts. Aranovich *et al.* (2013) experimentally found an increase in the orthoclase content of minimum melts in the haplogranite system with increasing salt concentration in coexisting H_2O–NaCl–KCl fluids and concluded that the compositions of K-rich granites, including A-type granites, are better explained by melting in the presence of aqueous–salt solutions rather than H_2O–CO_2 fluids. Our present experiments reproduce the model of Martin (2006) and expand the conclusions of Aranovich *et al.* (2013, 2014) to H_2O–CO_2–salt fluids and natural systems. The compositional characteristics of the melts produced in our experiments perfectly fit the compositional characteristics of A-type granitoids (Fig. 18a–c). The higher the salt content in the starting fluid the closer are the compositional parameters to those of A-type rocks. However, at X_{KCl} above 0·02 (Table 2), the H_2O–CO_2–KCl fluids produce melts with compositions that are highly unusual for natural granitoid magmas (very low Al_2O_3, ASI about 0·4 and A/NK $< 0·5$). This suggests that such concentrations of KCl are not realistic for the aqueous–carbonic fluids provoking melting of tonalite gneisses with the resultant formation of A-type granitoid associations.

Our experimental results also provide insights into the genetic relationships between granites and the more basic and alkalic members (syenites, monzonites, nepheline syenites) of A-type complexes. An increase of the NaCl/KCl ratio of the fluid and a decrease in temperature from 800 to 750°C assists in the formation of trachytic and trachyandesitic melts similar to syenites and monzonites (Fig. 9a and b). The silica-undersaturated composition of the melts from runs N13 and N12 (Tables 2 and 3) furthermore suggests that in the extreme case this process can result in the formation of nepheline-bearing assemblages. Compositional trends of melts produced from tonalite gneiss in the presence of H_2O–CO_2–(K, Na)Cl fluids at 800 and 750°C closely reproduce the compositional trends of rocks from ferroan (A-type) granitoid complexes that vary from peralkaline granite to syenite and monzonite (Fig. 19a and b). For example, formation of syenitic and feldspathoidal syenitic rocks via metasomatic transformation (fenitization) and subsequent partial melting of Archean tonalitic rocks has been proposed by Bea *et al.* (2001) for the Soustov intrusive complex in the Kola Peninsula. Those researchers suggested that this transformation proceeded via influx of H_2O–CO_2 fluids enriched in alkali chlorides released by mantle-derived magmas. Participation of such fluids is clearly reflected in the composition of the syenites, which contain up to 0·47 wt % Cl (Fig. 13a–c). Thus, the granite-to-syenite series of rocks in A-type complexes could be interpreted to have resulted from the progressive melting of tonalitic gneiss in the crustal basement under the influence of aqueous–carbonic fluids that are variably enriched in alkali salt components with variable K/Na ratios.

The metasomatic transformation of tonalitic gneiss seems to be an essential step in the formation of diverse granitoid and syenitic magmas. Experiments show that such transformation mostly leads to the formation of anhydrous pyroxene-bearing assemblages after biotite and hornblende. This has implications for the relationship between ferroan (A-type) granitoids and syenites and charnockites (Landenberger & Collins, 1996; Rajesh, 2008). From the results of our experiments the charnockite–granite–syenite link could be explained by variations in the fluid composition, particularly variations in the salinity of the fluids. Charnockites formed from precursor tonalite gneisses via H_2O–CO_2 low-salinity fluids transform to potassic A-type granitoids and, subsequently, to syenites with an increase in the fluid KCl concentration. For example, associations of charnockite with A-type plutons, which include both granitic and quartz-syenitic members, are well documented in southwestern India (Rajesh, 2008, and references therein). Local formation of charno-enderbitic veins, accompanied by syenitization (i.e. local formation of the Cpx ± Opx ± Kfs assemblage), in the Sand River Gneisses in the eastern part of the Central Zone of the Limpopo Complex, South Africa (Safonov *et al.*, 2012; Rajesh *et al.*, 2013), can be correlated by age (~2·0 Ga) with a large syenite body known as the Madiapala Complex in the western part of the Central Zone, suggesting that there may be a link between charnockite and syenite formation.

Application to dehydration zones in transitional amphibolite- to granulite-facies terrains

Our data on the dependence of mineral assemblages on temperature, salinity and the K/Na ratio in fluids allow speculation on mineral assemblages in local-scale and regional dehydration zones in Precambrian terrains. In most cases, they represent orthopyroxene-bearing assemblages developed after biotite–amphibole tonalitic gneisses, usually referred to as 'incipient charnockites' [see review

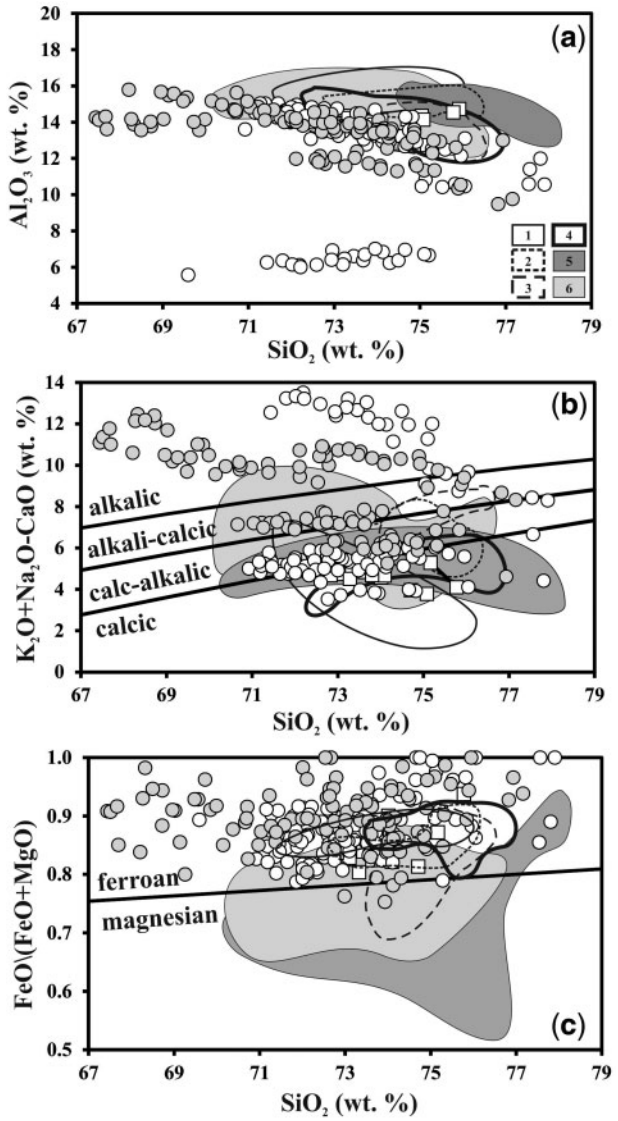

Fig. 17. Comparison of melts produced from partial melting of the gneiss in the presence of H_2O–CO_2, H_2O–CO_2–KCl and H_2O–CO_2–(K, Na)Cl fluids at 800°C (symbols as in Fig. 9) in terms of Al_2O_3 content (a), the MALI (b), and FeO/(FeO + MgO) ratio (c). The results are compared with fields for melts formed during dehydration and hydrous melting of tonalite at pressures of 400–1000 MPa as follows: 1, biotite gneiss (Bt + Pl + Qtz with minor K-feldspar, titanite, apatite, epidote) at 1000 MPa and 4 wt % H_2O (Gardien *et al.*, 2000); 2, hornblende-bearing biotite gneiss at 600 and 1000 MPa without fluid (Skjerlie & Johnston, 1993); 3, biotite–hornblende tonalite with K-feldspar and biotite–hornblende granodiorite at 400 and 800 MPa, vapor-absent (Patiño Douce, 1997); 4, hornblende and biotite tonalites at 800 and 1000 MPa, vapor-absent (Watkins *et al.*, 2007); 5, hornblende and biotite tonalites at 600 MPa with H_2O (Watkins *et al.*, 2007); 6, synthetic biotite gneiss at 300, 500, 700, and 1000 MPa, vapor-absent (Patiño Douce & Beard, 1997). The discrimination lines between calcic, calc-alkalic, alkali-calcic, and alkalic granites in (b) and ferroan and magnesian granites in (c) are after Frost *et al.* (2001).

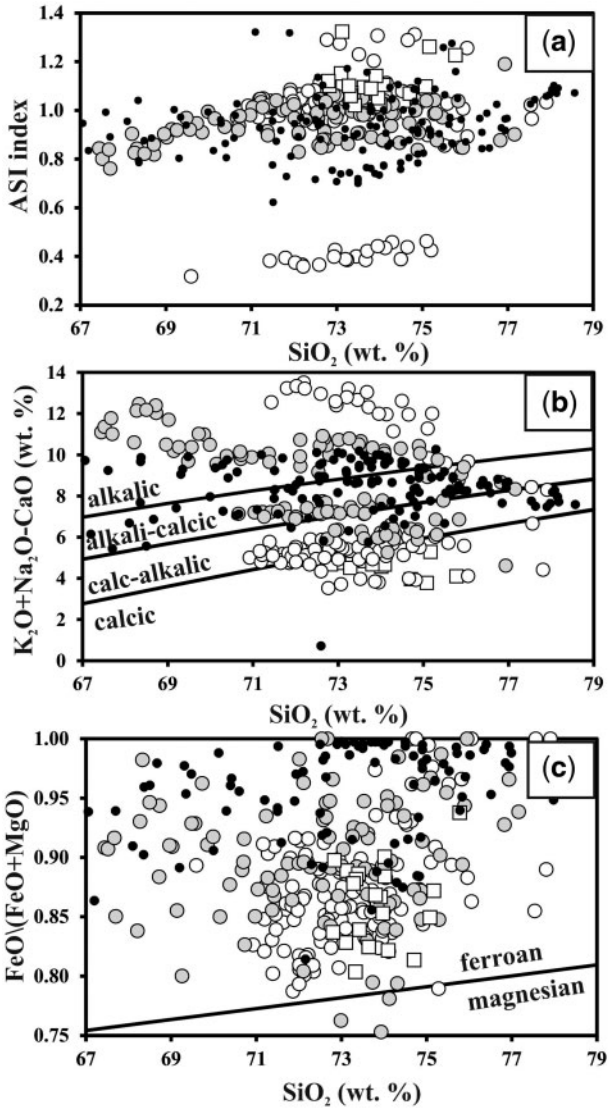

Fig. 18. Composition of melts produced from partial melting of the gneiss in the presence of H_2O–CO_2, H_2O–CO_2–KCl and H_2O–CO_2–(K, Na)Cl fluids at 800°C (symbols as in Fig. 9) compared with the compositions of A-type granites (black circles) (data from Eby, 1990) in terms of (a) ASI vs SiO_2, (b) MALI vs SiO_2, (c) FeO/(FeO + MgO) vs SiO_2.

and references given by Newton & Tsunogae (2014)]. Most researchers agree that their formation is a result of the passage of low-a_{H2O} fluids through the rocks at temperatures of 700–800°C and pressures of 500–700 MPa. Instead of a CO_2-rich fluid (e.g. Newton, 1986), preference is now given to more complex fluids involving both CO_2-rich and aqueous–salt portions (Hansen *et al.*, 1995; Newton, 1995; Newton *et al.*, 1998; Perchuk *et al.*, 2000; Ravindra Kumar, 2004). Clinopyroxene is very rare in the incipient charnockites of southern India and Sri Lanka

(e.g. Janardhan *et al.*, 1982). Perchuk *et al.* (2000) mentioned the presence of Al-poor clinopyroxene in a charnockite patch from the Kurunegala quarry (Sri Lanka); clinopyroxene was found in a leucocratic zone that surrounds the Opx- and Bt-bearing core of the charnockite patch. This zone is inferred to be of metasomatic origin formed via an increase of alkali activity in the fluid that transformed the gneiss to charnockite at about 700°C and 500–600 MPa. The results of our study support the conclusion that at constant temperature the appearance of clinopyroxene should reflect higher salinity of the fluid acting in the periphery of the charnockite patch in comparison with the core. From this point of view veins and patches of incipient charnockite exclusively containing orthopyroxene should be considered as dehydration zones that were initially produced by relatively low-salinity H_2O–CO_2 fluids at temperatures about 750–800°C.

Two-pyroxene-bearing local-scale dehydration zones have been documented in some gneissic terrains (Knudsen & Lidwin, 1996; Harlov *et al.*, 2006; Harlov, 2012; Safonov *et al.*, 2012; Rajesh *et al.*, 2013). Clinopyroxene in these zones shows a regular spatial distribution in close proximity to contacts with veins of charnockitic or enderbitic composition. This implies that crystallization of clinopyroxene in the dehydration zones was controlled not only by isochemical breakdown of amphibole (Knudsen & Lidwin, 1996; Harlov *et al.*, 2006), but also by the distribution or activity of fluid species. For dehydration zones within amphibole-rich mafic granulites of the Bamble sector (southern Norway), Knudsen & Lidwin (1996) noted that clinopyroxene appears at the immediate contact of orthopyroxene-bearing dehydration zones with enderbitic veins and concluded that the dehydration zones evolved under the influence of a complex (apparently heterogeneous) CO_2-, nitrogen- and chloride-rich brine at temperatures of 790–840°C and pressures of 590–910 MPa. Harlov *et al.* (2006) found that a similar dehydration zone developed at 650–700°C and pressures of 700–800 MPa around a clinopyroxene-bearing pegmatoid dyke in granitic gneisses at the Söndrum stone quarry (SW Sweden), which was zoned with respect to the distribution of clinopyroxene and orthopyroxene. Clinopyroxene occurs only over a short distance from the contact with the dyke or at the immediate contact with the host gneiss, whereas most of the dehydration zone is composed of an orthopyroxene-bearing rock with only minor clinopyroxene. Data from fluid inclusions and the log (f_{H2O}/f_{HCl}) value calculated by Harlov *et al.* (2006) show that the clinopyroxene-rich portion of the dehydration zone adjacent to the granitic dyke is related to fluids of higher salinity with respect to the orthopyroxene-rich portion. The source of these fluids is assumed to be melts from the dyke. Harlov *et al.* (2006) explained the appearance of clinopyroxene (and coexisting hornblende) by an increase in the Ca activity of the fluids within discrete portions of the dehydration zone. Our experiments show that the major reason for the apparent increase of Ca activity is more active participation of plagioclase in the reactions with increasing salinity of the fluids. Safonov *et al.* (2012) and Rajesh *et al.* (2013) documented the presence of clinopyroxene (+ rare orthopyroxene) and K-feldspar after biotite in amphibole–biotite gneiss that surrounds clinopyroxene-free charno-enderbite veins developed within shear zones at the Causeway locality, Limpopo Complex, South Africa. Safonov *et al.* (2012) showed that the clinopyroxene-bearing assemblage at the periphery of the dehydration zone was formed at lower temperature (below 750°C) than the veins (about 800°C) via a reaction similar to (1a). Those researchers suggested that the prevalence of clinopyroxene over orthopyroxene in the partially dehydrated gneiss corresponds to a higher K activity during the local formation of a two-pyroxene–K-feldspar coronitic assemblage compared with the formation of an

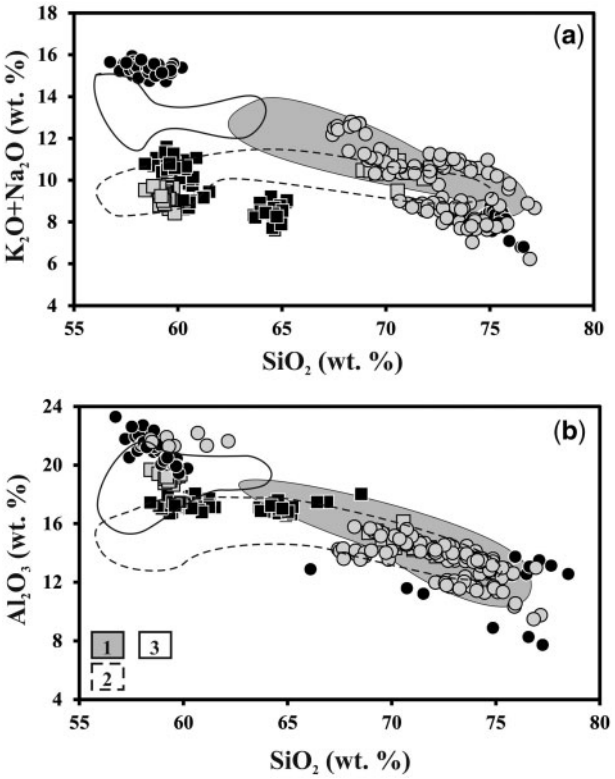

Fig. 19. Composition of melts produced from partial melting of the gneiss in the presence of H_2O–CO_2–NaCl fluids (black squares, 750°C; black circles, 800°C) and H_2O–CO_2–(K, Na)Cl fluids (gray squares, 750°C; gray circles, 800°C) compared with fields for the following compositions: 1, granitic and syenitic rocks from the A-type suites of the Bryansky Complex, Transbaikalia, Russia (Litvinovsky *et al.*, 2002); 2, the Red Mountain pluton, Wyoming, USA (Anderson *et al.*, 2003); 3, syenitic rocks of the Soustov complex, Kola Peninsula, Russia (Bea *et al.*, 2001).

orthopyroxene–K-feldspar assemblage in the charnoenderbitic vein, where clinopyroxene is absent. This conclusion is supported by our experiments.

Following our experimental results, the above examples suggest that the distribution of orthopyroxene and clinopyroxene could serve as an indicator of heterogeneity in the salinity of fluids within dehydration zones. Clinopyroxene-bearing assemblages would represent domains in dehydration zones that were affected by more saline fluids compared with domains in which orthopyroxene predominates. The above examples indicate that such heterogeneity is probably controlled by melts that expelled fluids of different salinity during their cooling and solidification (Kilink & Burnham, 1972; Shmulovich & Graham, 1996; Webster, 1997). Additional reasons for variations in the fluid salinity within specific dehydration zones include temperature changes, fluid–mineral reactions consuming either salt components or water (Trommsdorf *et al.*, 1985; Kullerud, 1996; Markl *et al.*, 1998; Scambelluri *et al.*, 1998; van den Kerkhof & Grantham, 1999; Yardley & Graham, 2002), and immiscibility within the salt-bearing fluid systems (e.g. Gilbert *et al.*, 1998).

Regular distribution of orthopyroxene and clinopyroxene is also deduced for regional-scale amphibolite-to-granulite transition zones (Harlov & Förster, 2002; Hansen & Harlov, 2007). Hansen & Harlov (2007) noted that a gradual transition from biotite–amphibole gneisses to charnockitic gneisses across a 95 km traverse in the Shevaroy Block, Tamil Nadu, southern India, occurred through a 30 km wide intermediate zone of clinopyroxene-bearing rocks. They specifically noted that the Cl contents of biotite, fluorapatite and amphibole in the clinopyroxene-bearing zone are higher compared with both the amphibolite and orthopyroxene-bearing zones. The action of saline fluids in the traverse is recorded in the rocks by K-feldspar micro-veining, the specific relationships of accessory minerals, and the depletion of the rocks in Rb, Cs, U and Th, supporting a model 'in which concentrated low H_2O activity brines migrated upwards from a source lower in the crust' (Hansen & Harlov, 2007, p. 1678) possibly locally accompanied by partial melting. Our experiments suggest that more saline fluids could represent a front of migrating fluid that provoked the formation of clinopyroxene-bearing assemblages. The additional factor for formation of the 'clinopyroxene front' could be a drop in temperature towards the amphibolite zone.

CONCLUSIONS

(1) Variations in the bulk chloride concentration and KCl/NaCl ratio of infiltrating H_2O–CO_2–(K, Na)Cl fluids at varying temperatures provoked the formation of diverse mineral assemblages after biotite–amphibole tonalitic gneiss. In most cases, chloride-rich fluids are responsible for the formation of anhydrous assemblages, reflecting the low water activity of these fluids (Aranovich & Newton, 1996, 1997, 1998; Schmulovich & Graham, 1996; Newton & Manning, 2010).

(2) Regular variations in mineral assemblage with the bulk chloride concentration and KCl/NaCl ratio of the fluid define an alkalinity facies, which, in general, reproduces a scheme suggested by Korzhinskii (1959) for granitoid rocks, and also mineralogical criteria for alkali activity suggested by Perchuk & Gerya (1993).

(3) Orthopyroxene-bearing charnockitic and mangeritic assemblages form at a temperature of 800°C and reflect the lowest salt concentration (alkali activity) in the fluids. Increase of the salt concentration (alkali activity) in the fluid and/or decrease of temperature (750°C) results in the stability of clinopyroxene with either K-feldspar or albite, depending on the predominant chloride component in the fluid. The aegirine content in clinopyroxene is a reflection of the salt content (alkali activity) of the fluids. Formation of amphibole is restricted to H_2O–CO_2–(K, Na)Cl fluids with relatively low concentrations of salts. The composition of amphibole is a sensitive indicator of the KCl/NaCl ratio of the fluids. Pargasite–edenite amphiboles form in equilibrium with the fluids if KCl is the predominant chloride component. With increasing NaCl content of the fluid the composition of the amphibole shifts toward winchite, barroisite or richterite. Experiments showed that KCl–NaCl-rich H_2O–CO_2 fluids provoke formation of silica-undersaturated assemblages, with characteristics close to those of fenites.

(4) Interaction of biotite–amphibole gneiss with H_2O–CO_2–(K, Na)Cl fluids at 750–800°C is accompanied by extensive partial melting, although the reaction progress vitally depends on temperature and the NaCl/KCl ratio of the fluid. Addition of NaCl significantly intensifies melting at both 750 and 800°C, whereas the presence of KCl suppresses melting.

(5) Interaction of biotite–amphibole gneiss with H_2O–CO_2–(K, Na)Cl fluids at 750–800°C results in the production of a wide spectrum of melts depending on temperature, salt concentration and the KCl/NaCl ratio of the fluid. At 800°C, KCl-dominated fluids lead to the formation of CaO- and Al_2O_3-poor rhyolitic melts with alkali contents that directly depend on the salt concentration of the fluid that provoked melting. In contrast, the presence of NaCl-dominated fluids shifts the composition of the melts towards SiO_2-poorer compositions. Decreasing temperature assists in the production of such SiO_2-poor melts.

(6) The present experiments demonstrate an importance of the aqueous–carbonic–salt fluids in the formation of ferroan A-type granite–syenite complexes by anatexis of tonalite–trondhjemite gneisses and suggest a possible link of these complexes with dehydration zones in amphibolite- to granulite-facies terrains in the middle crust.

ACKNOWLEDGEMENTS

The authors thank Leonid Aranovich, Daniel Harlov, Bernardo Cesare, Antonio Acosta-Vigil and an anonymous reviewer for their very detailed comments on two previous versions of the paper, which was greatly modified as a result. We thank Jörg Hermann for his organization of the reviews and for additional useful comments and support, and Jamie Connolly for consultation and providing additional options for the calculation of phase equilibria using the PERPLE_X software. We thank Konstantin Van, Alexei Nekrasov and Dmitrii Varlamov (group of microprobe analysis and microscopy, IEM RAS), Vasily Yapaskurt and Vasily Shcherbakov (Laboratory of Local Methods of Analysis, Department of Petrology, MSU) for assisting with the microprobe analyses, and Pavel Pletchov (Department of Petrology, MSU) for providing the facilities for the Raman analysis of the glasses in the run products.

FUNDING

The study was supported by the Russian Scientific Fund (project 14-17-00581 to O.G.S.). At the beginning, the study was supported by the Russian Foundation for Basic Research (projects 13-05-00353 to O.G.S. and 14-05-31243_mol to S.A.K.), by grants from the National Science Foundation of South Africa (GUN: 2053192) and the University of Johannesburg as part of a programme of Russian–South African scientific collaboration.

SUPPLEMENTARY DATA

Supplementary data for this paper are available at *Journal of Petrology* online.

REFERENCES

Abdel-Rahman, A.-F. M. & Martin, R. F. (1990). The Mount Gharib A-type granite, Nubian Shield: petrogenesis and role of metasomatism at the source. *Contributions to Mineralogy and Petrology* **104**, 173–183.

Acosta-Vigil, A., London, D., Morgan, G. B. & Dewers, T. A. (2003). Solubility of excess alumina in hydrous granitic melts in equilibrium with peraluminous minerals at 700–800°C and 200 MPa, and applications of the aluminum saturation index. *Contributions to Mineralogy and Petrology* **146**, 100–119.

Acosta-Vigil, A., London, D. & Morgan, G. B. (2006). Experiments on the kinetics of partial melting of a leucogranite at 200 MPa H_2O and 690–800°C: compositional variability of melts during the onset of H_2O-saturated crustal anatexis. *Contributions to Mineralogy and Petrology* **151**, 539–551.

Andersen, D. J. & Lindsley, D. H. (1985). New (and final!) models for the Ti-magnetite/ilmenite geothermometer and oxygen barometer. *EOS Transactions, American Geophysical Union* **66**, 416.

Anderson, I. C., Frost, C. D. & Frost, B. R. (2003). Petrogenesis of the Red Mountain pluton, Laramie anorthosite complex, Wyoming: implications for the origin of A-type granite. *Precambrian Research* **124**, 243–267.

Anderson, J. L. (1983). Proterozoic anorogenic granite plutonism of North America. In: Medaris, L. G., Jr, Byers, C. W., Mickelson, D. M. & Shanks, W. C. (eds) *Proterozoic Geology - Selected papers from an International Proterozoic Symposium,* Geological Society of America, Memoirs **161**, 133–154.

Aranovich, L. Ya. & Newton, R. C. (1996). H_2O activity in concentrated NaCl solutions at high pressures and temperatures measured by the brucite–periclase equilibrium. *Contributions to Mineralogy and Petrology* **125**, 200–212.

Aranovich, L. Ya. & Newton, R. C. (1997). H_2O activity in concentrated KCl and KCl–NaCl solutions at high temperatures and pressures measured by the brucite–periclase equilibrium. *Contributions to Mineralogy and Petrology* **127**, 261–271.

Aranovich, L. Ya. & Newton, R. C. (1998). Reversed determination of the reaction: Phlogopite + quartz = enstatite + potassium feldspar + H_2O in the ranges 750–875°C and 2–12 kbar at low H_2O activity with concentrated KCl solutions. *American Mineralogist* **83**, 193–204.

Aranovich, L. Ya., Shmulovich, K. I. & Fed'kin, V. V. (1987). The H_2O and CO_2 regime in regional metamorphism. *International Geology Review* **29**, 1379–1401.

Aranovich, L. Ya., Zakirov, I. V., Sretenskaya, N. G. & Gerya, T. V. (2010). Ternary system H_2O–CO_2–NaCl at high P–T parameters: an empirical mixing model. *Geochemistry International* **48**, 446–455.

Aranovich, L. Y., Newton, R. C. & Manning, C. E. (2013). Brine-assisted anatexis: Experimental melting in the system haplogranite–H_2O–NaCl–KCl at deep-crustal conditions. *Earth and Planetary Science Letters* **374**, 111–120.

Aranovich, L. Y., Makhluf, A. R., Manning, C. E. & Newton, R. C. (2014). Dehydration melting and the relationship between granites and granulites. *Precambrian Research*, doi:10.1016/j.precamres.2014.07.004.

Bea, F., Arzamastsev, A., Montero, P. & Arzamastseva, L. (2001). Anomalous alkaline rocks of Soustov, Kola: evidence of mantle-derived metasomatic fluids affecting crustal materials. *Contributions to Mineralogy and Petrology* **140**, 554–566.

Berman, R. G. (2007). *WinTWQ (version 2.3): A software package for performing internally-consistent thermobarometric calculations. Geological Survey of Canada Open File*, **5462.**

Berman, R. G. & Aranovich, L. Ya. (1996). Optimized standard state and solution properties of minerals. *Contributions to Mineralogy and Petrology* **126**, 1–24.

Bonin, B. (2007). A-type granites and related rocks; evolution of a concept, problems and prospects. *Lithos* **97**, 1–29.

Bowers, T. S. & Helgeson, H. C. (1983). Evaluation of the thermodynamic and geochemical consequences of non-ideal mixing in the system H_2O–CO_2–NaCl on phase relations in geological systems: equation of state for H_2O–CO_2–NaCl fluids at high pressure and temperature. *Geochimica et Cosmochimica Acta* **47**, 1247–1275.

Clemens, J. D., Holloway, J. R. & White, A. J. R. (1986). Origin of A-type granite: experimental constraints. *American Mineralogist* **71**, 317–324.

Coleyshaw, E. E., Crump, G. & Griffith, W. P. (2003). Vibrational spectra of hydrated carbonate minerals: ikaite, monohydrocalcite, lansfordite and nesquehonite. *Spectrochimica Acta, Part A* **59**, 2231–2239.

Collins, W. J., Beams, S. D., White, A. J. R. & Chappell, B. W. (1982). Nature and origin of A-type granites with particular reference to southeastern Australia. *Contributions to Mineralogy and Petrology* **80**, 189–200.

Condie, K. C., Allen, P. & Narayana, B. L. (1982). Geochemistry of the Archean low- to high-grade transition zone, Southern India. *Contributions to Mineralogy and Petrology* **81**, 157–167.

Connolly, J. A. D. (2005). Computation of phase equilibria by linear programming: A tool for geodynamic modeling and its application to subduction zone decarbonation. *Earth and Planetary Science Letters* **236**, 524–541.

Creaser, R. A., Price, R. C. & Wormald, R. J. (1991). A-type granites revisited: assessment of a residual-source model. *Geology* **19**, 163–166.

Duan, Z., Moller, N. & Weare, J. H. (1995). Equation of state for the $NaCl–H_2O–CO_2$ system: prediction of phase equilibria and volumetric properties. *Geochimica et Cosmochimica Acta* **59**, 2869–2882.

Ebadi, A. & Johannes, W. (1991). Beginning of melting and composition of first melt in the system $Qz–Ab–Or–H_2O–CO_2$. *Contributions to Mineralogy and Petrology* **106**, 286–329.

Eby, G. N. (1990). The A-type granitoids: a review of their occurrence and chemical characteristics and speculations on their petrogenesis. *Lithos* **26**, 115–134.

Franz, L. & Harlov, D. E. (1998). High-grade K-feldspar veining in granulites from the Ivrea–Verbano Zone, Northern Italy: fluid flow in the lower crust and implications for granulite facies genesis. *Journal of Geology* **106**, 455–472.

Frost, C. D. & Frost, B. R. (2011). On ferroan (A-type) granitoids: their compositional variability and modes of origin. *Journal of Petrology* **52**, 39–55.

Frost, B. R., Barnes, C. G., Collins, W. J., Arculus, R. J., Ellis, D. J. & Frost, C. D. (2001). A geochemical classification for granitic rocks. *Journal of Petrology* **42**, 2033–2048.

Gardien, V., Thompson, A. B. & Ulmer, P. (2000). Melting of biotite + plagioclase + quartz gneisses: the role of H_2O in the stability of amphibole. *Journal of Petrology* **41**, 651–666.

Gilbert, F., Guillaume, D. & Laporte, D. (1998). Importance of fluid immiscibility in the $H_2O–NaCl–CO_2$ system and selective CO_2 entrapment in granulites: experimental phase diagram at 5–7 kbar, 900°C and wetting textures. *European Journal of Mineralogy* **10**, 1109–1123.

Hansen, E. C. & Harlov, D. E. (2007). Whole-rock, phosphate, and silicate compositional trends across an amphibolite- to granulite-facies transition, Tamil Nadu, India. *Journal of Petrology* **48**, 1641–1680.

Hansen, E. C., Newton, R. C., Janardhan, A. S. & Lindberg, S. (1995). Differentiation of Late Archean crust in the Eastern Dharwar craton, South India. *Journal of Geology* **103**, 629–651.

Hansen, E., Ahmed, K. & Harlov, D. E. (2002). Rb depletion in biotites and whole rocks across an amphibolite to granulite facies transition zone, Tamil Nadu, South India. *Lithos* **64**, 29–47.

Harlov, D. E. (2004). Fluid induced dehydration of mafic lower crust from amphibolite to granulite facies: nature and experiment. *American Geophysical Union, Fall Meeting* , V31A-1409.

Harlov, D. E. (2011). Petrological and experimental application of REE- and actinide-bearing accessory minerals to the study of Precambrian high-grade gneiss terranes. In: Van Reenen, D. D., Kramers, J. D., McCourt, S. & Perchuk, L.L. (eds) *Origin and Evolution of Precambrian High-grade Terrains, with Special Emphasis on the Limpopo Complex in Southern Africa. Geological Society of America, Memoirs* **207**, 13–24.

Harlov, D. E. (2012). The potential role of fluids during regional granulite facies dehydration in the lower crust. *Geoscience Frontiers* **3**, 813–827.

Harlov, D. E. & Förster, H.-J. (2002). High-grade fluid metasomatism on both a local and regional scale: the Seward Peninsula, Alaska and the Val Strona di Omegna, Ivrea–Verbano Zone, northern Italy. Part I: Petrography and silicate mineral chemistry. *Journal of Petrology* **43**, 769–799.

Harlov, D. E. & Melzer, S. (2002). Experimental partitioning of Rb and K between phlogopite and concentrated (K, Rb)Cl brine: Implication for the role of concentrated KCl brines in the depletion of Rb in phlogopite and the stability of phlogopite during charnockite genesis. *Lithos* **64**, 15–28.

Harlov, D. E., Hansen, E. C. & Bigler, C. (1998). Petrologic evidence for K-feldspar metasomatism in granulite facies rocks. *Chemical Geology* **151**, 373–386.

Harlov, D. E., Wirth, R. & Förster, H.-J. (2005). An experimental study of dissolution–reprecipitation in fluorapatite: Fluid infiltration and the formation of monazite. *Contributions to Mineralogy and Petrology* **150**, 268–286.

Harlov, D. E., Johansson, L., Van den Kerkhof, A. & Förster, H. J. (2006). The role of advective fluid flow and diffusion during localized, solid-state dehydration: Sondrum Stenhuggeriet, Halmstad, SW Sweden. *Journal of Petrology* **47**, 3–33.

Heinrich, W. (2007). Fluid immiscibility in metamorphic rocks. In: Liebscher, A. & Heinrich, C. A. (eds) *Fluid–Fluid Interactions. Mineralogical Society of America and Geochemical Society, Reviews in Mineralogy and Geochemistry* **65**, 389–430.

Holness, M. B. (1997). Surface chemical controls on pore-fluid connectivity in texturally equilibrated materials. In: Jamtveit, B. & Yardley, B. W. D. (eds) *Fluid Flow and Transport in Rocks*. Chapman & Hall, pp. 149–169.

Holtz, F., Johannes, W., Tamic, N. & Behrens, H. (2001). Maximum and minimum water contents of granitic melts generated in the crust: a reevaluation and implications. *Lithos* **56**, 1–14.

Huizenga, J.-M., Perchuk, L. L., van Reenen, D. D., Flattery, Y., Varlamov, D. A., Smit, C. A. & Gerya, T. V. (2011). Granite emplacement and the retrograde *P–T*–fluid evolution of Neoarchean granulites from the Central Zone of the Limpopo Complex. In: van Reenen, D. D., Kramers, J. D., McCourt, S. & Perchuk, L. L. (eds) *Origin and Evolution of Precambrian High-Grade Gneiss Terrains, with Special Emphasis on the Limpopo Complex of Southern Africa. Geological Society of America, Memoirs* **207**, 125–142.

Janardhan, A. S., Newton, R. C. & Hansen, E. C. (1982). The transformation of amphibolite facies gneiss to charnockite in Southern Karnataka and Northern Tamil Nadu, India. *Contributions to Mineralogy and Petrology* **79**, 130–149.

Johannes, W. & Holtz, F. (1996). *Petrogenesis and Experimental Petrology of Granitic Rocks*. Springer.

Johnson, E. L. (1991). Experimentally determined limits for $H_2O–CO_2–NaCl$ immiscibility in granulites. *Geology* **19**, 925–928.

Khodorevskaya, L. I. (2004). Granitization of amphibolites: 2. Characterization of physical and chemical phenomena related to fluid filtration through a rock. *Petrology* **12**, 282–296.

Kilink, I. A. & Burnham, C. W. (1972). Partitioning of chloride between a silicate melt and coexisting aqueous phase from 2 to 8 kilobars. *Economic Geology* **67**, 231–235.

Knudsen, T. L. & Lidwin, A. (1996). Magmatic CO_2, brine and nitrogen inclusions in Sveconorwegian enderbitic dehydration veins and a gabbro from the Bamble sector, southern Norway. *European Journal of Mineralogy* **8**, 1041–1064.

Korzhinskii, D. S. (1959). *Physical-chemical Basis of the Analysis of the Parageneses of Minerals*. Consultant Bureau Inc..

Korzhinskii, D. S. (1962). The role of alkalinity in the formation of charnockitic gneisses. *Trudy Vostochno-Sibirskogo Instituta Akademii Nauk SSSR, Series of Geology* **5**, 50–61 (in Russian).

Kullerud, K. (1996). Chlorine-rich amphiboles: interplay between amphibole composition and an evolving fluid. *European Journal of Mineralogy* **8**, 355–370.

Landenberger, B. & Collins, W. J. (1996). Derivation of A-type granites from a dehydrated charnockitic lower crust: evidence from the Chaelundi Complex, Eastern Australia. *Journal of Petrology* **37**, 145–170.

Larikova, T. L. & Zaraisky, G. P. (2009). Experimental modeling of corona textures. *Journal of Metamorphic Geology* **27**, 139–151.

Le Maitre, R. W., Streckeisen, A., Zanettin, B., Le Bas, M. J., Bonin, B., Bateman, P., Bellieni, G., Dudek, A., Efremova, S., Keller, J., Lameyre, J., Sabine, P. A., Schmid, R., Sörensen, H. & Woolley, A. R. (2002). *Igneous Rocks—a Classification and Glossary of Terms. Recommendations of the IUGS Subcommission on the Systematics of Igneous Rocks*, 2edn. Cambridge University Press.

Litvinovsky, B. A. & Podladchikov, Y. Y. (1993). Crustal anatexis during the influx of mantle volatiles. *Lithos* **30**, 93–107.

Litvinovsky, B. A., Jahn, B., Zanvilevich, A. N., Saunders, A., Poulain, S., Kuzmin, D. V., Reichow, M. K. & Titov, A. V. (2002). Petrogenesis of syenite–granite suites from the Bryansky Complex (Transbaikalia, Russia): implications for the origin of A-type granitoid magmas. *Chemical Geology* **189**, 105–133.

Loiselle, M. C. & Wones, D. R. (1979). Characteristics and origin of anorogenic granites. *Geological Society of America, Abstracts with Programs* **11**, 468.

Manning, C. E. (2013). Thermodynamic modeling of fluid–rock interaction at mid-crustal and upper-mantle conditions. In: Stefánsson, A., Driesner, T. & Bénézeth, P. (eds) *Thermodynamics of Geothermal Fluids. Mineralogical Society of America and Geochemical Society, Reviews in Mineralogy and Geochemistry* **76**, 135–164.

Manning, C. E. & Aranovich, L. Y. (2014). Brines at high pressure and temperature: thermodynamic, petrological and geochemical effects. *Precambrian Research*, doi:10.1016/j.precamres.2014.06.021.

Markl, G. & Bucher, K. (1998). Composition of fluids in the lower crust inferred from metamorphic salt in lower crustal rocks. *Nature* **391**, 781–783.

Markl, G., Ferry, J. & Bucher, K. (1998). Formation of saline brines and salt in the lower crust by hydration reactions in partially retrogressed granulites from the Lofoten Islands, Norway. *American Journal of Science* **298**, 705–757.

Martin, R. F. (2006). A-type granites of crustal origin ultimately result from open-system fenitization-type reactions in an extensional environment. *Lithos* **91**, 125–136.

McMillan, P. F., Jakobsson, S., Holloway, J. R. & Silver, L. A. (1983). A note on the Raman spectra of water-bearing albite glasses. *Geochimica et Cosmochimica Acta* **47**, 1937–1943.

Montanini, A. & Harlov, D. E. (2006). Petrology and mineralogy of granulite-facies mafic xenoliths (Sardinia, Italy): Evidence for KCl metasomatism in the lower crust. *Lithos* **92**, 588–608.

Morgan, G. B. & London, D. (1996). Optimizing the electron microprobe analysis of hydrous alkali aluminosilicate glasses. *American Mineralogist* **81**, 1176–1185.

Mysen, B. O., Virgo, D., Harrison, W. J. & Scarfe, C. M. (1980). Solubility mechanisms of H_2O in silicate melts at high pressures and temperatures: a Raman spectroscopic study. *American Mineralogist* **65**, 900–914.

Newton, R. C. (1986). Fluids in granulite facies metamorphism. *Advances in Physical Chemistry* **5**, 36–59.

Newton, R. C. (1995). Simple-system mineral reactions and high-grade metamorphic fluids. *European Journal of Mineralogy* **7**, 861–881.

Newton, R. C. & Manning, C. A. (2010). Role of saline fluids in deep-crustal and upper-mantle metasomatism: insights from experimental studies. *Geofluids* **10**, 58–72.

Newton, R. C. & Tsunogae, T. (2014). Incipient charnockite: Characterization at the type localities. *Precambrian Research*, doi:10.1016/j.precamres.2014.06.

Newton, R. C., Aranovich, L. Y., Hansen, E. C. & Vandenheuvel, B. A. (1998). Hypersaline fluids in Precambrian deep-crustal metamorphism. *Precambrian Research* **91**, 41–63.

Newton, R. C., Touret, J. L. R. & Aranovich, L. Y. (2014). Fluids and H_2O activity at the onset of granulite facies metamorphism. *Precambrian Research*, doi:10.1016/j.precamres.2014.06.009.

Ni, H. & Keppler, H. (2013). Carbon in silicate melts. In: Hazen, R. N., Jones, A. P. & Baross, J. A. (eds) *Carbon in Earth. Mineralogical Society of America and Geochemical Society, Reviews in Mineralogy and Geochemistry* **75**, 251–287.

Patiño Douce, A. E. (1997). Generation of metaluminous A-type granites by low-pressure melting of calc-alkaline granitoids. *Geology* **25**, 743–746.

Patiño Douce, A. E. & Beard, J. S. (1995). Dehydration-melting of biotite gneiss and quartz amphibolite from 3 to 15 kbar. *Journal of Petrology* **36**, 707–738.

Perchuk, L. L. & Gerya, T. V. (1993). Fluid control of charnockitization. *Chemical Geology* **108**, 175–186.

Perchuk, L. L., Gerya, T. V. & Korsman, K. (1994). A model for charnockitization of gneissic complexes. *Petrology* **2**, 451–479.

Perchuk, L. L., Safonov, O. G., Gerya, T. V., Fu, B. & Harlov, D. E. (2000). Mobility of components in metasomatic transformation and partial melting of gneisses: an example from Sri Lanka. *Contributions to Mineralogy and Petrology* **140**, 212–232.

Rajesh, H. M. (2008). Petrogenesis of two granites from Nilgiri and Madurai blocks, southwestern India: implications for charnockite–calc-alkaline granite and charnockite–alkali (A-type) granite link in high-grade terrains. *Precambrian Research* **162**, 180–197.

Rajesh, H. M., Belyanin, G. A., Safonov, O. G., Kovaleva, E. I., Golunova, M. A. & van Reenen, D. D. (2013). Fluid-induced dehydration of the Paleoarchean Sand River biotite–hornblende gneiss, Central Zone, Limpopo Complex, South Africa. *Journal of Petrology* **54**, 41–74.

Ratajeski, K. & Sisson, T. W. (1999). Loss of iron to gold capsules in rock melting experiments. *American Mineralogist* **84**, 1521–1527.

Ravindra-Kumar, G. R. (2004). Mechanism of arrested charnockite formation at Nemmara, Palghat region, southern India. *Lithos* **75**, 331–358.

Rutter, M. J. & Wyllie, P. J. (1988). Melting of vapor-absent tonalite at 10 kbar to simulate dehydration melting in the deep crust. *Nature* **331**, 159–160.

Ryabchikov, I. D. & Hamilton, D. L. (1971). Possibility of separation of concentrated chloride solutions in course of acid magma crystallization. *Doklady Akademii Nauk SSSR* **197**, 933–937.

Safonov, O. G. (1998). The role of alkalis in the formation of coronitic textures in metamangerites and metaanorthosites from the Adirondack Complex, United States. *Petrology* **6**, 583–602.

Safonov, O. G. & Aranovich, L. Y. (2014). Alkali control of high-grade metamorphism and granitization. *Geoscience Frontiers* **5**, 711–727.

Safonov, O. G., Kovaleva, E. I., Kosova, S. A., Rajesh, H. M., Belyanin, G. A., Golunova, M. A. & van Reenen, D. D. (2012). Experimental and petrological constraints on local-scale interaction of biotite–amphibole gneiss with H_2O–CO_2–(K, Na)Cl fluids at middle-crustal conditions: Example from the Limpopo Complex, South Africa. *Geoscience Frontiers* **3**, 829–841.

Scambelluri, M., Pennacchioni, G. & Phillipot, P. (1998). Salt-rich aqueous fluids formed during eclogitization of metabasites in the Alpine continental crust (Austroalpine Mt. Emilius unit, Italian Western Alps). *Lithos* **43**, 151–167.

Shmulovich, K. I. & Graham, C. M. (1996). Melting of albite and dehydration of brucite in H_2O–NaCl fluids to 9 kbars and 700–900°C: implications for partial melting and water activities during high pressure metamorphism. *Contributions to Mineralogy and Petrology* **124**, 370–382.

Shmulovich, K. I. & Graham, C. M. (2004). An experimental study of phase equilibria in the systems H_2O–CO_2–$CaCl_2$ and H_2O–CO_2–NaCl at high pressures and temperatures (500–800°C, 0·5–0·9 GPa): geological and geophysical applications. *Contributions to Mineralogy and Petrology* **146**, 450–462.

Singh, J. & Johannes, W. (1996). Dehydration melting of tonalities. Part 1. Beginning of melting. *Contributions to Mineralogy and Petrology* **125**, 16–25.

Skjerlie, K. P. & Johnston, A. D. (1993). Fluid-absent melting behavior of an F-rich tonalitic gneiss at mid-crustal pressures: implications for the generation of anorogenic granites. *Journal of Petrology* **34**, 785–815.

Srikantappa, C. & Malathi, M. N. (2008). Solid inclusions of magmatic halite and CO_2–H_2O inclusions in the Closepet Granite from Ramnagaram, Dharwar Craton, India. *Indian Mineralogist* **42**, 84–89.

Srikantappa, C. & Zargar, S. A. (2009). First report on the halite-bearing fluid inclusions in the Precambrian granulites around Halaguru, Dharwar Craton, India. *Indian Mineralogist* **43**, 77–80.

Tamic, N., Behrens, H. & Holtz, F. (2001). The solubility of H_2O and CO_2 in rhyolitic melts in equilibrium with mixed CO_2–H_2O fluid phase. *Chemical Geology* **174**, 333–347.

Touret, J. L. R. (1985). Fluid regime in southern Norway: the record of inclusions. In: Tobi, A. C. & Touret, J. L. R. (eds) *The Deep Proterozoic Crust in the North Atlantic Provinces. Proceedings of NATO Advanced Study Institute Series* **C158**, 517–549.

Touret, J. L. R. (2009). Mantle to lower-crust fluid/melt transfer through granulite metamorphism. *Russian Geology and Geophysics* **50**, 1052–1062.

Touret, J. L. R. & Huizenga, J. M. (2011). Fluids in granulites. In: Van Reenen, D. D., Kramers, J. D., McCourt, S. & Perchuk, L.L. (eds) *Origin and Evolution of Precambrian High-grade Terrains, with Special Emphasis on the Limpopo Complex in Southern Africa. Geological Society of America, Memoirs* **207**, 25–37.

Touret, J. L. R. & Huizenga, J.-M. (2012). Fluid-assisted granulite metamorphism: a continental journey. *Gondwana Research* **21**, 224–235.

Trommsdorf, V., Skippen, G. & Ulmer, P. (1985). Halite and sylvite solid inclusions in high-grade rocks. *Contributions to Mineralogy and Petrology* **89**, 24–29.

Tropper, P. & Manning, C. E. (2008). Experimental constraints on the role of brines in the transformation of granulite-facies metapelites to eclogites. *Geophysical Research Abstracts* **10**, EGU2008-A-05012.

Tropper, P., Manning, C. E. & Harlov, D. E. (2011). Solubility of $CePO_4$ monazite and YPO_4 xenotime in H_2O and H_2O–NaCl at 800°C and 1 GPa: Implications for REE and Y transport during high-grade metamorphism. *Chemical Geology* **282**, 58–66.

Tropper, P., Manning, C. E. & Harlov, D. E. (2013). Experimental determination of $CePO_4$ and YPO_4 solubilities in H_2O–NaF at 800°C and 1 GPa: implications for rare earth element transport in high-grade metamorphic fluids. *Geofluids* **13**, 372–380.

Tsunogae, T. & van Reenen, D. D. (2014). High- to ultrahigh-temperature metasomatism related to brine infiltration in the Neoarchean Limpopo Complex: Petrology and phase equilibrium modeling. *Precambrian Research*, doi:10.1016/j.precamres.2014.07.001.

Van den Kerkhof, A. M. & Grantham, G. H. (1999). Metamorphic charnockite in contact aureoles around intrusive enderbite from Natal, South Africa. *Contributions to Mineralogy and Petrology* **137**, 115–132.

Watkins, J. M., Clemens, J. D. & Treloar, P. J. (2007). Archaean TTGs as sources of younger granitic magmas: melting of sodic metatonalites at 0·6–1·2 GPa. *Contributions to Mineralogy and Petrology* **154**, 91–110.

Watson, E. B. & Brenan, J. M. (1987). Fluids in the lithosphere, 1. Experimentally determined wetting characteristics of CO_2–H_2O fluids and their implications for fluid transport, host-rock physical properties, and fluid inclusion formation. *Earth and Planetary Science Letters* **85**, 594–615.

Webster, J. D. (1997). Exsolution of magmatic volatile phases from Cl-enriched mineralizing granitic magmas and applications for ore metal transport. *Geochimica et Cosmochimica Acta* **61**, 1017–1029.

Webster, J. D. & De Vivo, B. (2002). Experimental and modeled solubilities of chlorine in aluminosilicate melts, consequences of magma evolution, and implications for exsolution of hydrous chloride melt at Mt. Somma–Vesuvius. *American Mineralogist* **87**, 1046–1061.

Whalen, J. B., Currie, K. L. & Chappell, B. W. (1987). A-type granites: geochemical characteristics, discrimination and petrogenesis. *Contributions to Mineralogy and Petrology* **95**, 407–419.

Yardley, B. W. D. & Graham, J. T. (2002). The origins of salinity in metamorphic fluids. *Geofluids* **2**, 249–256.